TRANSITION METAL COMPLEXES AS PROBES OF DNA SEQUENCE-DEPENDENT STRUCTURE

Thesis by

Donna Campisi

in Partial Fulfillment of the Requirements

for the Degree of

Doctor of Philosophy

California Institute of Technology

Pasadena, California

1996

Submitted August 1, 1995

ACKNOWLEDGMENTS

First of all, I would like to express my gratitude to my advisor, Prof. Jackie Barton, for all her support and encouragement during my time as a graduate student. I believe that her optimism has truly transformed me from being an inveterate pessimist into someone who is more of a realist. Furthermore, I have learned that a realistic attitude is essential for doing good science. I would also like to thank Jackie for all the opportunities with which she has provided me.

Additionally, I would like to thank the members of my thesis committee, Prof. Doug Rees, Prof. Harry Gray, and Prof. Nate Lewis for their helpfulness. Thanks also to my undergraduate advisor, Prof. Marc Walters of New York University, who started me on the path of performing chemical research.

Next, I would like to acknowledge the members of the Barton Group, past and present, a special group of people who have also taught me much. I would specifically like to thank Dr. Takashi Morii, for being a wonderful collaborator who also trained me in many laboratory techniques and with whom I have had many discussions about science. I would additionally like to thank Dr. Sheila David, Dr. Cynthia Dupureur, Dr. Kevin Kingsbury, Ayesha Sitlani, and Yonchu Jenkins for cheerfully providing me with metal complexes. Thanks are also extended to former members of the Barton Group including Dr. Kaspar Zimmermann, Inho Lee, Dr. Achim Krotz, and Dr. Scott Klakamp. I would also like to thank current members of the group for their assistance and friendship, including R. Erik Holmlin, Tim Johann, Ai Ching Lim, Yonchu Jenkins, Susanne Lin, Brian Jackson, Brian Hudson, Bob Terbrueggen, Kitty Erkkila, Dan Hall, Marilena Fitzsimons, Dr. Eric Stemp, Michelle Arkin, Shana Kelley, Dr. Sonya Franklin, Dr. Sabine Coates, and Dr. Peter Dandliker. My sincere thanks go to Mo Renta for her assistance, advice, and friendship my entire time at Caltech.

On a more personal level, I would like to thank my friends and my family, who have been there for me over the years. I would especially like to acknowledge Drs. Ayesha Sitlani and Michael Pustilnik, who belonged to the "night crew" at lab, and have remained good friends to me to this day. Thanks also go to Sherin Halfon, my classmate and apartmentmate at Columbia University, who has also remained a good friend. Thanks go to my entire family, who have done a wonderful job of keeping in touch. I thank my parents, who have always understood the value of a good education. Finally, thanks go to my sister Debbie, for providing me with light moments, and to my sister Terry Ann, who will be receiving her Ph.D. in clinical psychology in a few months, for her understanding of the graduate school experience.

ABSTRACT

Different transition metal complexes have been applied in probing variations in the structure of double helical DNA. The following probes, which all bind DNA noncovalently, have been utilized: $Ru(phen)_3^{2+}$, $Ru(TMP)_3^{2+}$, $Rh(phen)_2phi^{3+}$, $Rh(TMP)_2phi^{3+}$, $Rh(dmbpy)_2phi^{3+}$, $Ru(phen)_2dppz^{2+}$, $Ru(bpy)_2dppz^{2+}$, and $Rh(bpy)_2dppz^{3+}$ (phen = 1,10 phenanthroline; TMP = 3,4,7,8,-tetramethyl-1,10-phenanthroline; phi = 9,10-phenanthrenequinone diimine; dmbpy = 5,5'-dimethyl-bipyridyl; bpy = bipyridyl; dppz = dipyrido[3,2-a;2',3'-c]phenazine). The local structure recognized by Δ-$Rh(phen)_2phi^{3+}$ has been defined by comparisons of photocleavage data on crystallographically characterized oligonucleotides with their structural parameters. A quantitative correlation has been determined between Δ-$Rh(phen)_2phi^{3+}$ photocleavage and extent of openness in the major groove due to differential propeller twisting, or interpurine angle. Therefore, Δ-$Rh(phen)_2phi^{3+}$ has been developed as a probe of DNA propeller twisting in solution. Differences in reaction pathway partitioning between enantiomers of $Rh(phen)_2phi^{3+}$ are attributed to differing extent of shape complementarity with DNA binding sites. $Rh(TMP)_2phi^{3+}$ has been explored in probing DNA mismatches in solution. Both Δ-$Rh(phen)_2phi^{3+}$ and $Rh(TMP)_2phi^{3+}$ sensitively mark local structural perturbations in an oligonucleotide, arising from substitution of a CG base pair with TG and AG mismatches. $Rh(phen)_2phi^{3+}$ and $Ru(TMP)_3^{2+}$ have also been applied in probing structural variations in the context of a long DNA strand. A C7 stretch is targeted by $Ru(TMP)_3^{2+}$, an A DNA probe and $Rh(phen)_2phi^{3+}$, a B DNA probe. These results indicate this sequence is heteronomous, containing wide major and minor grooves. Δ- and Λ-$Rh(phen)_2phi^{3+}$ also discriminate structural differences between bent and nonbent DNA fragments. Variations in metal complex-DNA interactions have also been examined by a gel electrophoretic mobility assay. Intercalator size, hydrophobicity of ancillary ligands, metal complex charge, and chirality all influence the extent of DNA retardation. Taken together, these studies demonstrate that transition metal complexes can be profitably and

uniquely applied towards exploring DNA structural heterogeneity.

TABLE OF CONTENTS

LIST OF FIGURES

Chapter 3:

Chapter 4:

Chapter 5:

LIST OF SCHEMES

page

Chapter 2:

LIST OF TABLES

page

Chapter 1:

Chapter 1:

Introduction: DNA Structural Heterogeneity and Probes of Sequence-Dependent Structure

1.1. DNA Global Conformational Variations

DNA is the repository for the genetic information necessary for life. By mechanisms which are not entirely understood, the sequence of DNA directs its three-dimensional structure. This DNA structure additionally plays an active role in the events involving molecular recognition, events which govern a great number of biological processes including transcription and replication. Therefore, an understanding of DNA structure is necessary in order to define its contribution to molecular recognition. Ultimately, it is envisioned that such knowledge could lead to therapeutic strategies for controlling biological recognition events.

The structure of DNA stores information on a number of levels, the most apparent of which include the features of its overall form. The global polymorphism of DNA has been well characterized by a variety of methods[1]. As shown in Figure 1.1, DNA adopts a range of conformations, which include the A, B, and Z forms. These structural families differ in many respects, including pitch, groove width, and even chirality. Some characteristics of these conformations are compared in Table 1.1. The A form of DNA has the smallest helical pitch of these three conformations, while the Z form is the most elongated. The A form additionally possesses a narrow, deep major groove, and a wide, shallow minor groove. The B form of DNA is characterized by a wide, deep major groove and a narrow, deep minor groove. Importantly, the B conformation exhibits a great variety of sequence-dependent local structure. The Z conformation is distinguished from the other two forms shown here by its left-handed chirality, a dinucleotide repeat, and a "zigzag" structure. Z DNA has a wide, almost convex major groove, and a very narrow, deep minor groove.

Figure 1.1. CPK models of the A, B, and Z global conformations of DNA structure. The sugar-phosphate backbone is depicted in red and the bases are shown in green. As may be seen, DNA exhibits notable structural polymorphism.

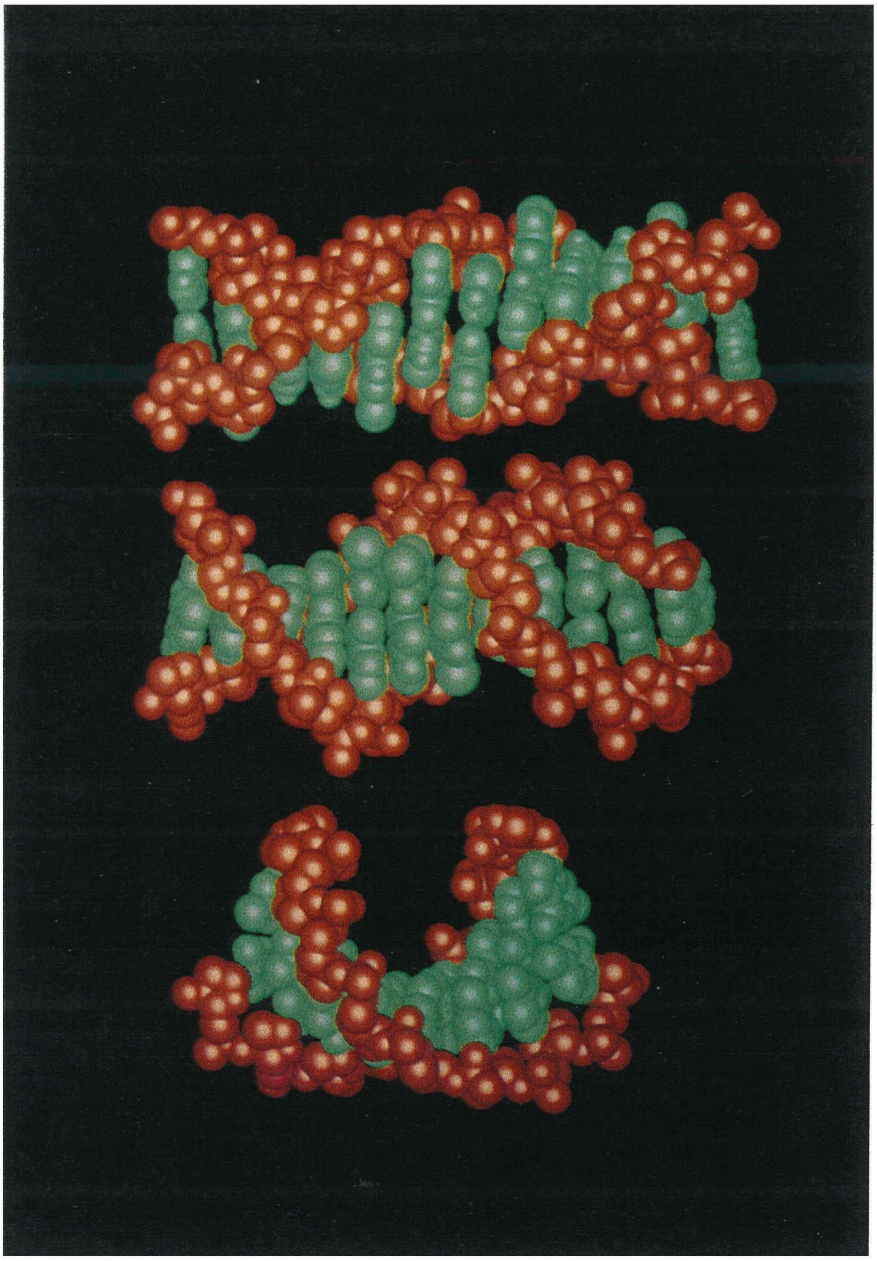

Table 1.1. Structural Characteristics of DNA According to Type[a]

Feature	A[b]	B[b]	Z
helix diameter	23 Å	19.3 Å	18.4 Å
pitch	28.2 Å	33.8 Å	45 Å
base pairs per turn	11 bp	10 bp	12 bp
groove width[c] -major[d]	2.7 Å	11.7 Å	-
minor	11.0 Å	5.7 Å	2.7 Å
groove depth[c] -major[d]	13.5 Å	8.5 Å	-
minor	2.8 Å	7.5 Å	9.0 Å
rise	2.56 Å	3.38 Å	3.7 Å
inclination	10° to 20°	-5.9° to -16.4°	-7°
base pair displacement	4.4 to 4.9 Å	-0.2 to -1.8 Å	positive[e]

[a]Data was originally obtained by X-ray fiber diffraction and X-ray crystallography methods. All entries are from compiled from Reference 1, except as indicated.
[b]Measurements are for random sequence DNA.
[c]Measurements based on van der Waals radii.
[d]These values can not be measured for Z form DNA.
[e]From Reference 9.

Global DNA structural characteristics necessarily influence molecular recognition. In general, due to steric considerations, grooves which are narrow afford less opportunity for sequence-specific recognition than grooves which are wide and accessible. Thus it is the major groove of B form DNA which is recognized by the majority of sequence-specific proteins. However, within the double helical regions of RNA which adopt the A form, specific recognition by proteins tends to predominate in the minor groove[2], or where the major groove is opened by other structural features, such as bulges. Nonspecific recognition by proteins does take place in the minor groove of B form DNA[3] and perhaps in the major groove of A form double helical RNA[4]. Recognition of Z DNA by proteins may have biological relevance[5] but is as yet poorly understood.

Aside from differences in groove widths, the global conformations of DNA also differ in more subtle respects such as sugar puckering, and positioning of the bases with respect to the sugar and with respect to the helical axis (inclination). Sugar puckering modes are shown in Figure 1.2A. The A conformation possesses the $C_{3'}$-*endo* conformation, and sugar puckering in the B form is $C_{2'}$-*endo*. Z DNA displays an alternating $C_{3'}$-*endo* for purines and $C_{2'}$-*endo* for pyrimidines. Sugar orientations are shown in Figure 1.2B. In correctly matched DNA in the A and B forms, the orientation of the base about the glycosidic bond is *anti*. For Z DNA, the pyrimidines adopt an anti orientation, and the purines adopt a *syn* orientation. Finally, although B form and Z form DNA contains bases which are nearly perpendicular to the helical axis, in the A form, the bases are notably inclined with respect to the helical axis normal (Table 1.1). All of these structural differences are components of the observed global variation.

It should be noted that each of the aforementioned global conformations occur within the context of straight, correctly paired DNA double helices. Structural aberrations such as DNA containing noncomplementary bases, and DNA bending have important biological consequences for repair and transcription respectively. The effects of these two structural features upon recognition will be further examined in Chapters 3 and 4.

Figure 1.2. Local structural variation involving the deoxyribose and bases. (top panel) The $C_{3'}$-*endo* sugar puckering mode (left) is present for A form helices and for purines in Z form DNA. The $C_{2'}$-*endo* sugar puckering mode (right) is present in B form DNA and for the pyrimidines of Z form. Adapted from Reference 6. (bottom panel) The rotation of the base about the glycosidic bond may be categorized as *syn* (left) or *anti* (right). In correctly paired B form and A form DNA, the *anti* orientation is exclusively used. The pyrimidines in Z form DNA also utilize the *anti* orientation. The *syn* orientation is adopted by the purines in Z form DNA, and by some mismatched bases in right-handed DNA. Adapted from Reference 7.

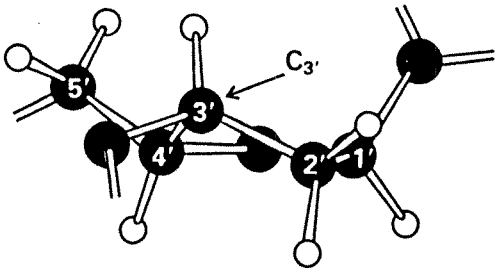

$C_{3'}$-*endo*

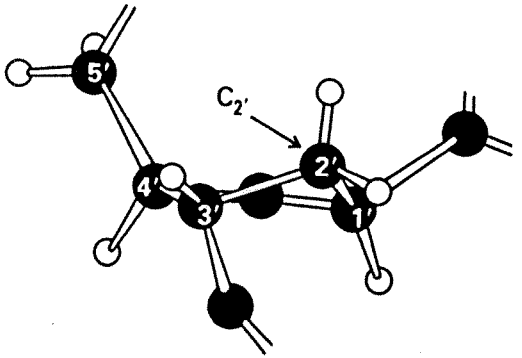

$C_{2'}$-*endo*

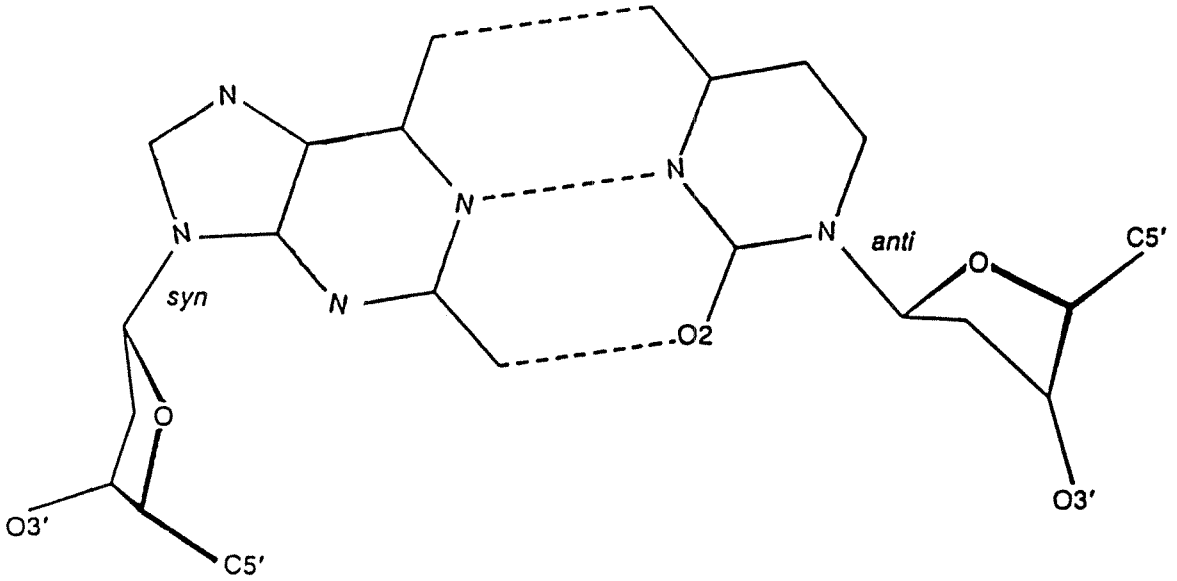

1.2. Parameters for Defining Local DNA Structure

The first high-resolution structure of DNA in the B conformation provided many details which were not apparent from examination of fiber diffraction studies alone[8]. Perhaps the most important outcome of these detailed crystallographic studies is that the structure of B form DNA, rather than rigidly adopting a fixed, regular conformation, shows *considerable, sequence-dependent heterogeneity*. That these variations in structure should be apparent in the crystal form of DNA is even more remarkable; it might be expected, then, that DNA in solution should display a breadth of structural variety at least as great as that found in the solid state.

The greatest variations in the local structure of B DNA are observed in the positioning of the bases with respect to one another, which is dictated primarily by stacking interactions. The complexity of local DNA structure has necessitated the use of a standardized coordinate reference frame and definitional parameters[9], which are depicted in Figure 1.3. These parameters fall into one of two categories, those parameters which define either (i) the position of the two bases of a base pair with respect to one another, or (ii) the positions of one base pair with respect to that of a neighboring base pair. Additionally, the parameters may be categorized as those which define translation of the base pair/step with respect to one of the coordinate axes, or those which denote the rotation of the base pair/step about one of the axes. These definitions are all irrespective of the DNA sequence involved. Although there are numerous parameters available for defining DNA structures obtained from crystallography, the most commonly reported are rise (D_z), propeller twist (ω), helical twist (Ω), tilt (τ), and roll (ρ).

1.3. Methods for Elucidation of DNA structure: X-ray Crystallography and Nuclear Magnetic Resonance Spectroscopy

As mentioned above, X-ray crystallography has provided a detailed picture of DNA structure in the solid state[10]. An important question is: how does the solution

Figure 1.3. The conventional coordinate frame of reference and parameters for defining DNA local structure. **A.** Definitions of parameters describing the rotation of bases and base pairs. Shown are parameters which define (top row) rotations of bases which are moving in the same direction, (center row) bases moving in opposite directions, and (bottom row) rotations of one base *pair* with respect to its neighboring base *pair*. **B.** Definitions of parameters delimiting the translation of bases and base pairs. Shown are parameters defining (top row) bases involved in a concerted motion (middle row) bases in an opposed, and (bottom row) the motion of two successive base pairs in a base step. Figure adapted from Reference 9.

A

ROTATION

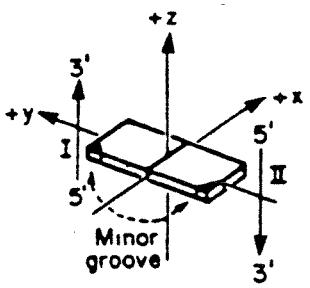

Coordinate frame

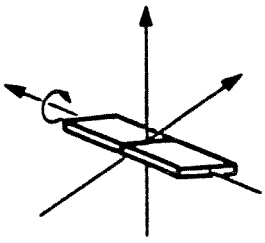

Tip (θ)

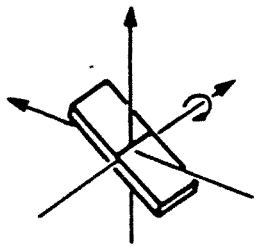

Inclination (η)

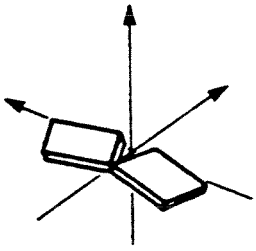

Opening (σ)

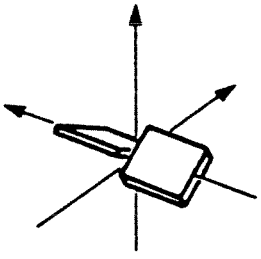

Propeller twist (ω)

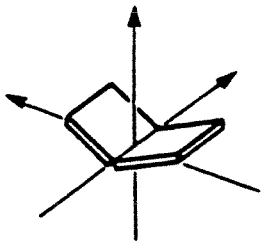

Buckle (κ)

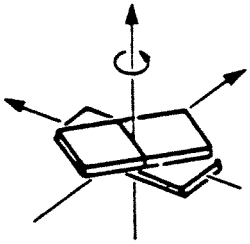

Twist (Ω)

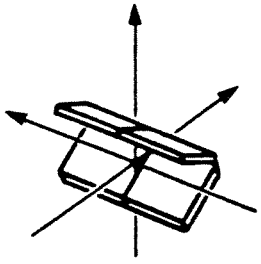

Roll (ρ)

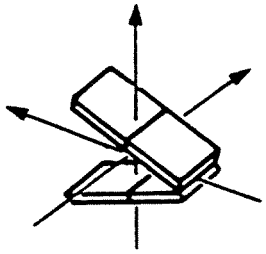

Tilt (τ)

B

TRANSLATION

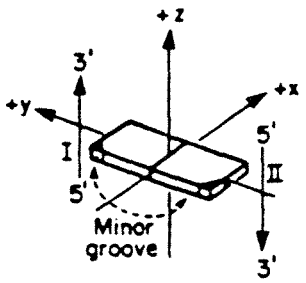

Coordinate frame

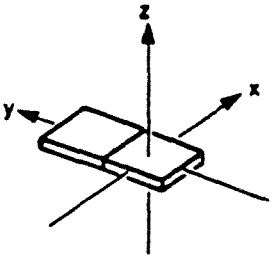

y displacement (dy)

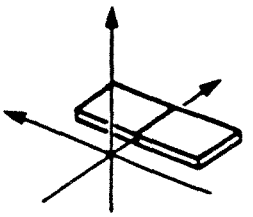

x displacement (dx)

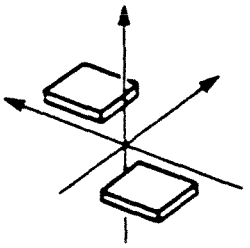

Stagger (Sz)

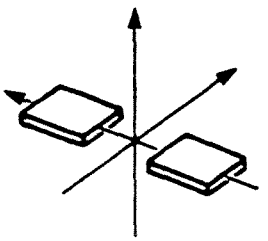

Stretch (Sy)

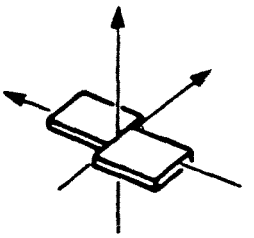

Shear (Sx)

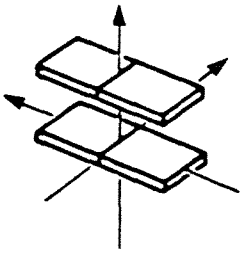

Rise (Dz)

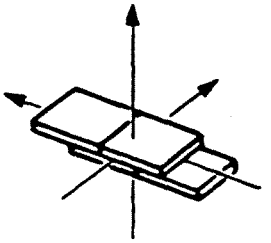

Slide (Dy)

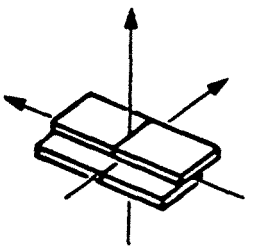

Shift (Dx)

structure, which is more likely to be biologically relevant, compare with structures obtained from the crystal? An important difference between the DNA environment in the crystal and in solution is the presence of forces which enable DNA helices to pack closely together in the ordered manner necessary for crystallization to occur. There are two types of crystallography experiments which address the problem of crystal packing effects on DNA structure. First, it is useful to examine closely related sequences with the same crystal packing for structural differences. Secondly, crystal structures of the same sequence in different packing environments may be examined for similarities. Studies of the former type indicate that there are sequence-dependent structural differences observed within a given packing geometry do exist[11]. However, several studies of DNA with identical sequences in two crystallographic environments shows that there are significant structural differences, which must be attributed to crystal packing forces[12]. Therefore consideration must be given to packing whenever evaluating crystallographically obtained DNA structures.

Structures acquired by nuclear magnetic resonance spectroscopy do not have the particular concern of packing influences. However, it does not appear that this technique is capable of determining a unique structure for a given oligonucleotide in solution in the same precise and detailed manner that characterizes DNA crystal structures[13]. The most commonly used nucleus in NMR experiments is the proton, and the structure of DNA is such that most of the protons are situated on the phosphate backbone, and not the bases. For this reason, the bases are not as well determined as the backbone by NMR spectroscopy. However, as mentioned above, it is the disposition of bases that define the most important local structural variation in B-form DNA. The use of multidimensional heteronuclear NMR with, e.g., ^{15}N-labelled bases does not yet appear to have surmounted this problem. Nevertheless, NMR spectroscopy has been appropriately and extensively utilized in examining ligand-DNA, and even protein-DNA interactions in solution[14]. Additionally, some dynamic structural information, such as rates of base pair openings,

can be uniquely obtained by this technique. How specific structures studied by NMR compare with those obtained by X-ray crystallography will be discussed in Chapter 2.

1.4. Enzymatic and Chemical Probes of DNA Structure

The limitations of X-ray crystallography and NMR in the study of DNA structural variation has led to the development of enzymatic and chemical probes. For example, a significant limitation of both aforementioned techniques is that the size of DNA amenable for study is under 20 base pairs; such considerations do not apply to studies with structural probes. These probes also have an advantage in that they allow for structural investigations of DNA under a large range of concentrations, and even in the presence of large, DNA binding proteins in solution. Therefore, utilization of structural probes importantly serves as an augmentation to the use of biophysical techniques, and provides a link between high resolution crystallography on oligonucleotides, and the sequence-dependent structure of long DNA polymers in solution.

The most commonly used enzymatic probe is DNase I. At higher concentrations, DNase I cleaves DNA fairly nonspecifically, and is used to map or "footprint" protein binding regions on DNA. However, this enzyme cleaves DNA in a somewhat selective manner at lower concentrations, and has been used to examine sequence-dependent structural variations of DNA in solution. It has been shown that DNase I preferentially cleaves DNA of mixed sequences, and cleaves poorly on both strands of homopolymeric stretches. What is the structural basis for this recognition? Since AT-rich DNA tends to exhibit a narrow minor groove, and CG-rich DNA possesses a wide minor groove, it is thought[15] that this enzymatic probe is recognizing DNA of medium minor groove width (approximately 13 Å). It is also possible that DNase I cleaves DNA sites having a high helical twist value[16]. The cleavage patterns of DNase II are complementary to those of DNase I, with DNase II having a preference for the purine strand of homopolymeric stretches[15b]. These opposing digestion patterns are believed to be the result of sequence-

dependent positioning of phosphates. Since DNase I performs nucleophilic attack across from the O3', it cleaves sites where the surface of the phosphorous atom opposite to the O3' is accessible to the solvent. Since DNase II attacks opposite the O5', it is perhaps not surprising that its site-selection is clearly different than that of DNase I. Thus DNase I and DNase II are useful in examining DNA groove width and conformation of the sugar-phosphate backbone.

Commonly used chemical probes of DNA structure and of protein-DNA interactions include $Cu(phen)_2^+$ and $Fe(EDTA)^{2-}$. The active form of $Cu(phen)_2^+$, which depends upon the presence of H_2O_2, has been shown by analysis of cleavage chemistry and examination of substituted phenanthroline ligands to bind the surface of the minor groove of DNA[17]. This complex prefers the minor groove conformation of B form DNA to A form DNA by a factor of 3[15a]. Additionally, like DNase I, $Cu(phen)_2^+$ also appears to recognize DNA possessing intermediate groove widths[13b]. Another chemical probe of local DNA structure is $Fe(EDTA)_2^{2-}$; this complex generates hydroxyl radicals which react with hydrogens in the minor groove of DNA. The reactivity of $Fe(EDTA)_2^{2-}$ tracks with the accessibility of these minor groove hydrogens. Although this complex employs a diffusable mechanism, it does provide information on altered groove widths, and has been particularly useful for examining the variations of the minor groove accessibility of bent DNA[18].

1.5. Transition Metal Complexes As Probes of DNA Local Structure

A special class of nucleic acid structural probes, consisting of octahedral metal complexes, has been developed by the Barton laboratory[19]. These complexes contain a transition metal center, most commonly rhodium or ruthenium, though osmium and iridium complexes have recently been synthesized[20]. This metal center is coordinately saturated by, in most cases, three bidentate ligands, which emanate from the metal center in a three-dimensional, propeller-like fashion. Since these metal complexes are

substitutionally inert, they have a well-defined, rigid structure. This rigidity simplifies to some extent the study of recognition, since it is known that the probe will be in the same conformation both before and after binding DNA. Significantly, many of these metal complexes possess ligands containing no hydrogen bonding functionalities. Therefore *their recognition is predicated upon shape-selection,* which may be defined as a match in the shape and symmetry of the DNA binding site with those of the metal complex probe.

This thesis concerns the application of several *transition metal complexes as probes of DNA sequence-dependent structure.* Short, well characterized DNA substrates have been examined in an attempt to refine our understanding of how these molecules interact noncovalently with DNA in solution. With these studies as a foundation, the metal complex probes have been also been applied to DNA sequences for which there are discrepancies between structures derived from other methods. Additionally, DNA conformation in the context of long strands has been probed by these complexes.

Octahedral metal complexes may interact with DNA by one of three major binding modes, as illustrated in the model in Figure 1.4: electrostatic interactions (top), surface binding (bottom), and intercalation (center). These metal complex-DNA interactions are located at the phosphate backbone, the minor groove, and the major groove, respectively. The metal complex which is shown in an electrostatic interaction with the negatively charged phosphates of DNA is $Ru(bpy)_3^{2+}$; the bipyridyl ligand does not possess a large enough hydrophobic area with which to stabilize any other binding modes. $Ru(phen)_3^{2+}$ is shown in a surface binding mode. The phenanthroline ligand is more hydrophobic than the bipyridyl, which favors intercalation, and to some extent, the depicted close association along the minor groove. The intercalative binding mode is illustrated in Figure 1.4 by the complex $Rh(phen)_2phi^{3+}$. Intercalation involves the insertion of the phi ligand between the DNA bases, with a concomitant unwinding of the helix. The phi ligand has a large enough surface area to ensure intercalation as the primary binding mode of $Rh(phen)_2phi^{3+}$.

Both surface binding and intercalating metal complexes have been used to probe

Figure 1.4. Types of metal complex-DNA noncovalent interactions. (top) $Ru(bpy)_3^{2+}$ in an electrostatic interaction with the negatively charged DNA sugar-phosphate backbone. (center) $Rh(phen)_2phi^{3+}$ binding by intercalation into the major groove of DNA. (bottom) $Ru(phen)_3^{2+}$ in a surface binding interaction in the minor groove.

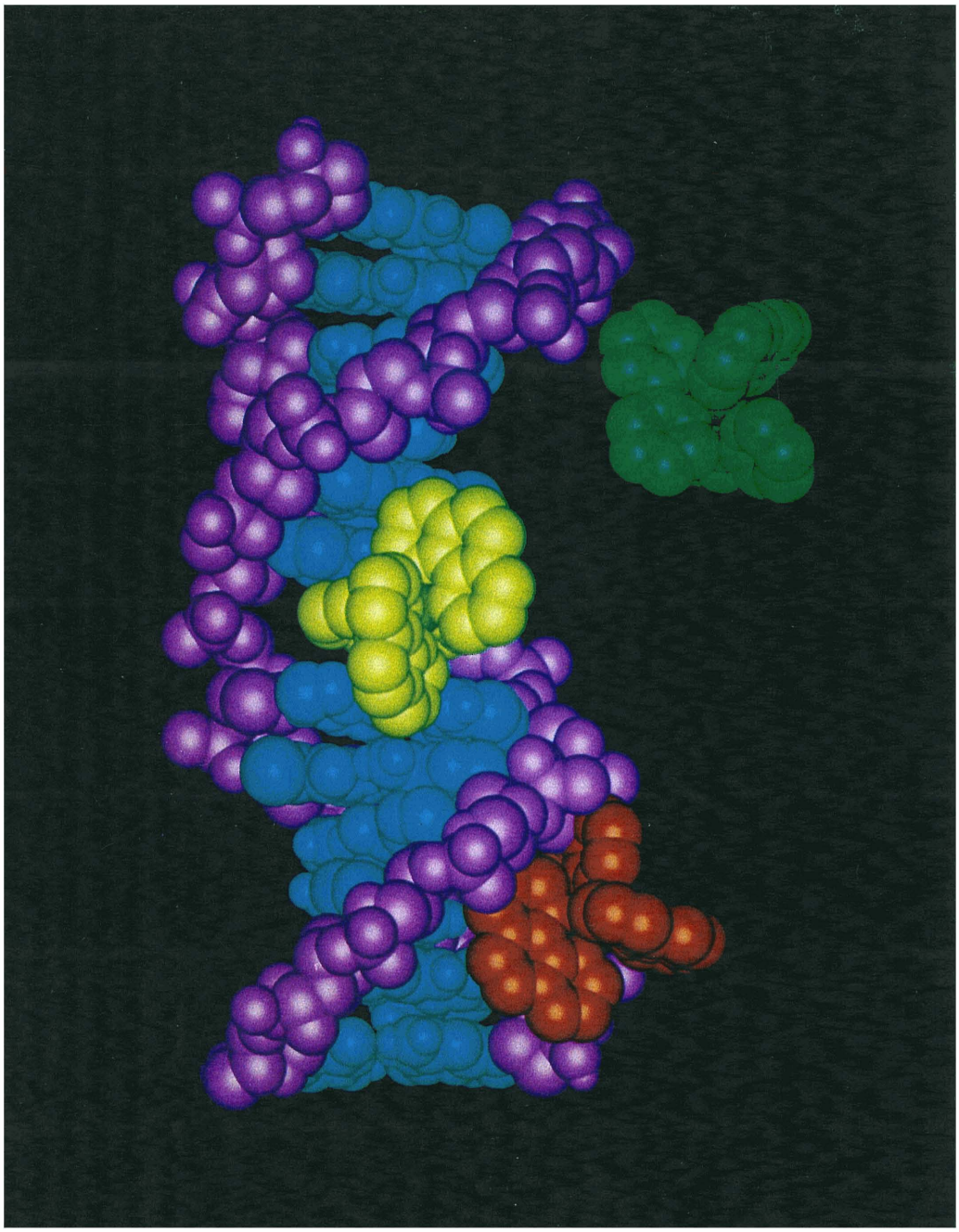

DNA conformation. An example of a surface-binding probe is $Ru(TMP)_3^{2+}$. The bulky nature of the 3,4,7,8 tetramethyl phenanthroline ligand in this complex precludes to a large extent an intercalative binding mode, which is present for the parent molecule $Ru(phen)_3^{2+}$. As shown in Figure 1.5, the large, hydrophobic surface area of $Ru(TMP)_3^{2+}$ is a close match in size and shape to that of the wide, shallow major groove of the A conformation. The width of the minor groove of B DNA, on the other hand, is not wide enough to accommodate the complex. Regions of DNA, or RNA, which show enhanced binding by $Ru(TMP)_3^{2+}$ over the parent molecule $Ru(phen)_3^{2+}$ are likely to be in the double helical A form[21]. The utility of this complex as a probe is enhanced by the fact that it cleaves DNA via a singlet oxygen mechanism upon irradiation with visible light.

Intercalating metal complexes have also been much utilized as probes. Two of the most important intercalating ligands have been the dppz (dipyrido [3,2: a-2', 3': c]-phenazine) and the previously mentioned phi (9,10 phenanthrenequinonediimine) ligands. These ligands are characterized by large aromatic areas available for stacking with the DNA bases. Both $Ru(phen)_2dppz^{2+}$ and $Rh(phen)_2phi^{3+}$ have been shown by NMR spectroscopy to bind primarily via intercalation in the major groove of DNA[22]. Dppz complexes of ruthenium and osmium have luminescent properties that may be used as a tag with which to explore protection of the dppz ligand by DNA bases. Phi complexes of rhodium have been used to examine DNA solution structure and explore molecular recognition. Phi complexes of rhodium and iridium, upon irradiation with ultraviolet light, cleave DNA by a nondiffusable mechanism. This useful property allows a direct visualization of the location of intercalation sites.

Shape-selection in combination with intercalation imparts a powerful array of recognition possibilities. $Rh(phi)_2bpy^{3+}$ and $Rh(phen)_2phi^{3+}$, shown in Figure 1.6, are two molecules whose recognition is governed by shape-selection. Although structurally similar, they have very different recognition properties. $Rh(phi)_2bpy^{3+}$ is a sequence-neutral complex, which has been used to photofootprint protein-DNA interactions[23]. On

Figure 1.5. Surface binding by $Ru(TMP)_3^{2+}$ as a probe of the A conformation of nucleic acids. Interactions between this complex and the minor groove of (top) B form DNA and (bottom) A form DNA. The bulky nature of the ligand in this metal complex hinders surface binding in the narrow, deep minor groove of B form DNA. However, a complementary surface for binding by this complex is present in the wide, shallow minor groove of DNA. This shape complementarity of $Ru(TMP)_3^{2+}$ with DNA is different than that of the parent molecule $Ru(phen)_3^{2+}$, which does surface bind the minor groove of the B form (shown in Figure 1.4). When $Ru(TMP)_3^{2+}$ cleaves DNA to a greater extent than does $Ru(phen)_3^{2+}$, an A form structure is indicated. Figure from Reference 19.

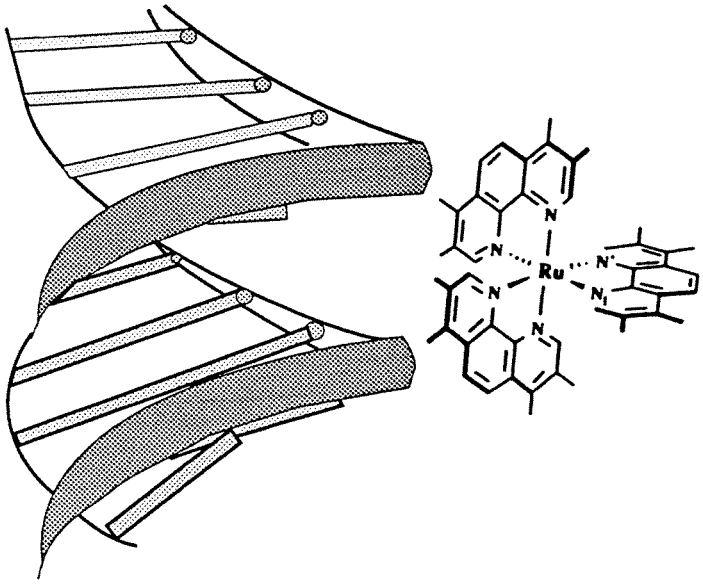
N
N
Ru
N'
N1
N
N

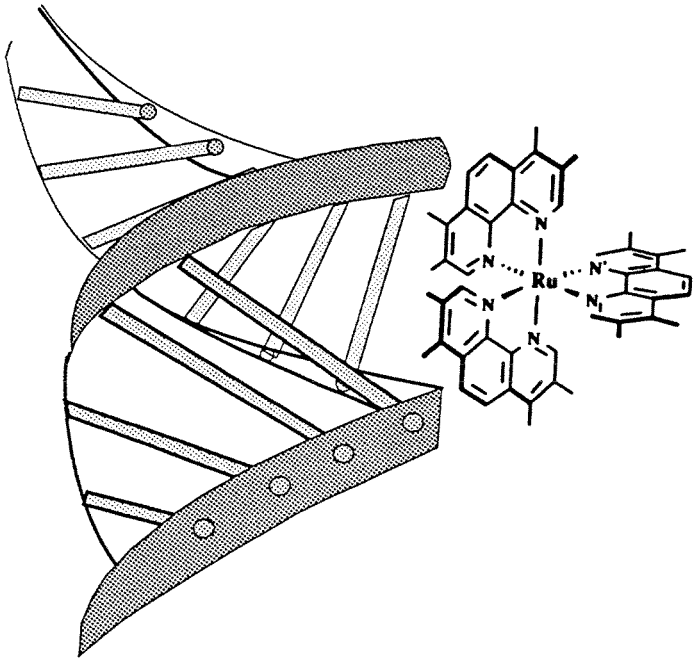
N
N
Ru
N'
N1
N
N

Figure 1.6. Shape selection in recognition of major groove structure by intercalating $Rh(phi)^{3+}$ complexes. (left) $Rh(phi)_2bpy^{3+}$ binds to DNA in a sequence-neutral fashion. It can be seen that the ancillary phi ligand is pulled away from the base stack, thereby permitting intercalation at many different types of sites. (right) $Rh(phen)_2phi^{3+}$ binds to DNA in a site-selective manner. Due to the overhanging phenanthroline ligands which clash with DNA bases at some sites, $Rh(phen)_2phi^{3+}$ can only bind to sequences possessing a structure which is open in the major groove.

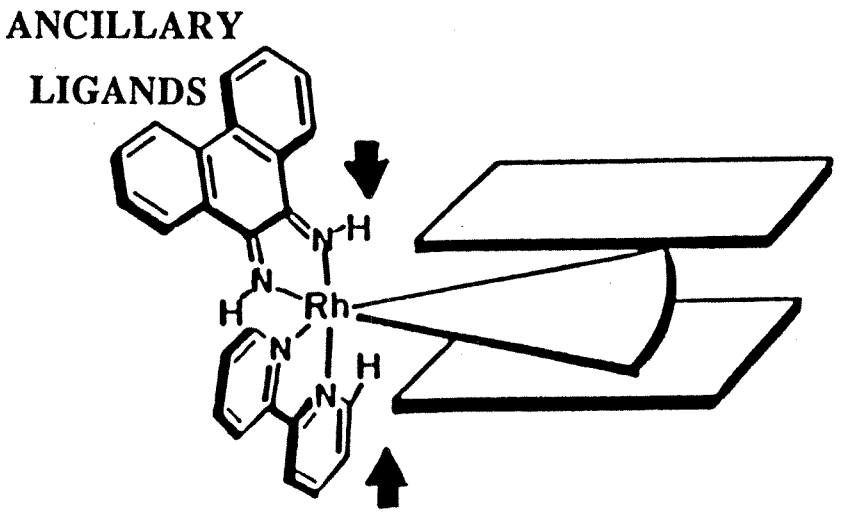

CANONICAL MAJOR GROOVE

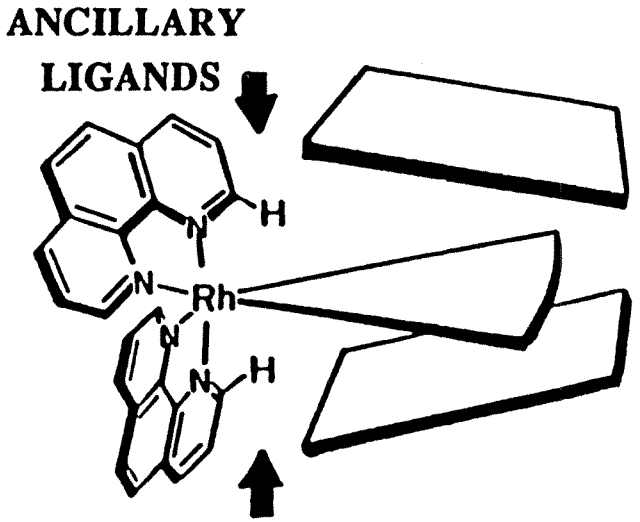

OPENED MAJOR GROOVE

the other hand, $Rh(phen)_2phi^{3+}$ exhibits a fair amount of site selectivity, and has been used as a probe of DNA sequence-dependent structure[24]. How may this be rationalized? One reason is that the bipyridyl ligand, being smaller than the phenanthroline ligand, provides less potential for steric hindrance. This notion is supported by the fact that $Rh(bpy)_2phi^{3+}$ is slightly less selective than $Rh(phen)_2phi^{3+}$ [25]. Another explanation is that $Rh(phi)_2bpy^{3+}$ has twice the number of binding modes as $Rh(phen)_2phi^{3+}$. Within a given intercalation site, the $Rh(phi)_2bpy^{3+}$ molecule may bind with the ancillary phi ligand directed either upwards or downwards with respect to the site. The third, and perhaps most significant, reason involves the positioning of the ancillary phi ligand in comparison with an ancillary phenanthroline ligand. As may be seen in Figure 1.6, the ancillary phi ligand is pulled away from the base column for the intercalated $Rh(phi)_2bpy^{3+}$ complex. This geometry allows the complex to bind to most DNA sites without a great degree of steric clashing. By way of comparison, the phenanthroline ligands of the intercalated $Rh(phen)_2phi^{3+}$ complex come in close proximity to the DNA bases. Therefore, there will be a consequential degree of steric hindrance at sites which are not in some way opened to accommodate the ancillary ligands. These steric interactions translate into a site selectivity for $Rh(phen)_2phi^{3+}$ which will be further examined below.

Another facet of DNA recognition by these metal complexes is their chirality. Each of these metal complex probes may be resolved into left- and right-handed mirror images, or Λ and Δ enantiomers. These enantiomers are chemically identical in every respect, except the disposition of the ligands about the metal center. Since DNA is a chiral molecule itself, the chirality of metal complex probe has a profound influence upon its recognition of DNA[26]. For example, for $Ru(phen)_3^{2+}$, the chirality of the molecule controls the binding mode selection. As shown in Figure 1.7, intercalation of this complex in the major groove takes place preferentially for the Δ-isomer over the Λ-isomer. This enantioselective binding results because the ancillary phenanthroline ligands are aligned with the groove for the right-handed isomer, whereas for the left-handed isomer, there is a

Figure 1.7. Basis for enantioselectivity in binding modes of Λ- (left) and Δ- (right) $Ru(phen)_3^{2+}$. (top) Shown are the interactions of both enantiomers in a surface bound mode in the minor groove of B form DNA, with one phenanthroline facing into solution. It can be observed that the Λ-$Ru(phen)_3^{2+}$ fits snugly in the minor groove, with minimal clashing with the DNA sugar phosphate backbone. However, the phenanthroline ligands of Δ- $Ru(phen)_3^{2+}$ do come in close proximity to the backbone, disfavoring this binding mode for the Δ-isomer. (bottom) Shown are the both isomers bound in the major groove of B form DNA by intercalation. When bound in an intercalative fashion, the ancillary ligands of the Λ-$Ru(phen)_3^{2+}$ are aligned against the groove, which results in significant steric clashing with the DNA backbone. On the other hand, the ancillary ligands of the Δ-$Ru(phen)_3^{2+}$ are aligned in the same direction as the groove, minimizing the steric interactions with the backbone and allowing the intercalative interaction to take place. Figure from Reference 19.

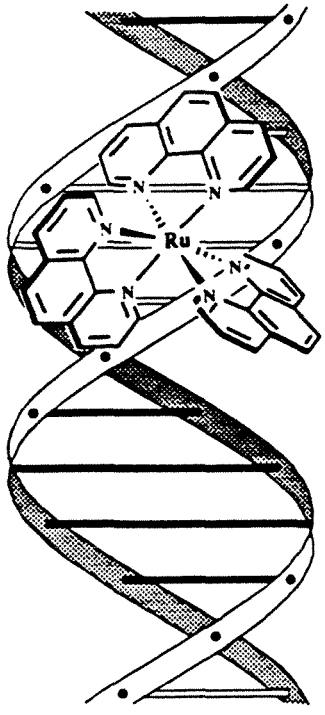

Λ

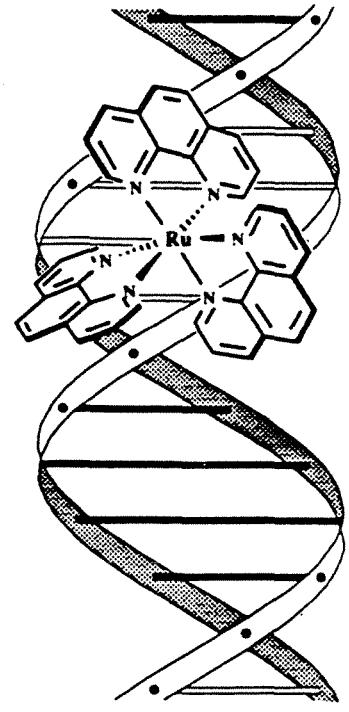

Δ

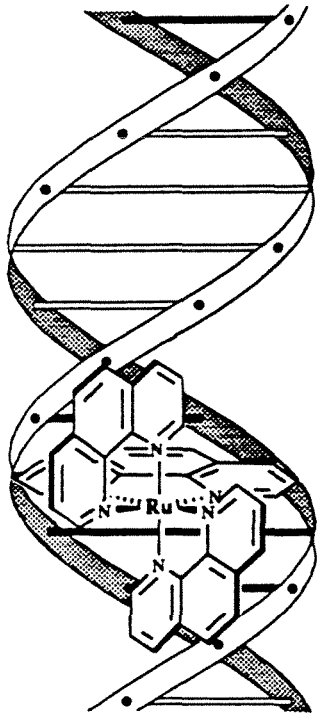

Λ

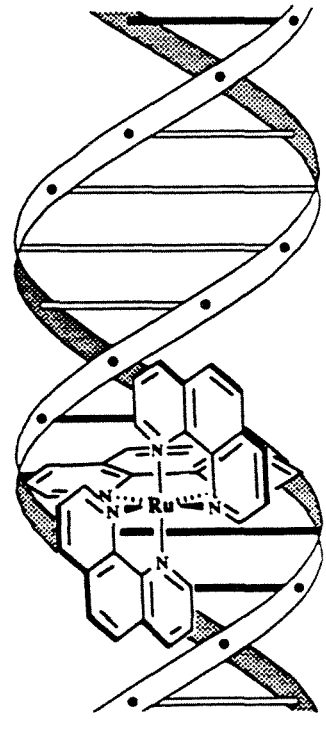

Δ

great deal of steric clash with the DNA sugar-phosphate backbone. However, for the minor groove surface binding interaction, which has one of the phenanthroline ligands directed outward towards solution, it is the Λ enantiomer which has fewer clashes with the DNA backbone. These models explain luminescence results which reveal that, indeed, the Δ enantiomer of $Ru(phen)_3^{2+}$ binds DNA to a greater extent by intercalation, and the Λ enantiomer binds preferentially by a surface bound mode[27].

For the $Rh(phi)^{3+}$ family of complexes, in which both enantiomers bind mainly by intercalation, metal complex chirality still has a great influence upon DNA *site* selection. For similar reasons to those described for $Ru(phen)_3^{2+}$, the Λ-isomer of $Rh(phen)_2phi^{3+}$, bound by intercalation in the major groove, clashes with the right-handed DNA backbone. Additionally, both enantiomers of $Rh(phen)_2phi^{3+}$ are also sensitive to base geometries. The arrangement of the ligands in either the Λ or Δ configuration has a significant contribution to site selectivity for $Rh(phen)_2phi^{3+}$, the basis for which will be described in a quantitative fashion in Chapter 3. When ancillary ligands are increased in size, enantioselectivity is enhanced. An extreme case of this type of enantioselective recognition occurs with the complex $Rh(diphenylbpy)_2phi^{3+}$, which has very bulky ancillary ligands. For this complex, the Δ enantiomer specifically recognizes the sequence 5'-CTCTAGAG-3', by shape-selective means, whereas the Λ enantiomer does not appear to bind DNA at all[28].

Do differences in the intercalating ligand affect enantioselectivity in binding to DNA? A metal complex with a long intercalating ligand, such as $Ru(phen)_2dppz^{2+}$, might be expected to show less enantiomeric discrimination in its interaction with DNA; the ancillary ligands are not necessarily in very close contact with the bases. This apparently is borne out by experimental evidence which suggests that both enantiomers of $Ru(phen)_2dppz^{2+}$ bind to canonical B form DNA with great affinity but with limited sequence selectivity[29]. However, the enantiomers of this complex do display some subtle differences in their geometry of intercalation, as observable by NMR[29b]. The effect of

such factors as the nature of the intercalating ligand and enantioselection upon binding to DNA will be further examined in Chapter 5.

References and Footnotes

1. Saenger, W. in *Principles of Nucleic Acid Structure*; Springer-Verlag: 1984.
2. Rould, M.A.; Perona, J.J.; Steitz, T.A. *Nature* **1991**, *352*, 213-218. Additionally, tertiary structural features of RNA are very important targets for recognition by proteins.
3. Churchill, M.E.A.; Travers, A.A. *T.I.B.S.* **1991**, *16*, 92-97.
4. (a) Saccomanno, L.; Bass, B.L. *Mol. Cell. Biol.* **1994**, *14*, 5425-5432. (b) Bass, B.L.; Hurst, S.R.; Singer, J.D. *Curr. Biol.* **1994**, *4*, 301-314. (c) St. Johnston, D.; Brown, N.H.; Gall, J.G.; Jantsch, M. *Proc. Natl. Acad. Sci., USA* **1992**, *89*, 10979-10983.
5. (a) Wittig, B.; Dorbic, T.; Rich, A. *Proc. Natl. Acad. Sci USA* **1991**, *88*, 2259-2263. (b) Kmeic, E.B.; Holloman, W.K. *Cell* **1986**, *44*, 545-554. (c) Holliday, R. *Trends Genet.* **1989**, *5*, 355-356.
6. Stryer, L. in *Biochemistry*; W.H. Freeman and Co., New York: 1988.
7. Dickerson, R.E. *Sci. Am.* **1983**, *249*, 94-cont.
8. Dickerson, R.E.; Drew, H.R. *J. Mol. Biol.* **1981**, *149*, 761-786.
9. EMBO Workshop on DNA Curvature and Bending *EMBO J.*, **1989**, *8*, 1-4.
10. Kennard, O; Hunter, W.N. *Q. Rev. Biophys.* **1989**, *22*, 327-379.
11. Yanagi, K.; Privé, G.G.; Dickerson, R.E. *J. Mol. Biol.* **1991**, *217*, 201-214.
12. (a) Lipanov, A.; Kopka, M.L.; Kaczor-Grzeskowiak, M.; Quintana, J.; Dickerson, R.E. *Biochemistry* **1993**, *32*, 1373-1389. (b) Shakked, Z.; Guerstein-Guzikevich, G.; Eisenstein, M.; Frolow, F.; Rabinovich, D. *Nature* **1989**, *342*, 456-460. (c) Jain, S.; Sundaralingam, M. *J. Biol. Chem.* **1989**, *264*, 12780-12784. (d) Ramakrishnan, B.; Sundaralingam, M. *Biochemistry* **1993**, *32*, 11458-11468.

13. (a) Wemmer, D.E. *Curr. Op. Struct. Biol.* **1991**, *1*, 452-458. (b) Metzler, W.J.; Wang, C.; Kitchen, D.B.; Levy, R.M.; Pardi, A. *J. Mol. Biol.* **1990**, *214*, 711-736.

14. (a) Patel, D.J.; Shapiro, L.; Hare, D. *Ann. Rev. Biophys. Biophys. Chem.* **1987**, *16*, 423-54. (b) Reid, B.R. *Q. Rev. Biophys.* **1987**, *20*, 1-34. (c) Patel, D.J.; Shapiro, L.; Hare, D *Q. Rev. Biophys.* **1987**, *20*, 35-112.

15. (a) Drew, H.R. *J. Mol. Biol.* **1984**, *176*, 535-557. (b) Drew, H.R.; Travers, A.A. *Cell* **1984**, *37*, 491-502. (c) Drew, H.R.; Travers, A.A. *Nuc. Acids Res.* **1985**, *13*, 4445-4467. (d) Drew, H.R.; Travers, A.A. *J. Mol. Biol.* **1985**, *186*, 773-790. (e) Fox, K.; Waring, M. *Nuc. Acids Res.* **1984**, *12*, 9271-9285. (f) Low, L.; Drew, H.R.; Waring, M. *Nuc. Acids Res.* **1984**, *12*, 4865-4879.

16. Lomonossoff, G.P.; Butler, P.J.G.; Klug, A. *J. Mol. Biol.* **1981**, *149,* 749-760.

17. (a) Sigman, D.S. *Acc. Chem. Res.* **1986**, *19*, 180-186. (b) Thederahn, T.B.; Kuwabara, M.D.; Larsen, T.A.; Sigman, D.S. *J. Am. Chem. Soc.* **1989**, *111*, 4941-4946.

18. Tullius, T.D. *Methods Enzymol.* **1992**, *212*, 219-242.

19. Sitlani, A.; Barton, J.K. in *Handbook of Metal-Ligand Interactions of Biological Fluids*; Marcel Dekker, Inc., New York.: 1993.

20. (a) Holmlin, R.E.: Barton, J.K. *Inorg. Chem.* **1995**, *34*, 7-8. (b) Erkkila, K.E.; Barton, J.K., unpublished results.

21. (a) Mei, H.-Y.; Barton, J.K. *J. Am. Chem. Soc.* **1986**, *108*, 7414-7416. (b) Mei, H.-Y.; Barton, J.K. *Proc. Natl. Acad. Sci., USA* **1988**, *85*, 1339-1343. (c) Chow, C.S.; Barton, J.K. *J. Am. Chem. Soc.* **1990,** *112*, 2839-2841.

22. (a) David, S.D.; Barton, J.K. *J. Am. Chem Soc.* **1993** *115,* 2984-2985. (b) Dupureur, C.M.; Barton, J.K. *J. Am. Chem Soc.* **1994**, *116*, 10286-10287.

23. Uchida, K.; Pyle, A.M.; Morii, T.; Barton, J.K. *Nuc. Acids Res.* **1989**, *17*, 10259-10279.

24. (a) Huber, P.W.; Morii, T.; Mei, H.-Y.; Barton, J.K. *Proc. Natl. Acad. Sci., USA* **1991**, *88*, 10801-10805. (b) Pyle, A.M.; Morii, T.; Barton, J.K. *J. Am. Chem. Soc.* **1990**, *112*, 9432-9434. (c) Campisi, D.; Morii, T.; Barton, J.K. *Biochemistry* **1994**, *33*, 4130-4139.

25. Sitlani, A., Ph.D. thesis, California Institute of Technology, Pasadena, 1993.

26. Barton, J.K. *Science* **1986**, *233*, 727-732.

27. (a) Barton, J.K.; Goldberg, J.M.; Kumar, C.V.; Turro, N.J. *J. Am. Chem. Soc.* **1986**, *108*, 2081-2088. (b) Kumar, C.V.; Barton, J.K.; Turro, N.J. *J. Am. Chem. Soc.* **1985**, *107*, 5518-5523.

28. Sitlani, A.; Dupureur, C.M.; Barton, J.K. *J. Am. Chem. Soc.* **1993**, *115*, 12589-12590.

29. (a) Haq, I.; Lincoln, P.; Suh, D.; Nordén, B.; Chowdhry, B.Z.; Chaires, J.B *J. Am. Chem. Soc.* **1995**, *117*, 4788-4796. (b) Dupureur, C.M.; Barton, J.K., manuscript submitted, 1995. (c) Jenkins, Y.C.; Barton, J.K., unpublished results.

Chapter 2:

Photocleavage by Enantiomers of $Rh(phen)_2phi^{3+}$ as a Probe of DNA Propeller Twisting in Solution†

2.1. Introduction

Although utilization of X-ray crystallography has provided a wealth of detailed information about DNA structure, the available techniques for examining DNA structure in solution are not as precise[1]. Since NMR spectroscopy is not useful for examining oligonucleotides longer than about 14 bp in length, the development of chemical and enzymatic probes of DNA local structure becomes necessary. Important DNA structural parameters such as propeller twisting, which was first observed by high-resolution crystallography, are difficult to characterize in solution using NMR methods[2]. How propeller twisting varies as a function of sequence, and whether such variation influences recognition are interesting questions to consider.

To this end, we have developed a probe of DNA propeller twisting based on enantioselective recognition of DNA by Δ- and Λ-$Rh(phen)_2phi^{3+}$, shown in Figure 2.1. This metal complex efficiently binds DNA by intercalation, and upon photoactivation, effects strand scission by a nondiffusable mechanism[3]. Major groove intercalation via the phi ligand of this complex has been confirmed by two-dimensional NMR experiments[4].

The potential suitability of $Rh(phen)_2phi^{3+}$ enantiomers in probing DNA propeller twisting was first recognized by comparison of the sequences cleaved on restriction fragments[5]. Resolution of $Rh(phen)_2phi^{3+}$ into its Δ and Λ enantiomers provides discrete structural probes whose difference in cleavage depends only upon shape considerations. The Δ- and Λ-isomers both cleave to a moderate extent at 5'-N*Y*YN-3' steps, (where the italic Y denotes the site of cleavage) and neither show appreciable

† Adapted from Campisi, D.; Morii, T.; Barton, J.K. *Biochemistry* **1994**, *33*, 4130-4139.

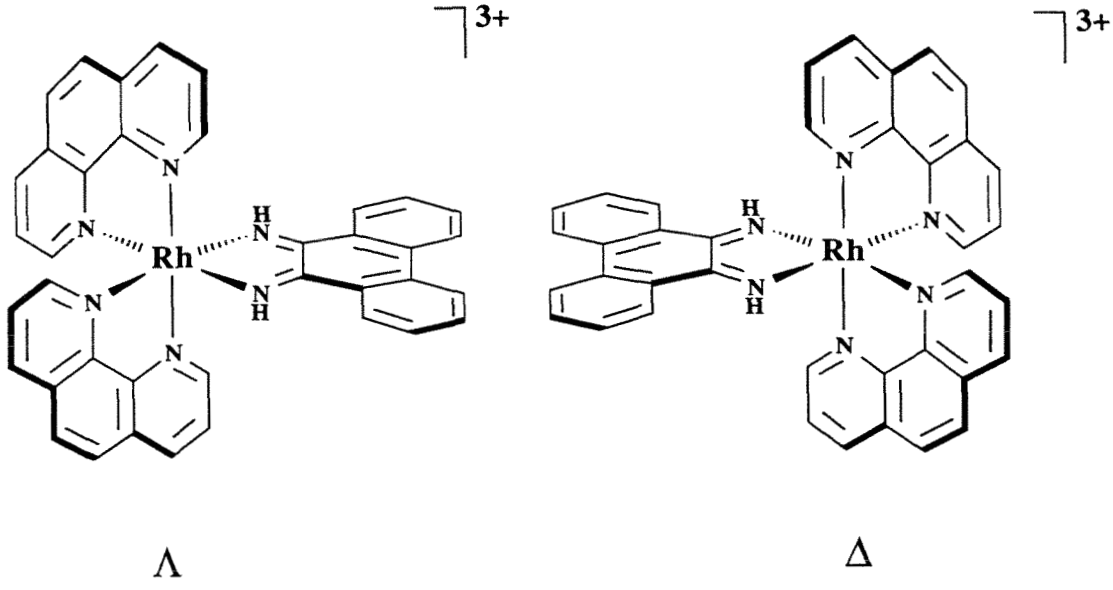

Figure 2.1. The enantiomers of $Rh(phen)_2phi^{3+}$

Figure 2.2. Schematic representation of enantiomeric discrimination in binding by Λ-(left) and Δ-Rh(phen)$_2$phi^{3+} (right) as a probe of DNA propeller twisting. 5'-YR-3'(top) and 5'-RY-3' (bottom) steps are viewed from the major groove. The phi ligand (heavy line) of the enantiomers is oriented into the page for intercalative binding. Intercalation by the octahedral metal complex at canonical DNA base steps yields steric clashes between the 2, 9 hydrogens (circled) of Rh(phen)$_2$phi^{3+} and the bases, unless the local conformation leads to an opening in the major groove. Differential propeller twisting at 5'-YR-3' steps provides an opening in the major groove for the Δ-isomer; in contrast there are clashes at this step between the phenanthroline ancillary ligands and the pyrimidine bases for the Λ-isomer. At the 5'-RY-3' step, neither enantiomer may bind with facility since there are clashes between the larger purines and the ancillary ligands of both enantiomers; the major groove is closed.

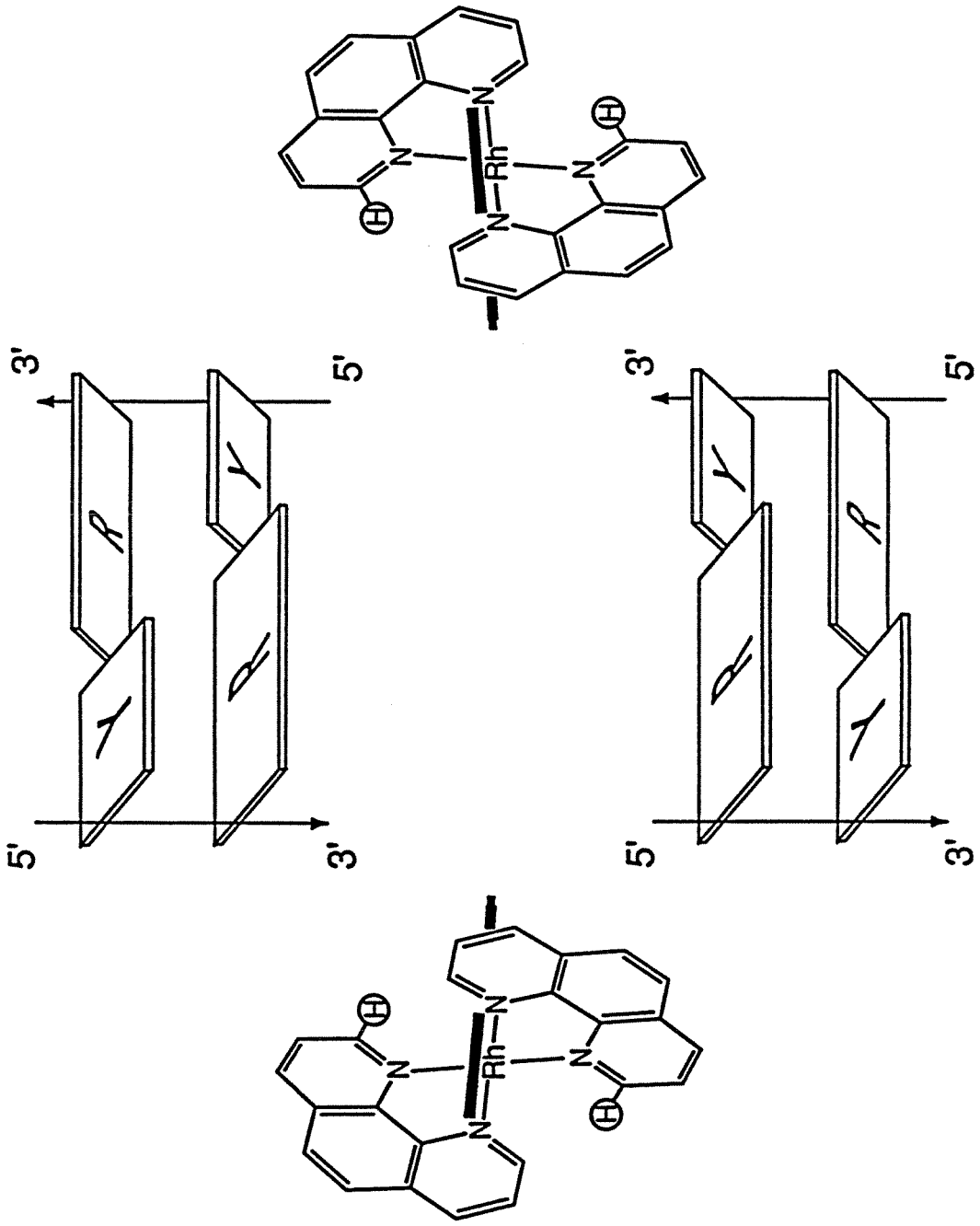
3'
5'
R
Y
Y
R
5'
3'
3'
5'
Y
R
R
Y
5'
3'
Rh
Rh

cleavage at 5'-N*R*YN-3' steps[6]. However, at 5'-N*Y*RN-3' steps, particularly 5'-Y*Y*RR-3' steps, there is strong cleavage by the Δ-Rh(phen)$_2$phi^{3+} but not by the Λ enantiomer. Those sites which are cleaved preferentially were found to be those which are characterized by a high degree of differential propeller twisting[7]. Thus, these results suggested that the shape-selective metal complex might serve to recognize and distinguish the propeller twisting of DNA sites in solution on the basis of matching shape and symmetry. Figure 2.2 schematically summarizes the proposed basis for this enantioselective discrimination at propeller twisted sites.

Variations in the chemical reactivity of DNA have also been found to be subtly dependent upon shape-complementarity. Photoproducts produced by Rh(phen)$_2$phi^{3+} have been consistent with a reaction mechanism of C3'-hydrogen abstraction by the photoexcited intercalated phi ligand[3b]. This C3'-hydrogen atom abstraction is partitioned between two different reaction pathways[8]. The oxygen-independent pathway yields a fragment containing a 5'-phosphate terminus as well as one possessing a 3'-phosphate terminus, with free base release. The oxygen-dependent pathway produces a 5'-phosphate terminus, and a 3'-phosphoglycaldehyde terminus accompanied by base propenoic acid release. The differences in partitioning along the pathways at a given site are directed by the distinct shapes and binding modes of Δ- and Λ-Rh(phen)$_2$phi^{3+}. Thus reaction pathway partitioning as a function of sequence provides an additional measure of the complementarity in structure between these enantiomers and DNA.

This chapter describes studies performed to develop Rh(phen)$_2$phi^{3+} recognition and reaction as a probe of DNA structure in solution. Here the correlation between enantioselectivity in cleavage by Rh(phen)$_2$phi^{3+} with differential propeller twisting is examined quantitatively. Correlations between enantioselective cleavage and other helical parameters is also examined. Three crystallographically characterized oligonucleotides were studied in solution with Δ- and Λ-Rh(phen)$_2$phi^{3+}: (i)The Dickerson-Drew dodecamer[9], (ii) the *Nar* I dodecamer[10], and (iii) the CG decamer[11].

```
5' C G C G A A T T C G C G 3'
3' G C G C T T A A G C G C 5'

5' A C C G G C G C C A C A 3'·
3' T G G C C G C G G T G T 5'

5' C C A A C G T T G G 3'
3' G G T T G C A A C C 5'
```

These oligonucleotides were chosen because each crystallizes in the B-form and each structure had a different crystal packing. A correlation is established in this work between enantioselectivity of photocleavage by $Rh(phen)_2phi^{3+}$ and a local structural feature of DNA as obtained from crystallographic parameters in the absence of metal complex. In addition, the reactivity of this rhodium complex within a site appears to be influenced by DNA structure in a sequence-dependent fashion. Thus this work provides a foundation for utilization of $Rh(phen)_2phi^{3+}$ as a probe of DNA conformational variations in solution.

2.2. Experimental

Materials. Oligonucleotides were synthesized via the phosphoramidite method[12], using 1.0 μM columns on an ABI 391 DNA-RNA synthesizer. A reversed- phase, C18 Dynamax column was used on a Waters HPLC for the purification of DNA. Labelling reactions were done with γ^{32}P-ATP (NEN) and polynucleotide kinase. Labelled oligonucleotides were purified by Nensorb columns, and stored dry at 4°C. For non-self-complementary oligonucleotides, equimolar concentrations of each strand were heated to 90°C and cooled over several hours to allow proper annealing to occur. $Rh(phen)_2phi^{3+}$ was synthesized as previously described[13]. Enantiomers were resolved by column chromatography with a chiral eluent[4]. Quantitation of metal and oligonucleotide concentrations was accomplished using a CARY 219 spectrometer, based on $\varepsilon(362) = 19{,}400\ M^{-1}\ cm^{-1}$.

Photocleavage Reactions. Reactions contained 480μM nucleotides , 50mM sodium cacodylate buffer, pH 7.0, and 25μM rhodium complex, and were irradiated at 313 nm with a 1000W Hg-Xe lamp. Irradiation times were typically 4.5 minutes. Different irradiation times gave the same distribution of cleavage, although the total amount cleaved was increased with longer irradiation. After photocleavage, an aliquot of each reaction mixture was taken and dried in vacuo. These aliquots, along with Maxam-Gilbert sequencing reactions[14] and controls were then taken up in a NaOH- formamide dye, heated to 90°C for 3 minutes, chilled on ice for 1 minute, and loaded on a 20%/ 8.3 M urea polyacrylamide gel. Gels were eluted about 4 hours at 1600V. Upon completion, gels were wrapped and exposed to a phosphorimaging plate for 12 hours. These plates were scanned on a Molecular Dynamics Phosphorimager.

Quantitation of Cleavage: Gel electrophoresis experiments were quantified using Molecular Dynamics software. DNA was irradiated in the absence of metal (light control) to provide a control for damage due to irradiation. Cleavage at each base was corrected for any damage shown in this light control as follows:

$$c_{corr,i} = \left(\frac{x}{c_{tot}}\right)c_i - \left(\frac{x}{h_{tot}}\right)h_i, \qquad (1)$$

where $c_{corr,i}$ is the corrected value of a cleavage band; c_i is the uncorrected integration volume of a cleavage band; h_i is the intensity value of the corresponding band in the light control; c_{tot} and h_{tot} are the total number of counts in the cleavage and light control lanes, respectively, and x is a factor arbitrarily set to 10 million counts which allows comparison of sites in non-self-complementary strands (which are corrected to different light control values.)

After this correction was made for Λ and Δ cleavage at each position, a normalization which allows for comparison between experiments is performed. The Δ cleavage for each experiment was normalized to 4% total cleavage of the self-complementary oligonucleotides. For the *Nar*I dodecamer, cleavage was normalized so that corrected *Δ* cleavage from both strands added together represented 8% of the uncut

material. This correction was accomplished to preserve any reactivity differences present between the two strands. Λ cleavage was also normalized relative to 4% Δ cleavage, thus leaving enantioselectivities (Δ/Λ) unaffected by the normalization. Actual percent cleaved was varied to establish such variations did not affect the distribution of cleavage intensities.

The total cleavage at each *base* was then obtained by adding together the intensities for cleavage to form the 3'-phosphate and 3'-phosphoglycaldehyde termini observed on the gel. The amount of cleavage at each site is best represented as a sum of cleavage from each strand. Thus, total cleavage at each base step was obtained by adding together the corrected cleavage on both strands to the 5' side across the intercalation site, as shown below. This

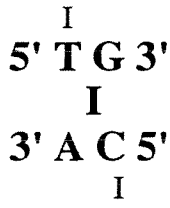

summation is necessary since cleavage may occur on either strand. Cleavage intensities are added in the 5'-direction because in general, photoactivation of $Rh(phen)_2phi^{3+}$ promotes cleavage with single base 5' asymmetry, that is, the C3' hydrogen atom of the deoxyribose to the 5'-side of the intercalation site appears to be preferentially abstracted[3b].

Calculation of Differential Propeller Twisting, x_p: There are two parameters which describe the rotation of a base pair /step about its long axis. Propeller twist (ω) is the angle at which the bases in a base pair twist with respect to one another; roll (ρ) is the angle which describes the angle between the mean plane of the first base pair in a base step with the mean plane of the second base pair of that step. Both parameters then contribute to a base step opening or closing toward the major groove. This opening may be approximated as the angle between purine planes (neglecting helical twist), as shown

in Figure 2.3. For each of the four base steps, the calculation of this angle differs. However, the pyrimidine roll angle is added in all cases. The expressions are

$x_p = a + b + \rho$ (2)

for the 5'-YR-3' step,

$x_p = -(a + b) + \rho$ (3)

for the 5'-RY-3' step,

$x_p = (a - b) + \rho$ (4)

for the 5'-YY-3' step, and

$x_p = (b - a) + \rho$ (5)

for the 5'-RR-3' step, where a is one-half the propeller twisting value (ω) at the 5' side of the base step, and b is one-half the ω value at the 3' side of the base step. a, b, and ω are all negative by convention[15]. Just as a negative roll angle describes major groove opening, a negative x_p value also describes major groove opening. It may be seen that for a 5'-YR-3' step, the greater the propeller twisting, the greater the major groove opening, whereas for a 5'-RY-3' step, the greater the propeller twisting, the more closed the major groove becomes. All values for ω and γ were taken from the referenced crystallographic parameters. Differential propeller twist angle neglecting roll angle, $x_p$nr, was also calculated as a comparison. Errors for x_p and $x_p$nr, when included, are represented by the range of values calculated using both ends of a self-complementary but nonsymmetrical crystal structure[9a].

2.3. Results

2.3.1. General Features of Photocleavage by $Rh(phen)_2phi^{3+}$

Cleavage by the Δ and Λ enantiomers differs in position, intensity and in partitioning between reaction pathways. For all three oligonucleotides, the cleavage by

Figure 2.3. Geometrical projections of each of the four base steps. The view is along the long axis of the base pairs, with the major groove to the left side of the projection and the minor groove to the right side. The purines are shown in white and the pyrimidines in gray. The front strand is in the 3'- 5' direction, and is represented by thick outlines. The back strand is in the 5'-3' direction and is represented by thin outlines. Roll (ρ) and x_p angles show direction of opening.

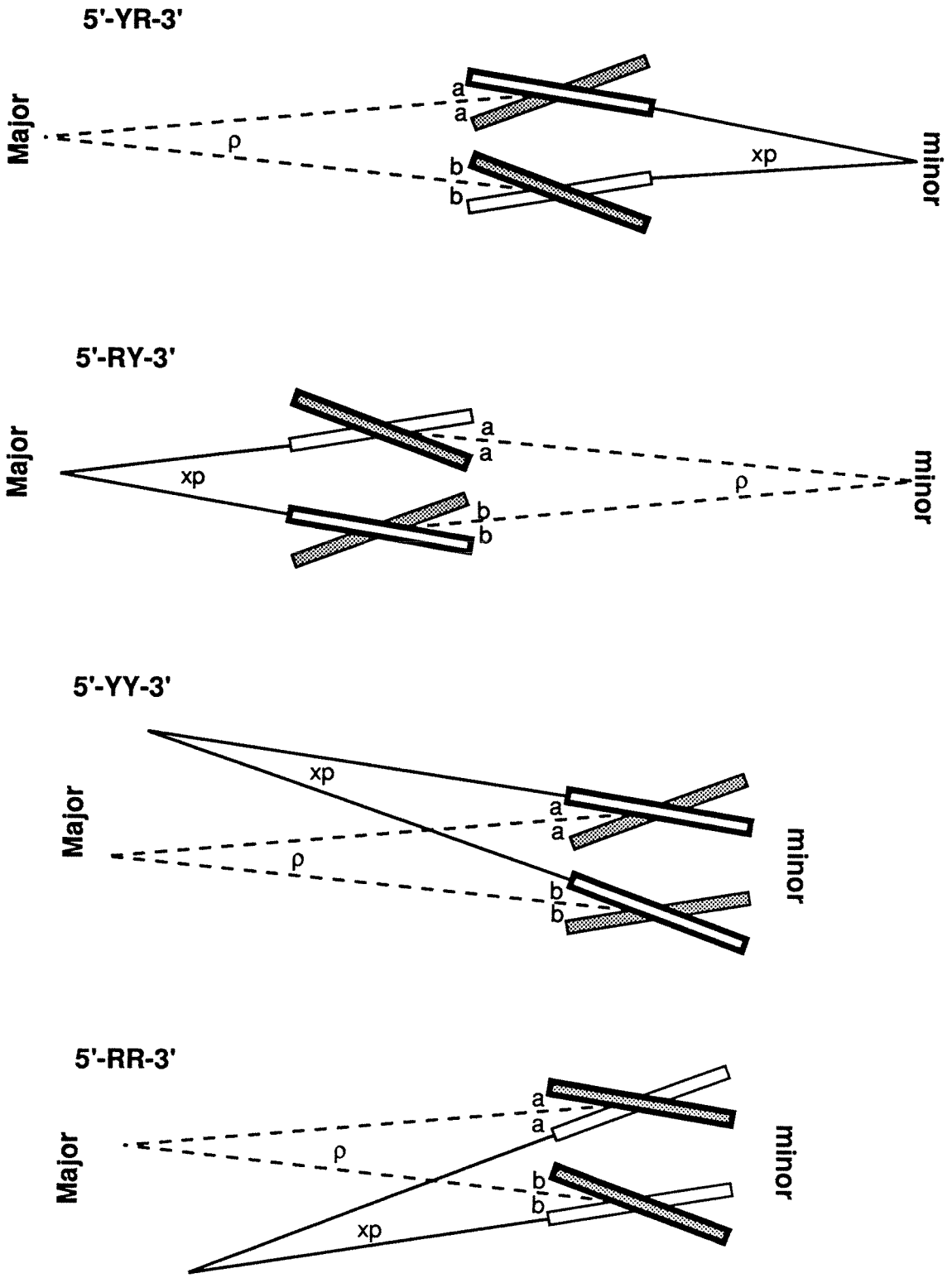
5'-YR-3'
Major
a
a
ρ
b
b
xp
minor
5'-RY-3'
Major
a
a
xp
ρ
minor
b
b
5'-YY-3'
xp
Major
a
a
ρ
b
b
minor
5'-RR-3'
Major
a
a
ρ
b
b
xp
minor

the racemic mixture shows characteristics of both enantiomers, with more similarity to that of the Δ enantiomer. Autoradiograms of polyacrylamide gels which indicate sites of cleavage on all three oligonucleotides are shown in Figure 2.4, and the results are quantitated in Table 2.1.

Dickerson -Drew dodecamer: In the Dickerson-Drew dodecamer, the Δ enantiomer cleaves predominately at C_9, with a lesser amount of cleavage at the C_3 which is across from C_9 at the same base step (Figure 2.4A). There is also a moderate amount of cleavage at the T_8 site by the Δ enantiomer. The Λ enantiomer, however, shows an equivalent amount of cleavage at the T_8 and C_9 sites.

Nar I *dodecamer:* This oligonucleotide contains two intercalation sites which display enantioselective cleavage. As can be seen in Figure 2.4B, at both cytosines at the C_3 site, C_3 and C_{21}, Δ-Rh(phen)$_2$phi^{3+} cleaves significantly more than the Λ-isomer. At the C_9-T_{15} intercalation site, cleavage by the Δ enantiomer is greater than that of Λ for C_9, but equivalent at T_{15}. Δ- and Λ-Rh(phen)$_2$phi^{3+} cleave at C_6 and C_{18} to a similar extent, although it is a 5'-YR-3' step. This cleavage is less than that seen for the Δ-isomer at the two more highly enantioselective sites.

CG oligonucleotide: There is one highly enantioselective cleavage site for Δ-Rh(phen)$_2$phi^{3+} on this oligonucleotide, as shown in Figure 2.4C. At C_5, Δ cleaves more than Λ at this site by a factor of 6. The second strongest site for the Δ enantiomer, T_8, is cleaved almost equally by the Λ enantiomer.

It should be also be noted that differences in total amounts of bases released for the Δ and Λ enantiomers, analyzed by HPLC, agree with the cleavage data obtained by gel quantitation (data not shown).

2.3.2. Asymmetry of Photocleavage

In addition to cleavage position, the 5' asymmetry associated with cleavage also provides some information as to how these complexes are bound to DNA. Of the four

Figure 2.4. Images of photocleavage of 5'- ^{32}P endlabelled oligonucleotides of differing sequences by the enantiomers of $Rh(phen)_2phi^{3+}$.

A. The Dickerson-Drew dodecamer. Lanes 1 and 2 are Maxam-Gilbert C+T and G+A reactions respectively. Lanes 3, 4, and 5 contain the oligonucleotide (480μM nucleotides) irradiated for 1 min. at 313 nm in the presence of Δ, Λ, and racemic $Rh(phen)_2phi^{3+}$ respectively; lane 6 shows the oligonucleotide in the absence of metal complex but with irradiation, and lane 7 in the absence of metal complex and without irradiation.

B. The *Nar* I dodecamer, showing cleavage on strand 1 (left) and strand 2 (right). Lanes 1 and 8 as well as 2 and 9 are A+G and C+T Maxam Gilbert reactions respectively. Lanes 3 and 10 show labelled oligonucleotide without irradiation or metal complex. Lanes 4, 5 and 6 and lanes 11, 12, and 13 show the oligonucleotide irradiated for 4.5 min. in the presence of racemic, Δ, and Λ $Rh(phen)_2phi^{3+}$, respectively. Lanes 7 and 14 show irradiation in the absence of metal complex. The fragments indicated by **a** and **b** correspond to the 3'-phosphate and 3'-phosphoglycaldehyde terminus respectively; note that **b** shows slower mobility than its corresponding 3'-phosphate.

C. The CG decamer. Lane 1 shows DNA in the absence of light and metal complex. Lanes 2 and 3 show Maxam-Gilbert G+A and C+T reactions, respectively. Lane 4 contains the oligonucleotide after irradiation in the absence of metal, and lanes 5, 6, and 7 show cleavage by the Δ, Λ, and racemic complexes, respectively after irradiation for 5 min.

D. A schematic illustration summarizing sites of primary intercalation based upon cleavage data for Δ- and Λ- $Rh(phen)_2phi^{3+}$.

A

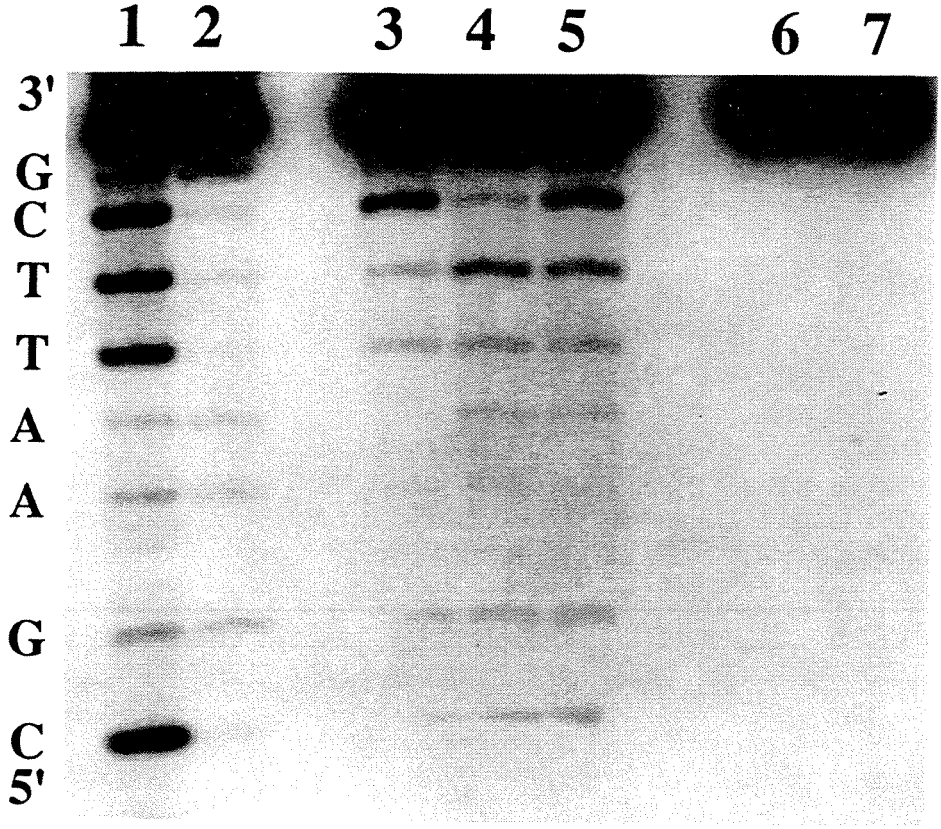

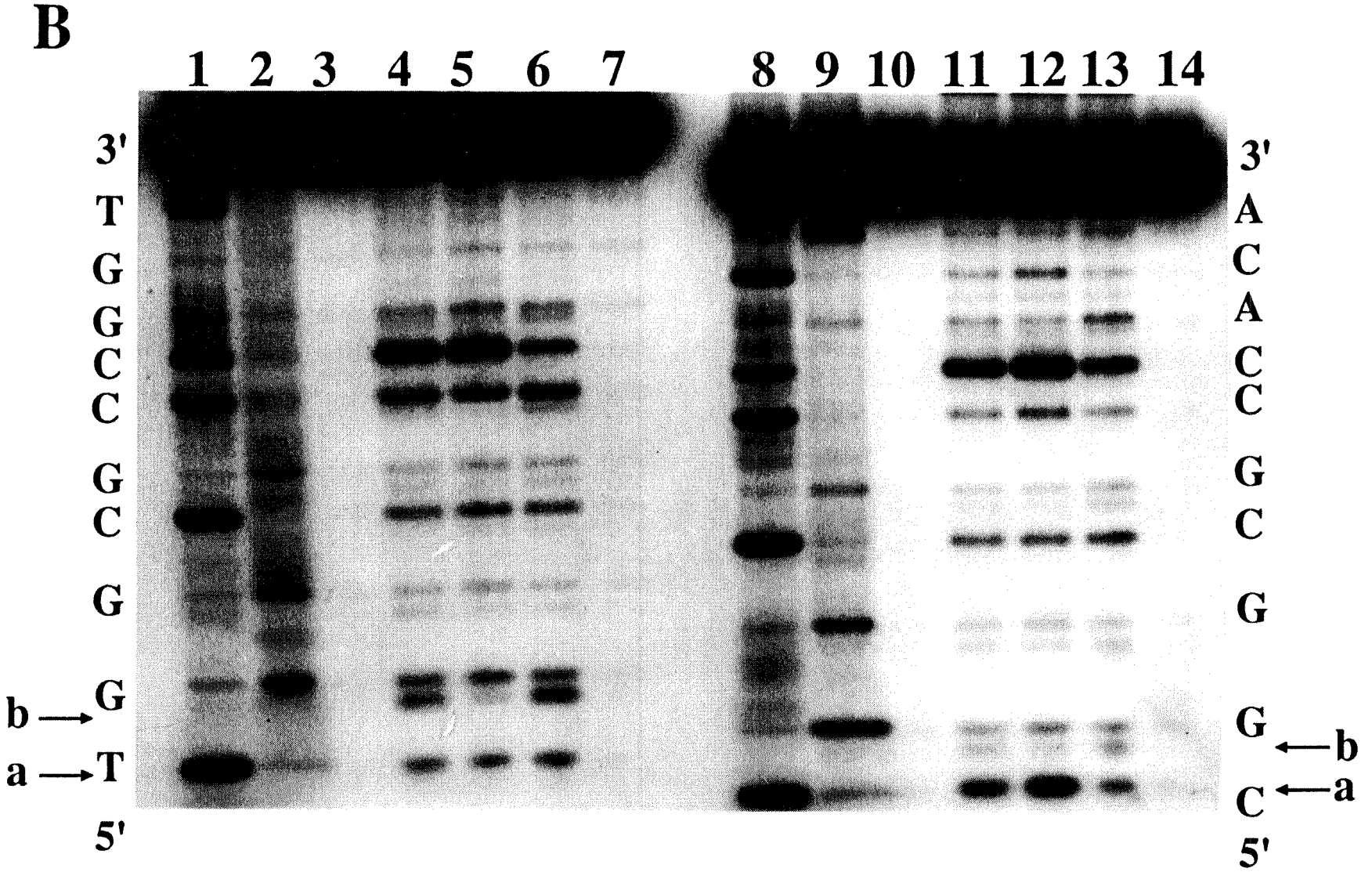
B
1 2 3 4 5 6 7 8 9 10 11 12 13 14
3'
T
G
G
C
C
G
C
G
G
T
5'
b
a
3'
A
C
A
C
C
G
C
G
G
C
5'
b
a

C

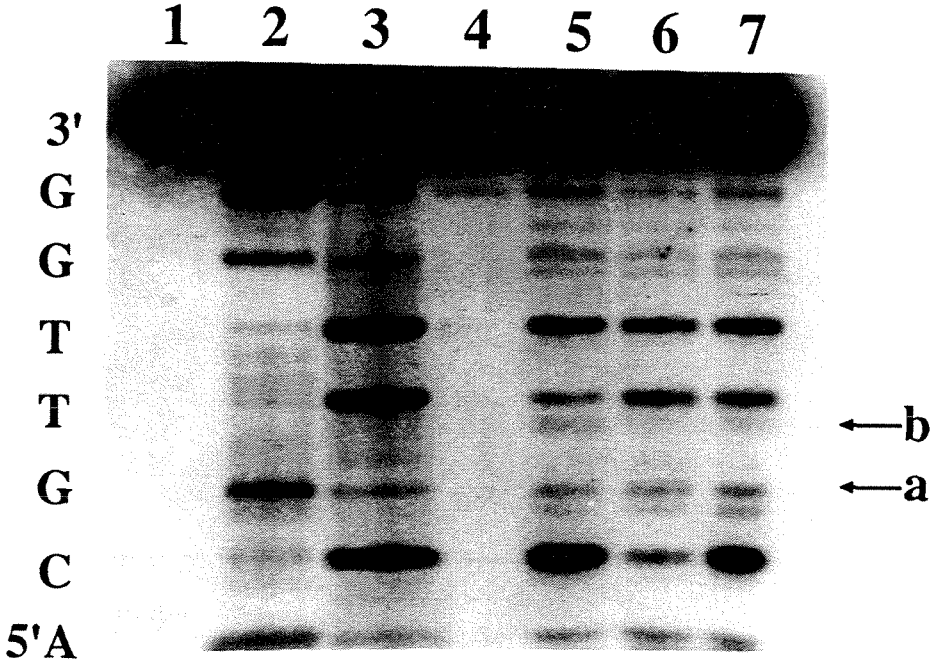

D

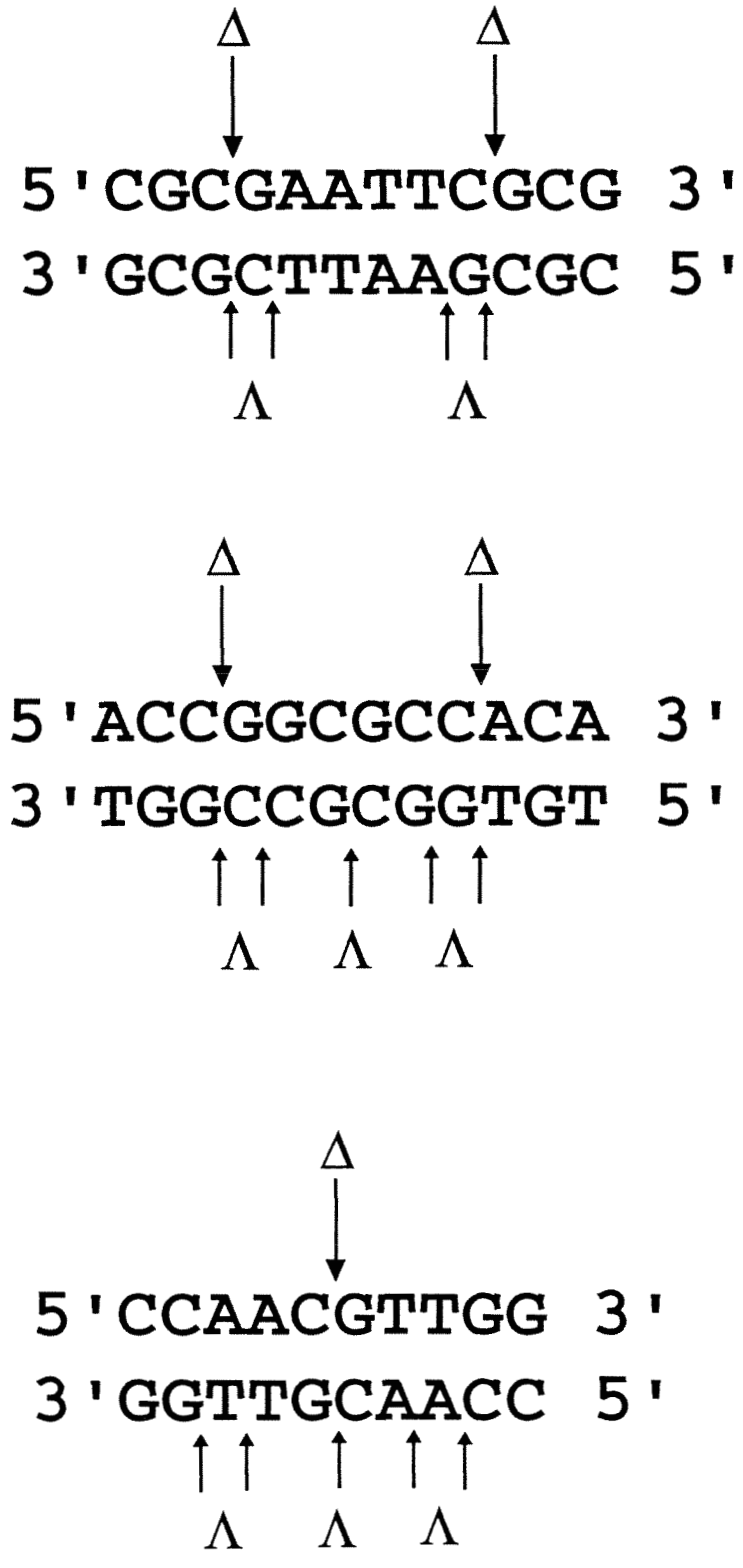
Δ Δ
5'CGCGAATTCGCG 3'
3'GCGCTTAAGCGC 5'
Λ Λ
Δ Δ
5'ACCGGCGCCACA 3'
3'TGGCCGCGGTGT 5'
Λ Λ Λ
Δ
5'CCAACGTTGG 3'
3'GGTTGCAACC 5'
Λ Λ Λ

strongest cleavage sites for Δ-Rh(phen)$_2$phi^{3+}, two, C_9-C_3 on the Dickerson-Drew dodecamer and C_9-T_{15} on the *Nar*I dodecamer, show an appreciable asymmetry in the extent of cleavage at each side of the site, as shown in Table 2.1. (For the center of the self-complementary CG oligonucleotide, this asymmetry can not be determined.) In the case of the Dickerson dodecamer, C_9 strikingly yields about 23 times as much cleavage as the corresponding C_3, and for the *Nar*I oligonucleotide, C_9 is cleaved about 9 times as strongly as the corresponding T15. These two sites correspond to 5'-*YY*RN-3' steps. We ascribe this asymmetry to the canting of the molecule in the site to one strand[3b].

Not every 5'-YR-3' step shows appreciable asymmetry. A 5'-CA-3' step examined earlier[3b], in the context of 5'-GCAT-3', does not show appreciable asymmetry for the racemic complex, and the central 5'-GCGC-3' of the *Nar* I dodecamer does not show asymmetry for the Δ, Λ, or racemic complexes.

These observations indicate that flanking sequence may have an influence over the manner in which the complex binds to a site. That is, generally speaking, the complex binds preferentially at a 5'-YR-3' step which has a pyrimidine to the 5' side of that step. If only one side has a flanking pyrimidine, cleavage by the complex appears to be skewed toward that side. If the step is flanked on the 5' side of both bases by pyrimidines, there is not as much asymmetry in cleavage, but the overall cleavage is still high, whereas if the step is flanked on both sides by purines, the canting and cleavage tend to be lower.

2.3.3. Correlation of Enantioselectivity with Major Groove Opening

Both enantioselectivity and absolute cleavage by the Δ-isomer show correlations with differential propeller twisting. This correlation between differential propeller twist and cleavage by Δ-Rh(phen)$_2$phi^{3+} is shown in Figure 2.5. Shown are plots of cleavage by Δ-Rh(phen)$_2$phi^{3+} versus differential propeller twisting with and without contributions of roll. At positive values for x_p, where the major groove is closed, the amount of Δ

Table 2.1. Quantitation of Photoinduced Cleavage by $Rh(phen)_2phi^{3+}$ on Different Oligonucleotides[a]

Dickerson-Drew			*Nar* I sequence		Δ		Λ		CG		
sequence	Δ	Λ	1	2	1	2	1	2	sequence	Δ	Λ
C3	0.11	0.07	C3	G22	1.11	0.31	0.19	0.15	A3	0.06	0.12
G4	0.12	0.08	G4	C21	0.22	1.86	0.12	0.26	A4	0.15	0.25
A5	0.05	0.06	G5	C20	0.11	0.33	0.06	0.20	C5	2.05	0.32
A6	0.05	0.07	C6	G19	0.27	0.10	0.20	0.09	G6	0.22	0.17
T7	0.22	0.14	G7	C18	0.10	0.27	0.07	0.18	T7	0.23	0.44
T8	0.31	0.32	C8	G17	0.25	0.11	0.09	0.06	T8	0.68	0.56
C9	2.54	0.25	C9	G16	2.12	0.32	0.40	0.21			
G10	0.61	0.23	A10	T15	0.27	0.26	0.25	0.33			

[a]Data are derived from gel analysis of the oligonucleotides photocleaved by $Rh(phen)_2phi^{3+}$ as shown in Figure 2.4. Phosphor-imagery was used to determine relative band intensities for each base and values were corrected for differences in loading and any slight damage due to light alone as described in the text. Each value shown represents the average percentage cleavage on the oligonucleotides. The uncertainty in these photocleavage values is estimated to be about ±6%

cleavage is low. However, when the major groove is open, values for cleavage by Δ-Rh(phen)$_2$phi^{3+} are substantially higher. These sites all correspond to 5'-YR-3' steps.

An important exception is found in 5'-G$_5$*C*$_6$G$_7$-3' in the *Nar*I dodecamer, which shows little cleavage. Although strongly propeller twisted in the crystal structure, this site appears to show anomolously low cleavage and enantioselectivity. It is interesting that in this segment of the oligonucleotide in the crystal, two helices are packed closely against one another. It is likely that this type of packing has a deforming effect in the crystal in this region of the helix. Thus, the strong differential propeller twist at this site in the crystal may not represent the structure in solution based upon the data presented here. Supportive evidence for this idea may be found in the crystallographic structures[16] for the oligonucleotide 5'-CCAACITGG-3'. This sequence crystallized both with a monoclinic packing and a trigonal packing similar, though not identical to that found in the *Nar*I crystal structure. Significant (ca. 6°) differences in propeller twisting were found between the two packing forms.

Parallel results are observed in plots of enantioselectivity versus differential propeller twist relative to Δ cleavage versus differential propeller twist (data not shown). Since Λ-Rh(phen)$_2$phi^{3+} does not produce significantly strong sites, relative to Δ, the same correlation pertains. Although enantioselectivity is correlated with Δ cleavage, the site which shows the highest enantioselectivity (C$_9$ of Dickerson-Drew) is not the same as the site which shows the highest Δ cleavage (C$_5$ of the CG decamer). Both are CG steps, but the first is not completely symmetrical (considering flanks), while the latter is symmetrical. It is possible that the flanks may influence the structures in a way which may make them less accessible to the Λ enantiomer. Plots of enantioselectivity, however, contain higher uncertainty at weak cleavage sites (positive values of x_p), since ratios between small values are required.

Figure 2.5. Plots showing the correlation between the percentage cleavage by Δ-$Rh(phen)_2phi^{3+}$ and propeller twisting corrected for roll angle (top, x_p), and without inclusion of roll angle (bottom, $x_p nr$). Data are shown for cleavage on the Dickerson-Drew dodecamer (●), the *Nar*I dodecamer (▲), and the CG decamer (Δ). Cleavage was quantitated at each site as described in the text. The differential propeller twisting was determined based upon the crystallographic structural parameters[9a,10,11]. Errors for cleavage intensity are represented by the standard deviations between experiments.

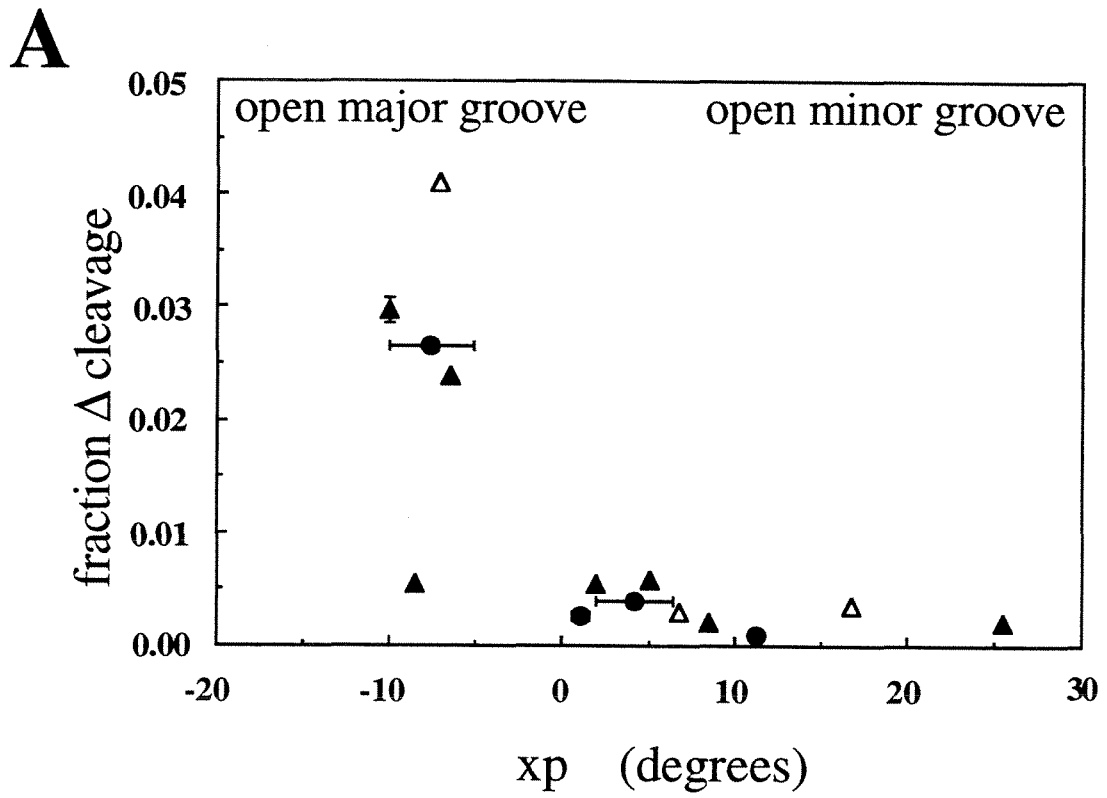
A
open major groove
open minor groove
fraction Δ cleavage
0.05
0.04
0.03
0.02
0.01
0.00
-20
-10
0
10
20
30
xp (degrees)

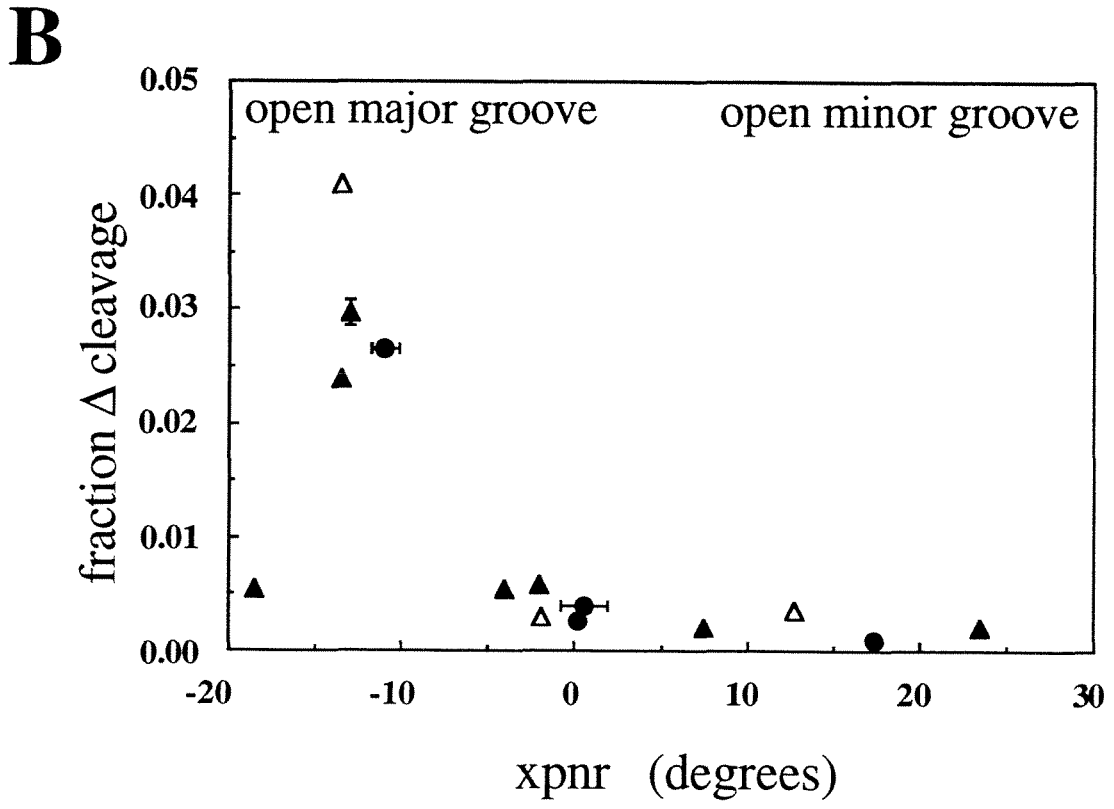
B
open major groove
open minor groove
fraction Δ cleavage
0.05
0.04
0.03
0.02
0.01
0.00
-20
-10
0
10
20
30
xpnr (degrees)

2.3.4. Correlation of Δ and Λ Cleavage with Other Helical Parameters

It might be expected that other parameters which describe the structure of a base step may show some correlation with cleavage by $Rh(phen)_2phi^{3+}$. Examples of commonly reported parameters include helical twist, rise, tilt and roll. A weak correlation was found between helical twist values and enantioselectivity. For two of the three oligonucleotides examined, there was a good correlation between the two values, consistent with the right-handed helicity of the duplex[17]. However, for the Dickerson-Drew dodecamer this correlation did not hold. There was also no significant correlation found between Δ cleavage, enantioselectivity, or Λ cleavage with any of the following: rise, tilt, groove width (phosphate-phosphate distances) or roll (in isolation). This lack of correlation may arise because none of these parameters contain a symmetry axis along the dyad, except the helical twist.

2.3.5. Enantioselectivity in Cleavage Photoproducts

In addition to cleavage position and cleavage asymmetry, the cleavage product distribution observed as a function of sequence gives some insight into the interactions of these enantiomers with DNA. As described earlier[3b], and represented in Scheme 3.1, oligonucleotide photocleavage through an O_2-independent pathway yields 5'- and 3'-phosphate termini, whereas the O_2- dependent pathway produces 5'-phosphate and 3'-phosphoglycaldehyde ends. The termini may be differentiated using gel electrophoresis, as shown in Figure 2.4. Hence, information may also be obtained regarding the sequence-dependence in partitioning along these pathways. Since a close shape-complementarity between the complex and the base step would block oxygen access to the C3'-radical for subsequent reaction, a high concentration of oxygen-dependent photoproduct may reflect a poor fit of the metal complex into the site.

The reaction pathway partitioning is indeed found to be sequence-dependent. In general, at a given site, Λ-$Rh(phen)_2phi^{3+}$ produces a greater concentration of oxygen-

Scheme 2.1. Summary of the different photoproducts obtained after partitioning along the O_2- independent and O_2- dependent pathways for strand cleavage following C3'-H abstraction. The structures labelled **a** and **b** correspond to the marked photoproducts in Figure 2.4.

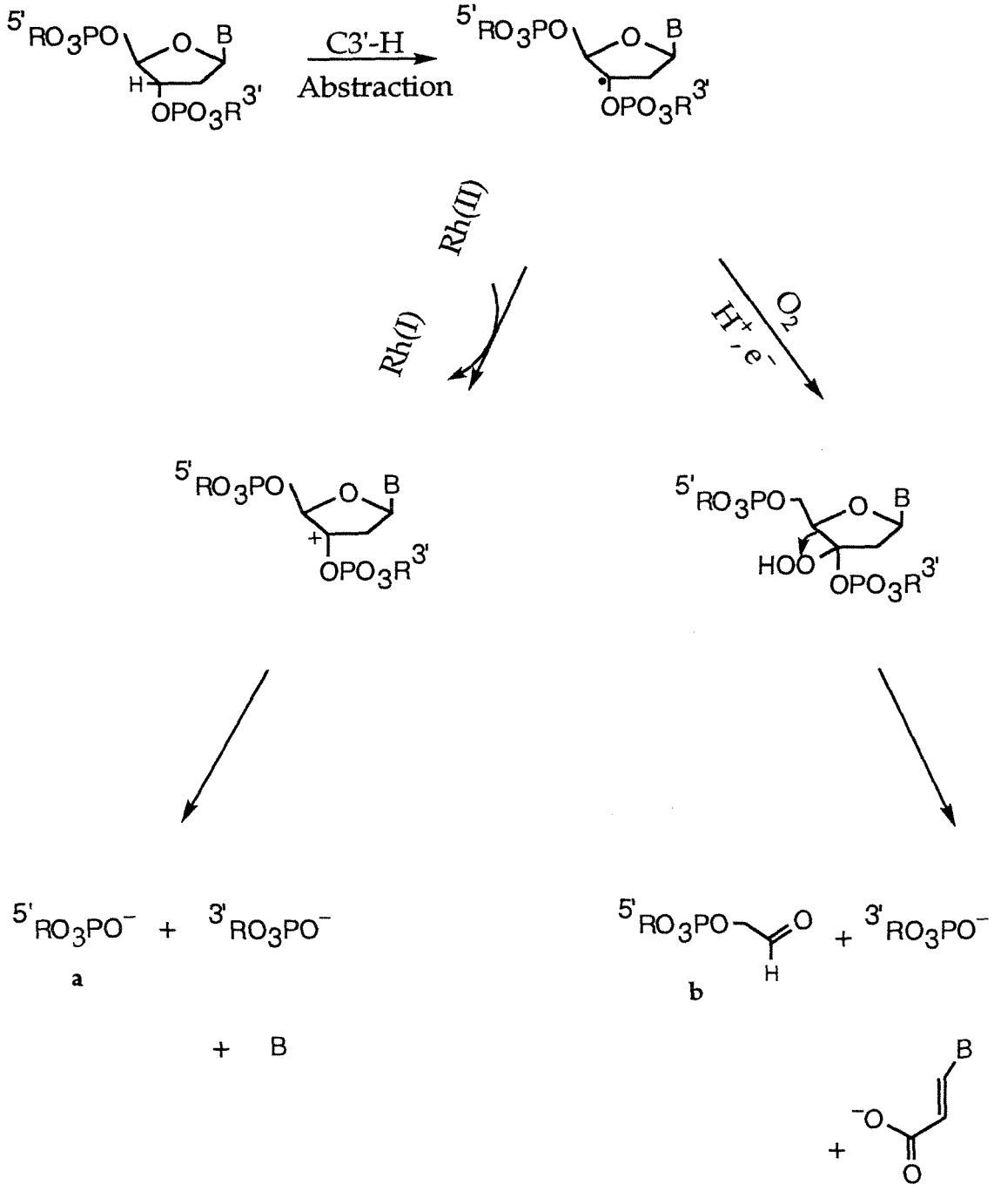
5'RO3PO
B
C3'-H
Abstraction
OPO3R3'
Rh(II)
Rh(I)
O2
H+, e-
HOO
a
b
+ B

dependent photoproducts than does Δ-Rh(phen)$_2$phi^{3+}, likely reflecting the poorer match of the left-handed isomer into the right-handed helix[17]. The presence of oxygen-dependent photoproducts also correlates with the asymmetry in cleavage on the duplex, suggesting that canting of the complex in the helix to one strand allows oxygen access to the other.

Two illustrative examples from different oligonucleotides are shown in Table 2.2, and the products obtained are evident in Figure 2.4. These sites both show a high intensity of 3'-phosphoglycaldehyde product, but one site represents an example of high cleavage overall and the other of low cleavage. In both cases there is little or no O_2-dependent photoproduct detected for one strand, and a significant amount of phosphoglycaldehyde for the complementary strand; for a given base step, the greater the intensity of cleavage, the lower the concentration of phosphoglycaldehyde. Additionally quantitative, sequence-dependent differences in reaction pathway partitioning are observed between enantiomers. In the 5'-T_{15}G$_{16}$-3' · 5'-C_9G$_{10}$-3' step from the *Nar*I dodecamer, neither enantiomer shows a significant amount of phosphoglycaldehyde at C_9, which shows the greater amount of cleavage at this base step. However, on the complementary strand at T_{15}, both enantiomers show some reaction via this oxygen-dependent pathway. In fact, a greater percent of the total cleavage by Λ–Rh(phen)$_2$phi^{3+} for this 5'-YR-3' step is by this oxygen-dependent pathway, as can be seen in Table 2.2. Also, at the 5'-G_6T$_7$-3' · 3'-A_4C5-5' step from the CG decamer, cleavage at A_4 occurs predominately by the O_2-independent pathway for both enantiomers. However, both enantiomers show cleavage by the O_2-dependent pathway at G_6. Indeed, as can be seen in Table 2.2, now a greater proportion of the total cleavage by Δ-Rh(phen)$_2$phi^{3+} occurs via the O_2-dependent pathway at this base. Thus, while the 5'-RY-3' step does not prove to be a suitable binding site for either enantiomer, the fit at this site tends to be worse for Δ than for Λ. (This observation may be rationalized by steric clashes between the 2, 9 hydrogens of the phenanthroline and the functional groups on the purine bases in the

Table 2.2. Quantitative Comparison of Products Obtained as a Result of Partitioning between Reaction Pathways[a]

Oligomer	Site	Product	Δ[b]	Λ[b]	product[c] Δ	product[c] Λ
Nar I dodecamer	5' T_{15} G_{16} 3'	5'-RO_3PO^-	0.21	0.20	81	59
		5'-RO_3POCH_2CHO	0.05	0.14	19	41
	3' A_{10} C_9 5'	5'-RO_3PO^-	2.08	0.38	98	95
		5'-RO_3POCH_2CHO	0.04	0.02	2	5
CG decamer	5' G_6 T_7 3'	5'-RO_3PO^-	0.14	0.13	61	76
		5'-RO_3POCH_2CHO	0.09	0.04	39	24
	3' C_5 A_4 5'	5'-RO_3PO^-	0.15	0.25	100	100
		5'-RO_3POCH_2CHO	0	0	0	0

[a] Data obtained in the same fashion as data from Table 2.1. Quantitation refers to the products formed at italicized bases.

[b] Cleavage intensities shown represent the percentage cleavage on the fragment.

[c] Values represent the percentage partitioning along either pathway, based upon the relative amount of product formed.

Table 2.3. Summary of Sequence-Dependent Photoproducts Observed in Reaction with $Rh(phen)_2phi^{3+}$ Enantiomers [a].

sequence	overall intensity of cleavage	enantioselectivity in cleavage	enantioselectivity in formation of O_2-dependent products
5' Y*Y*RN 3'	high	$\Delta >> \Lambda$	$\Lambda > \Delta$
5' R*Y*RN 3'	intermediate	$\Delta \geq \Lambda$	$\Lambda > \Delta$
5' N*Y*YN 3' [b] and 5' N*R*RN 3'	intermediate	$\Delta \sim \Lambda$	$\Lambda > \Delta$
5' N*R*YN 3'	low	$\Delta \sim \Lambda$	sequence-dependent[c]

[a]Comparisons refer to reaction at italicized bases. [b]Except 5'G*Y*YN3'. [c]For some sequences there is too little product for detection.

major groove.) Furthermore, the generally low cleavage at these sites is to be expected since they are closed in the major groove (*vide supra*). The relative amount of phosphoglycaldehyde photoproduct at a particular site can therefore serve as an indicator of the accessibility of dioxygen to that site and thus of the fit between the shape of the metal complex and the shape of that site. The sequence-dependence in photoproducts observed is summarized in Table 2.3 and may be generally considered in that context.

2.4. Discussion

2.4.1. Major Groove Intercalation

The features which govern DNA recognition by $Rh(phen)_2phi^{3+}$ determine both its binding and cleavage characteristics. Strong sites of cleavage often display single base 5'-asymmetry, consistent with binding from the major groove[18]. In the case of $Rh(phen)_2phi^{3+}$, with asymmetric binding, one furthermore observes the production of 3'-phosphoglycaldehyde *termini*, a cleavage product consistent with reaction at the C3'-hydrogen atom in the major groove. The fact that the complex binds by intercalation from the major groove[3b,4] importantly differentiates $Rh(phen)_2phi^{3+}$ from many natural products and chemical probes which bind in the minor groove[19]. This contrast becomes evident in comparing probes on the Dickerson-Drew dodecamer. Δ-$Rh(phen)_2phi^{3+}$ cleaves mainly at C_9, which corresponds to binding at the 5'-C_9G_{10}-3' step. The Λ enantiomer binds and cleaves at the 5'-T_8C_9-3' and the 5'-C_9G_{10}-3' step. Each differs from minor-groove binding $Cu(phen)_2^+$, which cleaves at all positions of this oligonucleotide[19a], and the green bleomycin-cobalt (III) complex, which cleaves predominately at the C_3 and C_{11} positions[19b]. They also differ in distribution of cleavage from minor groove binding DNaseI which cleaves strongly at T_8[19c].

Each step which is cleaved strongly by Δ-$Rh(phen)_2phi^{3+}$ is a 5'-N*Y*RN-3' step. This step is thought to be favorable for classical intercalators[20] because of the stability which may be gained by overlap with the intercalator. Although intercalation has been

demonstrated as the primary binding mode for this complex, the chiral discrimination at all sites, favoring the Δ- isomer, also shows that this intercalative overlap with the base pairs is not the sole factor governing site recognition. In other words, the disposition of the ancillary phenanthroline ligands about the metal center provides another structural element in distinguishing one site from another. The feature being discerned by means of steric repulsion on the helix is, likely, the angle of opening of the purines towards the major groove.

2.4.2. Enantioselectivity in $Rh(phen)_2phi^{3+}$-DNA Interactions

The following all give information about the differences in interaction between the enantiomers of this complex and a given site: total intensity of cleavage, cleavage asymmetry, and mechanistic partitioning of the photoproducts. As may be seen in Tables 3.1 and 3.2 and summarized in Table 2.3, the greatest difference in total cleavage between the enantiomers is at 5'-YR-3' steps, in particular 5'-Y*Y*RR-3' steps. Enantioselectivity (Δ cleavage/ Λ cleavage) of up to a factor of 10 has been observed for these steps, particularly when flanked by a 5' pyrimidine. The Δ enantiomer also shows a greater degree of cleavage asymmetry at 5'-YR-3' steps than does the Λ enantiomer. This asymmetry is dependent on neighboring bases as well. If only one base of the base step possesses a 5' flanking pyrimidine, cleavage is weighted towards that side for *both* enantiomers, but the asymmetry is more dramatic for the Δ enantiomer. While asymmetric intercalation has also been demonstrated in crystal structures[21] of some planar intercalators bound to 5'-CG-3' dinucleotide steps, this work shows that flanks may influence the local structure and recognition of 5'-YR-3' steps. Again, the disposition of the ancillary phenanthrolines is likely to enhance the discrimination.

The enantiomers also show differences in how cleavage products are partitioned along the two pathways. The amount of O_2-dependent photoproducts, along with asymmetry of cleavage, gives information as to the fit of the bound molecule in the site,

the shape-complementarity of the metal complex to the local structure of DNA. For example, as shown in Table 2.3, at the 5'-Y*Y*RN-3' and 5'-R*Y*RN-3' steps, it is the Δ enantiomer which yields a relatively small amount of phosphoglycaldehyde terminus, and which thus has the better fit for this site. The better fit of the Δ-isomer in most sites is evident, based upon this criterion, including 5'-GC-3' steps. At low sites of cleavage, where neither enantiomer likely fits well, both isomers may yield O_2-dependent product; indeed, at the 5'-AC-3' step of the CG decamer, it is the Δ-isomer which yields more 3'-phosphoglycaldehyde. It should be noted that at some sites the total cleavage is so low that no O_2-dependent photoproduct is detectable. These cases suggest the worst fit between both enantiomers and the site, with steric clashes between the ancillary ligands and the bases.

2.4.3. Recognition Structure

What then are the structural features of DNA which are being recognized by Δ-$Rh(phen)_2phi^{3+}$? It may be said that this complex is recognizing groove width in a coarse fashion. $Rh(phen)_2phi^{3+}$ specifically cleaves B-form DNA, or other nucleic acid structures where the major groove is open enough to allow binding. On the other hand, the rhodium complex does not cleave the double-helical regions of tRNA[22] because the narrow major groove precludes binding by the complex. Thus the first aspect of the "open major groove" is a groove possessing a width large enough to accommodate the complex. From comparisons with groove widths obtained from coordinates of the Dickerson-Drew dodecamer and the CG decamer, however, it does not appear that the complex is recognizing small variations in groove width within the range evident in the B conformation. There are two possible explanations for this. Crystal packing affects groove width values more than it does most other parameters. Differences dependent on packing have been observed for the B conformation[16] and the A conformation[23]. Therefore, small variations in groove widths in crystal structures may not be wholly

indicative of the solution structure. Alternatively, the binding characteristics of this molecule, an intercalator rather than a large groove binding molecule, do not lend themselves to subtle comparisons with variations in groove width.

A related aspect is the inclination of the base pairs with respect to one another, the base pair tilt. While it does not appear that the complex is recognizing tilt in a strictly quantitative fashion, all of the strong cleavage sites for the Δ enantiomer in these oligonucleotides have a tilt angle which is less than or equal to zero. It also does not appear that tilt correlates with the asymmetry of the cleavage.

Other parameters can define opening in the major groove. Although it had been suggested[24] that sequence could dictate opening towards or away from the major groove through variations strictly in their roll angle, cleavage by neither enantiomer, nor enantioselectivity in cleavage by $Rh(phen)_2phi^{3+}$, correlate with the roll angle in isolation. There also does not appear to be a correlation between cleavage by either enantiomer and the sequence-dependent rise of a base step. As this rise is determined by the C1'-C1' distance in a step, it would be surprising to find this parameter to be sensitive to considerations of intercalator chirality.

However, one parameter which might be expected to govern enantioselectivity in cleavage is the helical twist. Although there is a weak direct correlation between the two sets of values, this correlation holds only for the *Nar*I dodecamer and the CG decamer; it does not hold for the Dickerson-Drew dodecamer. The explanation for this may lie in the high twist profile (HTP) and low twist profile (LTP)[25] gleaned from crystal structure analysis. The HTP describes steps having a high twist, low rise and negative roll, whereas the LTP describes steps having a low twist, large rise, and positive roll. The 5'-YR-3' step has been shown, from a body of crystallographic structures[25] and calculations[26] to exhibit both types of behavior. Correlations made which factor in helical twist, roll, and rise are not straightforward. Thus, although helical twist is not

explicitly accounted for in the differential propeller twisting calculation, it may contribute in part to the resultant enantioselectivity in cleavage.

What the Δ enantiomer locally appears to recognize is the rotation of the base pairs about their long axes, e.g., the angle between the purine planes caused by the propeller twisting of the base pairs, and as defined in Figure 2.3. $Rh(phen)_2phi^{3+}$ is therefore unique in recognizing an important element in DNA local structure. Both propeller twist angles and the roll angle contribute to this parameter, which also may be considered as a measure of the major groove opening of DNA. As Figure 2.5 reveals, *there is a strong correlation between the intensity of cleavage by Δ-$Rh(phen)_2phi^{3+}$ at a site with the openness in the major groove as a result of sequence-dependent base pair propeller twisting.* The sign of this parameter shows opening (negative) or closing (positive) of the major groove, in the same convention as the roll angle. The extent of the opening may be approximated by the values of the parameter. Importantly, it is not the propeller twist itself which is recognized by the metal complex, but instead *the change* in propeller twist. Sites of substantially enantioselective cleavage are observed both where there is a 26° propeller at one base pair and 0° at the next (in the C_3G_4 base step of *Nar*I) and where the angle is 13° at one base pair and 14° at the next (in the C_9A_{10} base step of *Nar*I). Both geometries lead to sites which are open in the major groove.

In order to test the contribution of the roll angle to this opening, $x_p$nr, the differential propeller twisting without inclusion of the roll angle, was calculated. While the general agreement between enantioselectivity and differential propeller twisting still holds, it does not appear to correlate as well as when the roll angle is included. Particularly, there are two sites (C_3 and C_9 of the *Nar*I dodecamer) which have the same $x_p$nr, but quite different cleavage values. It should be noted that neither x_p nor $x_p$nr correlates with the corresponding roll angle alone.

It is also interesting to compare these cleavage results to structural parameters obtained for these oligonucleotides in solution by NMR. Such a comparison may be

drawn in particular in the case of the Dickerson-Drew dodecamer where several laboratories have carried out relevant NMR experiments[2a,2c-d]. In one case[2c], NMR analysis revealed a more substantial kink at the C_3G_4 base step, the site of strongest cleavage by Δ-Rh(phen)$_2$phi^{3+}, than is evident in the crystal, indeed a structural kink similar to that found in the crystal with bound *Eco*RI[27]. Other analyses show general agreement between the structure in the crystal and in solution but emphasize that propeller twisting is among the inherently least well-determined parameters available by NMR[2a]. In the case of the CG decamer, solution NMR analysis has also been performed and compared to the crystal structure[28]. Here while detailed structural parameters are not available, general agreement between the solution and crystal structure appears to be found. Hence, in both these cases correlations appear to be present between site-specific cleavage by the rhodium complex with solution as well as crystallographically determined oligonucleotide structure.

2.4.4. Biological Relevance

It has been demonstrated that Rh(phen)$_2$phi^{3+} recognizes a particular structural feature of DNA. Does this have any relevance to protein-nucleic acid recognition? Binding by the Δ enantiomer shows several similarities to that of sequence-specific proteins. Firstly, both bind primarily from the major groove and are therefore recognizing major groove structure. Secondarily, both bind through a hierarchy of noncovalent interactions. In the case of the metal complex, the primary driving force is intercalation, but the ancillary ligands modulate site recognition, mainly through steric considerations. In the case of DNA-binding proteins, often nonspecific electrostatic interactions provide a substantial driving force for binding to the nucleic acid. Flanking sequences can also affect binding specificity either directly or by altering the local shape of the site. For example, in this set of data, having a guanine to the 5' side strongly reduces the affinity of

the complex for a 5'-CG-3' step. Likewise, flanks[29] can reduce/ increase protein binding affinity to particular sites.

Another similarity rests in the ability of both the rhodium complex and some proteins to change the structure of DNA upon binding. $Rh(phen)_2phi^{3+}$ necessarily deforms every site to which it binds due to its intercalation. Proteins as well cause changes in the B-form structure upon binding. For example, in the co-crystal[27] of *Eco*RI with its recognition sequence, the Dickerson-Drew dodecamer, the sequence 5' TCG3' shows a kink which increases the phosphate-phosphate distance between nucleotides C_9 and G_{10}, and of particular interest, the propeller twist of the C_3 and G_{10} steps. Specifically, C_3 adopts an unusual angle. This structure is not observable in the DNA crystal lacking the protein, but as described above, a similar kink may be apparent in solution in the absence of protein[2c] and may influence binding both by the protein and $Rh(phen)_2phi^{3+}$. The co-crystal[30] of the *met* repressor-operator complex shows that the central CG step exhibits a conformation altered from the B-form; changes in this step affect the binding affinity of the *met* repressor[31]. It is interesting that in this case and in that of *Eco*RI, $Rh(phen)_2phi^{3+}$ appears to be cleaving at sites whose structures are perturbed by protein binding. It is possible then that propeller twisting could be in part responsible for mediating post-binding alterations of DNA structure.

More generally, there are similarities between the actual sequences recognized by $Rh(phen)_2phi^{3+}$ and those recognized by proteins. One site which is cleaved very strongly by Δ-$Rh(phen)_2phi^{3+}$, which is not a 5'-Y*Y*RN-3' step is the 5'-AC_5G_6T-3' of the CG oligonucleotide. This sequence appears to be particularly prevalent in transcription factor binding sites. These include, for example, the ATF promoter[32]. 5'-ACGT-3' is also part of the recognition sequence for the *met* repressor[31]. Another group of sites are the recognition sequences for the TFIIIA family of zinc fingers. A recent crystal structure of five-finger GLI with a 21-mer[33] shows two fingers which are bound most closely in the opened major groove containing 5'-CCAC-3', a sequence also contained in

the *Nar*I dodecamer, and which is recognized by $Rh(phen)_2phi^{3+}$. The general correspondence of cleavage sites with protein recognition sites may reflect the importance of an open major groove for binding by a family of proteins[34]. A structure which is open in the major groove may serve as a landmark for the binding of proteins and small molecules alike. This correlation of sites recognized by $Rh(phen)_2phi^{3+}$ with protein binding is particularly striking in the case of 5S RNA[35].

A related question is whether $Rh(phen)_2phi^{3+}$ is recognizing sequence-dependent structure or sequence-dependent deformability. The fact that correlations have been found between cleavage and structures which have been crystallized *without metal complex present* offers support to the notion that the structure which is present in the DNA before binding by the metal complex correlates well with the strength of the metal complex-DNA interaction after binding. The enantioselective discrimination at these sites also suggests structural recognition as a predominant signal. Indeed, the strong correlation found between cleavage at sites with a large differential propeller twist rather than, for example, at the ends of the oligonucleotide helix, irrespective of sequence, suggests that transient openings in the helix are insufficient for site-specific cleavage. Nonetheless, just as with DNA-protein binding, the recognition of sequence-dependent structure and of sequence-dependent deformability are difficult to unravel. Here, too, the deformability of a particular sequence toward a more opened propeller-twisted state may be one feature of site recognition.

2.5. Conclusions

Therefore, in direct comparisons of cleavage by $Rh(phen)_2phi^{3+}$ with different, crystallographically characterized oligonucleotides, we have determined factors which govern sequence-selective recognition by $Rh(phen)_2phi^{3+}$. Both binding and reaction at sites are governed by considerations of shape and symmetry. In particular, enantioselective cleavage favored by the Δ-isomer is governed locally by the opening of

the site in the major groove. The change in base pair propeller twisting of the site correlates most closely with recognition by Δ-$Rh(phen)_2phi^{3+}$. Hence, these results provide support for site recognition which depends upon DNA propeller twisting in solution. Therefore, these results indicate that $Rh(phen)_2phi^{3+}$ may be uniquely and powerfully applied as a chemical probe for sequence-dependent propeller twisting of DNA.

References and Footnotes

1. Chapter 1, this work.
2. (a) Pardi, A.; Hare, D.R.; Wang, C. *Proc. Natl. Acad. Sci. U.S.A.* **1988**, *85*, 8785-8789. (b) Metzler, W.J.; Wang, C.; Kitchen, D.B.; Levy, R.M.; Pardi, A. *J. Mol. Biol.* **1990**, *214*, 711-736. (c) Nerdal, W.; Hare, D.R.; Reid, B.R. *Biochemistry* **1989**, *28*, 10008-10021. (d) Kaluarachchi, K.; Meadows, R.P.; Gorenstein, D.G. *Biochemistry* **1991**, *30*, 8785-8797.
3. (a) Pyle, A.M.; Long, E.C.; Barton J.K. *J. Am. Chem. Soc.* **1989**, *111*, 4520-4522. (b) Sitlani, A.; Long, E.C.; Pyle, A.M.; Barton, J.K. *J. Am. Chem Soc.* **1992**, *114*, 2303-2312.
4. David, S.D.; Barton, J.K. *J. Am. Chem Soc.* **1993**, *115*, 2984-2985.
5. Pyle, A.M.; Morii, T.; Barton, J.K. *J. Am. Chem Soc.* **1990**, *112*, 9432-9434.
6. Y denotes pyrimidine; R denotes purine; N denotes any base.
7. We define differential propeller twisting as the interpurine angle projected onto a plane defined by the dyad and helical axes.
8. Stubbe, J.; Kozarich, J.W. *Chem. Rev.* **1987**, *87*, 1107-1136.
9. (a) Dickerson, R.E.; Drew, H.R. *J. Mol. Biol.* **1981**, *149*, 761-786. (b) Drew, H.R.; Wing, R.M.; Takano, T.; Broka, C.; Tanaka, S.; Itakura, K.; Dickerson, R.E. *Proc. Natl. Acad. Sci. U. S. A.* **1981**, *78*, 2179-2183. (c) Frantini, A.V.; Kopka, M.L.; Drew, H.R.; Dickerson, R.E. *J. Mol. Biol.* **1982**, *257*, 14686-14707.
10. Timsit, Y.; Westhof, E.; Fuchs, R. P. P.; Moras, D. *Nature* **1989**, *341*, 459-462.
11. Privé, G.G.; Yanagi, K.; Dickerson R.E. *J. Mol. Biol.* **1991**, *217*, 177-199.
12. Carruthers, M.H.; Barone, A.D.; Beaucage, S.L.; Dodds, D.R.; Fisher, E.F.; Mc Bride, L.J.; Matteucci, M.; Stabinsky, Z.; Tang, J.-Y. *Methods Enzymol.* **1987**, *154*, 287-313.

13. Pyle, A.M.; Chiang, M.; Barton, J.K. *Inorg. Chem.* **1990**, *29*, 4487-4495.

14. Maniatis, T.; Fritsch, E.F.; Sambrook, J. in *Molecular Cloning*; Cold Spring Harbor Laboratory Press: 1982 .

15. EMBO Workshop on DNA Curvature and Bending *EMBO J.*, **1989**, *8*, 1-4.

16. Lipanov, A.; Kopka, M.L.; Kaczor-Grzeskowiak, M.; Quintana, J.; Dickerson, R.E. *Biochemistry* **1993**, *32*, 1373-1389.

17. Barton, J.K. *Science* **1986**, *233*, 727-732.

18. Dervan, P.B. *Science* **1986**, *232*, 464-471.

19. (a) Sigman, D.S. *Acc. Chem. Res.* **1986**, *19*, 180-186. (b) Saito, I.; Morii, T.; Sugiyama, H.; Matsuura, T.; Meares, C.F.; Hecht, S.M. *J. Am. Chem. Soc.* **1989**, *111*, 2307-2308. (c) Lomonossoff, G.P.; Butler, P.J.G.; Klug, A. *J. Mol. Biol.* **1981**, *149*, 749-760.

20. Krugh, T.R.; Reinhardt, C.G. *J. Mol. Biol.* **1975**, *97*, 133-162.

21. Sakore, T.D.; Jain, S.C.; Tsai, C.-C.; Sobell, H.M. *Proc. Natl. Acad. Sci., U.S.A.* **1977**, *74*, 188-192.

22. Chow, C.S.; Behlen, L.S.; Uhlenbeck, O.; Barton J.K. *Biochemistry* **1992**, *31*, 972-982.

23. (a) Shakked, Z.; Guerstein-Guzikevich, G.; Eisenstein, M.; Frolow, F.; Rabinovich, D. *Nature* **1989**, *342*, 456-460. (b) Jain, S.; Sundaralingam, M. *J. Biol. Chem.* **1989**, *264*, 12780-12784. (c) Ramakrishnan, B.; Sundaralingam, M. *Biochemistry* **1993**, *32*, 11458-11468.

24. Calladine, C.R. *J. Mol. Biol.* **1982**, *161*, 343-352.

25. Yanagi, K.; Privé, G.G.; Dickerson, R.E. *J. Mol. Biol.* **1991**, *217*, 201-214.

26. Hunter, C.A. *J. Mol. Biol.* **1993**, *230*, 1025-1054.

27. McClarin, J.A.; Frederick, C.A.; Wang, B.-C.; Greene, P.; Boyer, H.W.; Grable, J.; Rosenberg, J.M. *Science* **1986**, *234*, 1526-1541.

28. Nibedita, R.; Kumar, R.A.; Majumdar, A. *J. Biomol. NMR* **1992**, *2*, 477-484.

29. (a) Drew, H.R.; Travers, A.A. *Nuc. Acids Res.* **1985**, *13*, 4445-4467. (b) Koudelka, G.B.; Harrison, S.C.; Ptashne, M. *Nature* **1987**, *326*, 886-888.

30. Somers, W.S.; Phillips S.E.V. *Nature* **1992**, *359*, 387-393.

31. Phillips, S.E.V.; Manfield, I.; Parsons, I.; Davidson, B.E.; Rafferty, J.B.; Somers, W.S.; Maragarita, D.; Cohen, G.N.; Saint-Girons, I.; Stockley, P.G. *Nature* **1989**, *341*, 711-715.

32. Hai, T.; Fang, L.; Coukos, W.J.; Green, M.R. *Genes Dev.* **1989**, *3*, 2083-2090.

33. Pavletich, N.P.; Pabo, C.O. *Science* **1993**, *262*, 1701-1707.

34. Huber, P.; Morii, T.; Mei, H.-Y.; Barton, J.K. *Proc. Natl. Acad. Sci. U.S.A.* **1991**, *88*, 801- 805.

35. Chow, C.S.; Hartmann, K.M.; Rawlings, S.L.; Huber, P.W.; Barton, J.K. *Biochemistry* **1992**, *31*, 3534-3542.

Chapter 3:

Photocleavage by $Rh(X)_2phi^{3+}$ Complexes on a K-*ras* -Derived Oligonucleotide and Mutants Possessing Mispaired Bases: Sensitivity to Local Structural Deformations.

3.1. Introduction

The pairing of noncomplementary bases within a DNA duplex has important biological consequences. Such mispairing results from the deamination of cytosine, DNA replication errors, and genetic recombination. Mismatches in DNA lead to transitions and transversions of DNA sequence in the daughter molecules upon DNA replication. This altered genetic material serves as a template for the formation of mutant proteins, potentially resulting in oncogenesis in eukaryotic organisms. Mechanisms of repair have evolved in order to reduce the frequency of DNA mismatches, and have been identified in both prokaryotes and eukaryotes[1]. How DNA structure and dynamics influence repair efficiency are areas which are as yet not well understood.

In order to determine the fundamental basis for DNA repair, many detailed structural studies have been performed on short oligonucleotides containing one or more mispairs. However, these mismatched base pairs show a great deal of structural variation, depending upon a number of factors, including sequence context and the crystal or solution environment. For example, the GA mismatch adopts a range of conformations with respect to the rotation of each base about the glycosidic bond. For example, as determined by NMR, the GA mismatch adopts a G(*anti*)-A(*anti*) conformation at neutral pH; this is the same conformation which is found in correctly paired DNA. However, at lower pH in solution, the G(*syn*)-A(*anti*) structure is observed. Crystal structures have shown all three possibilities: G(*anti*)-A(*anti*), G(*syn*)-A(*anti*), and G(*anti*)-A(*syn*). It should be noted that the G(*anti*)-A(*anti*) structure has only been observed

crystallographically for an oligonucleotide containing two adjacent GA mispairs[2]. This example, and others where two mismatches occur within 12 base pairs or less, are unlikely to have a high level of occurrence in biological systems.

One characterized DNA structure that has biological relevance is that of the *ras* oncogene, which is often found in human cancer. This gene has been highly conserved through evolution, and encodes the protein p21. The *ras* gene contains a mutation hot spot in codon 12; if residue 12 of p21 is changed from a glycine to any other amino acid except proline, an activated protein results[3]. For example, an AG mismatch in position 34 of the K-*ras* gene leads to a GGT-> TGT transversion, found in human colon cancer[4]. Therefore, only one mismatched base pair can have a deleterious effect. This particular mismatch is poorly repaired, for reasons which are as yet unknown. An oligonucleotide containing the region of the *ras* gene from position 29 to 39, with an AG mismatch at position 34, has been characterized by NMR spectroscopy[5] and molecular dynamics[6].

Another method of investigating such issues as mismatch-induced alterations in DNA structure, and how structural variations may effect recognition, entails the development and use of probes of nucleic acid solution structure. The transition metal complex $Rh(phen)_2phi^{3+}$ recognizes nucleic acid structural features through intercalative binding and shape-selection. The racemic complex has been applied towards an understanding of RNA tertiary structure, and the effects of mutations upon this tertiary structure[7]. Additionally, the enantiomers of this molecule have been utilized to examine the sequence-dependent structure of double helical DNA[8]. Thus $Rh(phen)_2phi^{3+}$ is sensitive to such features of nucleic acid structure as stacking and disposition of the bases. It has also been demonstrated, with the closely related metal complexes $Rh(bpy)_2phi^{3+}$ and $Rh(phi)_2bpy^{3+}$, that shape-selection may be further modulated by appending hydrophobic groups onto the ancillary ligands[9]. This chapter concerns the synthesis of the complex $Rh(TMP)_2phi^{3+}$ (TMP = 3,4,7,8-tetramethyl-phenanthroline),

Figure 3.1. Structures of rhodium complexes utilized to probe DNA mismatches . $Rh(phen)_2phi^{3+}$ (top) and $Rh(TMP)_2phi^{3+}$ (center) were used to probe the structure of oligonucleotides containing AG and GT mismatches. $Rh(dmbpy)_2phi^{3+}$ (bottom) was used as a comparison to these two molecules in photocleavage on a long DNA fragment.

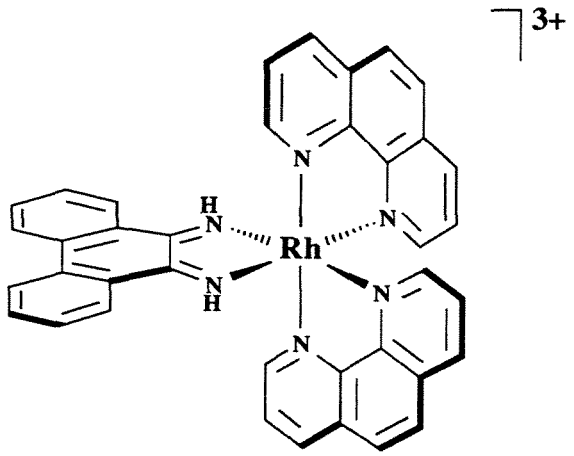
3+
H
N
N
H
Rh
N
N
N
N

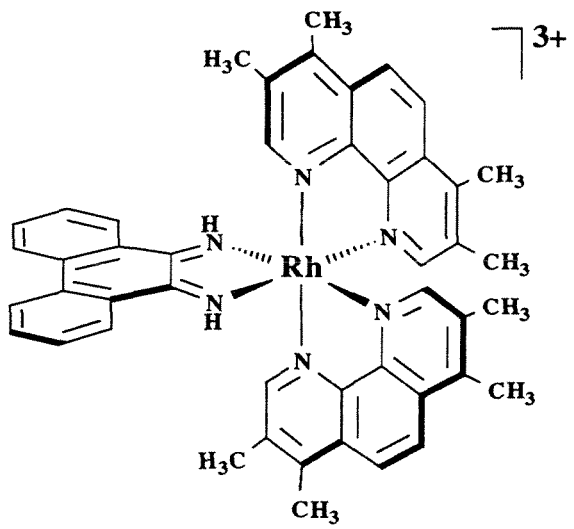
CH3
H3C
3+
H
N
N
H
Rh
N
N
N
N
CH3
CH3
CH3
CH3
H3C
CH3

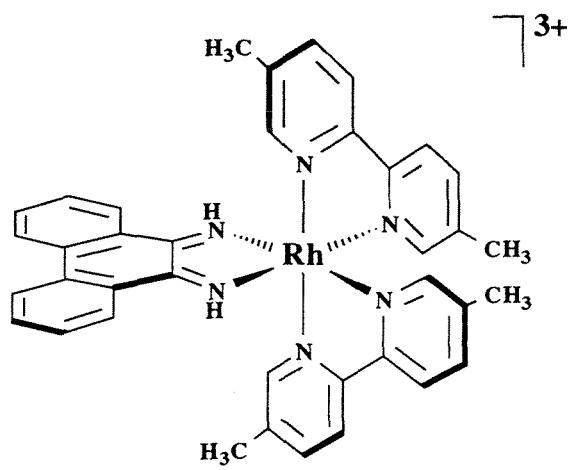
H3C
3+
H
N
N
H
Rh
N
N
N
N
CH3
CH3
H3C

and its application to the study of DNA mismatches in solution. Metal complexes used in this chapter are shown in Figure 3.1.

Three oligonucleotides corresponding to the K-*ras* gene were probed with $Rh(phen)_2phi^{3+}$ and $Rh(TMP)_2phi^{3+}$. These include a portion of the protooncogene, a mutant containing a AG mismatch, and another mutant containing a TG mismatch. For the purposes of this study, they will be referred to as K-*ras* CG, K-*ras* AG, and K-*ras* TG respectively. The sequences are as follows:

```
5'-G C C A C C A G C T C-3'
3'-C G G T G G T C G A G-5'

5'-G C C A C A A G C T C-3'
3'-C G G T G G T C G A G-5'

5'-G C C A C T A G C T C-3'
3'-C G G T G G T C G A G-5'
```

3.2. Experimental

3.2.1. Synthesis of $Rh(TMP)_2phi^{3+}$

Materials and Instrumentation. The starting materials for the synthesis of $Rh(TMP)_2phi^{3+}$ were commercially obtained as follows. $RhCl_3$ (42.5% Rh) was from Aesar Johnson Matthey, (Seabrook, NH); 3,4,7,8-1,10-tetramethyl phenanthroline (TMP), and 9,10-diaminophenanthrene (DAP), and Sephadex resin were from Aldrich (Milwaukee, WI). Absorption spectra were recorded on a Cary 219 spectrophotometer, and NMR spectra were recorded on a GE-300 MHz spectrometer.

Synthesis, Purification, and Characterization of $[Rh(TMP)_2phi]Cl_3$. This metal complex was synthesized using a different methodology than those described previously for $Rh(X)_2phi^{3+}$ complexes, where X= an aromatic ligand. The method used here is closer to that described for the synthesis of $[Rh(NH_3)_4phi]Cl_3$ [10]. Specifically, 0.39 mmoles of $RhCl_3$ was dissolved in 3 mL water; this solution was degassed and put under

a nitrogen atmosphere. Next 0.39 mmoles DAP was added in a solid form. This solution was refluxed with a condenser at 100°C for 1 hour. The reaction was then cooled to room temperature, and 20 mL of degassed DMF was transferred with a nitrogen-flushed airtight syringe. The reaction was then heated under reflux to 100°C for 5 minutes, and cooled to room temperature again. The reaction flask was then placed in liquid nitrogen, until the solid was completely frozen. Solid TMP (0.78 mmoles) was next added to the frozen solution; the reaction was degassed. This reaction mixture was brought up to room temperature, and then heated to 120-125°C for 2.5 hours. After cooling the reaction to room temperature, 100 mL water and 220 mL ethanol were added. The solution was stirred in the dark for 2-3 days, to allow for the air oxidation from coordinated DAP to coordinated phi. The complex was subsequently purified by use of the cation exchange resin Sephadex CM C-25. A bright orange band is eluted at 0.5 M NaCl. Salt was removed by extraction first with ethanol and then methylene chloride. $[Rh(TMP)_2phi]Cl_3$ was characterized by NMR, uv-visible absorption, and mass spectrometry. As described previously for other $Rh(X)_2phi$ complexes, the NMR spectrum of this complex is sensitive to pH[11]. The addition of trifluoroacetic acid fumes sharpens the entire spectrum and improves the peak resolution considerably. The NMR and uv-visible spectra are shown in Figure 3.2. The TFA treated NMR in D_2O showed the following shifts in ppm: 2.25 (s), 2.6 (s), 2.85 (s), 2.95 (s), 7.45 (s), 7.55 (t), 7.85 (t), 8.2 (d), 8.3 (d), 8.5 (multiplet), 8.6 (s). UV visible absorption spectra in water show maxima at 282nm, 312nm, 336nm, and 377nm. FAB Mass Spec ion mass: 816, $[Rh(TMP)_2phi+Cl]^+$; 780, $[Rh(TMP)_2phi^{2+}-H]^+$; 610, $[Rh(TMP)_2+Cl]^+$; 575, $[Rh(TMP)_2]^+$; 545, $[Rh(TMP)(phi)]^+$; 339, $[Rh(TMP)]^+$; 236, TMP.

Resolution of Δ-$Rh(TMP)_2phi^{3+}$: The Δ-isomer of $Rh(TMP)_2phi^{3+}$ was resolved by cation exchange chromatography with a chiral eluent, as described[12].

Figure 3.2. Characterization of $[Rh(TMP)_2phi^{3+}]Cl_3$. (first panel) NMR spectrum of $Rh(TMP)_2phi^{3+}$ in D_2O. Enlargement of the aromatic region is shown below. (second panel) Uv-visible absorption spectrum of $Rh(TMP)_2phi^{3+}$ in H_2O.

^{1}H NMR spectrum

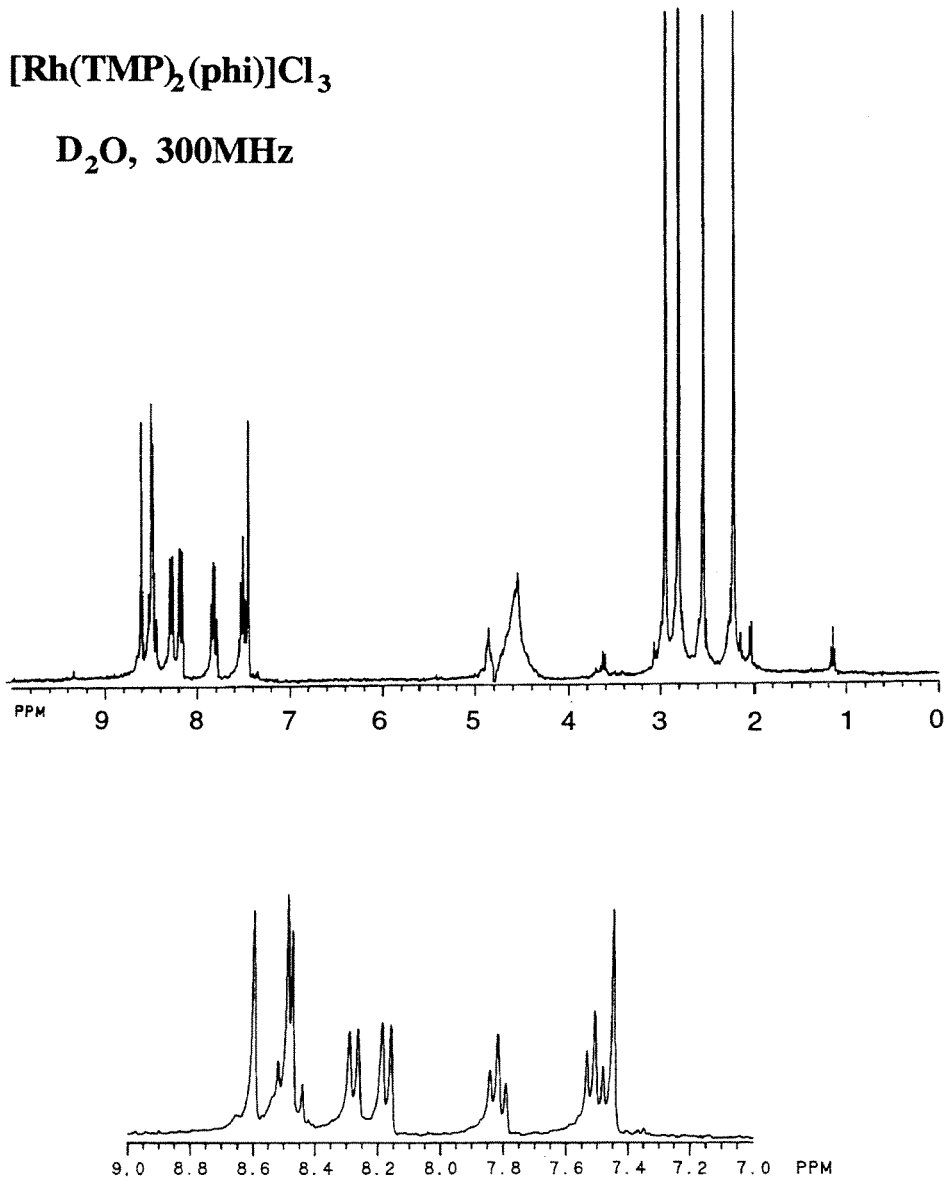

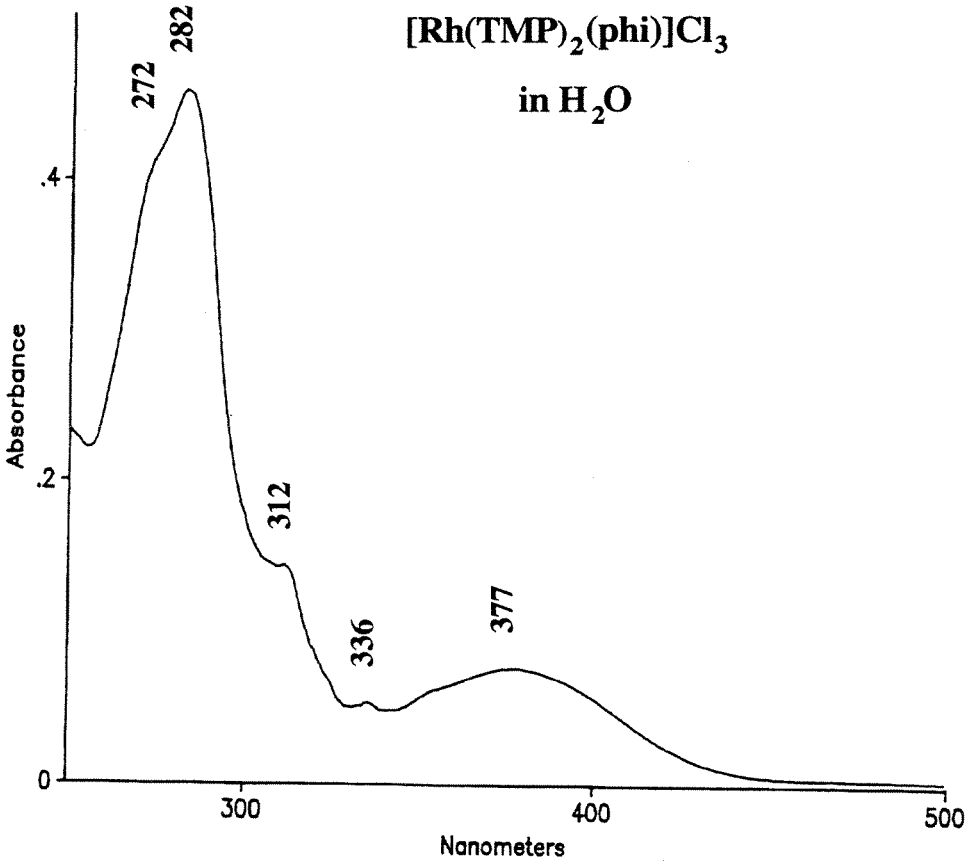
[Rh(TMP)2(phi)]Cl3
in H2O
272
282
312
336
377
Absorbance
.4
.2
0
300
400
500
Nanometers

3.2.2. Photocleavage Experiments

Materials. Oligonucleotides were synthesized via the phosphoramidite method[13], using 1.0 μM columns on an ABI 391 DNA-RNA synthesizer. A reversed- phase, C18 Dynamax column was used on a Waters HPLC for the purification of DNA. Labelling reactions were done with γ^{32}P-ATP (NEN) and polynucleotide kinase. Labelled oligonucleotides were purified by Nensorb columns, and stored dry at 4°C. For each of the three oligonucleotides, equimolar concentrations of each strand were heated to 90°C and cooled over several hours to allow proper annealing to occur. $Rh(phen)_2phi^{3+}$ was synthesized as previously described[14]. Enantiomers of this complex were kindly donated[15]. Quantitation of metal complex and oligonucleotide concentrations was accomplished using a CARY 219 spectrometer. $Rh(phen)_2phi^{3+}$ concentration was based on $\varepsilon(362) = 19{,}400\ M^{-1}\ cm^{-1}$ at pH=7.0. The same extinction was used in calculating concentrations of $Rh(TMP)_2phi^{3+}$ and $Rh(dmbpy)_2phi^{3+}$. $Rh(dmbpy)_2phi^{3+}$ and other $Rh(X)_2phi^{3+}$ complexes have extinction coefficients which differ from $Rh(phen)_2phi^{3+}$ by less than 10%[11]. Extinction coefficients were calculated for each oligonucleotide taking base composition into consideration.

Photocleavage Reactions on 11mer Oligonucleotides. Reactions contained 480μM nucleotides, 50mM sodium cacodylate buffer, pH 7.0, and 25μM rhodium complex, and were irradiated at 313 nm with a 1000W Hg-Xe lamp. Irradiation times were typically 2 minutes. After photocleavage, an aliquot of each reaction mixture was taken and dried in vacuo. These aliquots, along with Maxam-Gilbert sequencing reactions[16] and controls were subsequently taken up in a NaOH- formamide dye, heated to 90°C for 3 minutes, chilled on ice for 1 minute, and loaded on a 20% polyacrylamide gel which was 8.3 M in urea . Gels were eluted about 4 hours at 1600V. Upon completion, gels were wrapped and exposed to a phosphorimaging plate for 12 hours. These plates were scanned on a Molecular Dynamics Phosphorimager.

Photocleavage Reactions on *EcoRI-PvuII *fragment 180mer Fragment from pUC18*: The conditions for the cleavage experiment were prepared as follows : 50mM sodium cacodylate buffer at pH 7.0, 40μM bp calf thymus DNA, and 1μM and 5μM $Rh(TMP)_2phi^{3+}$, $Rh(dmbpy)_2phi^{3+}$ or $Rh(phen)_2phi^{3+}$. Irradiations were at 313nm for 2 minutes. Samples were twice precipitated with ethanol and 7.4 M ammonium acetate, rinsed with 80% ethanol and dried. Loading was the same as described above for the oligonucleotides. Samples were run on an 8% denaturing polyacrylamide gel.

3.3. Results

3.3.1. Photocleavage by $Rh(phen)_2phi^{3+}$, $Rh(TMP)_2phi^{3+}$, and $Rh(phen)_2phi^{3+}$ on a Long DNA Fragment.

In order to characterize the recognition properties by $Rh(TMP)_2phi^{3+}$, cleavage on DNA fragments not containing mismatches was examined, and compared to the known recognition of DNA by $Rh(phen)_2phi^{3+}$ and $Rh(dmbpy)_2phi^{3+}$ (dmbpy = 5,5'-dimethyl-bipyridyl). Table 3.1 shows a comparison between racemic $Rh(TMP)_2phi^{3+}$, $Rh(dmbpy)_2phi^{3+}$, and $Rh(phen)_2phi^{3+}$. Interestingly, there seems to be a closer similarity between photocleavage by $Rh(phen)_2phi^{3+}$ and $Rh(dmbpy)_2phi^{3+}$ than between $Rh(TMP)_2phi^{3+}$ and either of these complexes. Although there are not that many strong sites for $Rh(phen)_2phi^{3+}$ on the fragment used, there are a few high affinity sites for $Rh(TMP)_2phi^{3+}$. These are characterized by either an A or a T to the 5' side of the cleavage site, in most cases.

Notably, $Rh(TMP)_2phi^{3+}$ is excluded from the site 5'-CCAG-3', which is cleaved strongly by $Rh(phen)_2phi^{3+}$ and $Rh(dmbpy)_2phi^{3+}$. There are other 5'-CA-3' sites which are cleaved by $Rh(TMP)_2phi^{3+}$, but in all cases they are flanked by either an A or T to the 5' side. Van der Waals interactions between the methyl groups of the TMP ancillary ligand and the DNA thymine methyl groups may be stabilizing an otherwise less than favorable interaction at these 5'-A/TCAN-3' sites. The same may also be said of reaction

Table 3.1. A Comparison of Cleavage Selectivity for $Rh(TMP)_2phi^{3+}$, $Rh(dmbpy)_2phi^{3+}$ and $Rh(phen)_2phi^{3+}$ [a]

site 5' ->3'	TMP 5 μM	TMP 1 μM	dmbpy 5μM	dmbpy 1 μM	phen 5μM	phen 1μM
AGGA	++	+	++	+	++	+
ACAG	++++	+++	+++	++	+++	++
ACAC	++	+	+++	+	+++	+
TCAC	++	+	+++	+	+++	+
ACAA	++	-	+	-	+	-
AGCG	+++	-	-	-	-	-
TGTG	++	++	+	+	-	-
TGTG	+++	+++	+	+	-	-
TCCG	+++	+++	+	-	++	+
ACTC	+++	++	+	++	+	+
TGTG	+++	+++	-	+	-	-
AGTG	++	++++	+	++	-	+
CTGG	+++	++++	+	+++	+	+++
CCAG	-	-	+	+	++	++

[a] Data from photocleavage performed as described in the experimental section.

by $Rh(TMP)_2phi^{3+}$ at the 5'-RY-3' steps, which are not favored sites for reaction by $Rh(phen)_2phi^{3+}$. Stabilization of binding of $Rh(phi)^{3+}$ complexes by methyl-methyl interactions with DNA has also been previously observed[9a,17].

3.3.2. Photocleavage by $Rh(phen)_2phi^{3+}$ and $Rh(TMP)_2phi^{3+}$ on Oligonucleotides Containing a CG base pair, an AG Mismatch, and a TG Mismatch

These photocleavage experiments utilized high oligonucleotide and high metal complex concentrations. For this reason, it appears that there is a small amount of nonspecific cleavage at every site in these three oligonucleotides by each of the complexes examined. This cleavage is clearly above the controls, as may be seen in the gels shown in Figure 3.3A-C. These weak cleavage sites will not be discussed unless there is a change in intensity of the site between different oligomers. Photocleavage results are summarized in Figure 3.3D.

K-ras *CG oligomer:* As shown in the gel in Figure 3.3A, one strand of this correctly paired oligonucleotide is cleaved more strongly by several complexes than the other strand. Cleavage is strongest at C5 and C6. There are, however, differences in intensity of cleavage at these two positions by the different metal complexes examined. Δ-, Λ-, and racemic $Rh(phen)_2phi^{3+}$ each cleave these sites fairly evenly. However, racemic $Rh(TMP)_2phi^{3+}$ cleaves more strongly at C5 and Δ-$Rh(TMP)_2phi^{3+}$ cleaves more strongly at C6. It appears likely then that it is Λ-$Rh(TMP)_2phi^{3+}$ cleaves C5 to a greater extent.

Δ-$Rh(phen)_2phi^{3+}$ cleaves C3 on this same strand to a moderate extent. Additionally, T16 is cleaved to a moderate extent by Δ-, Λ- and racemic $Rh(phen)_2phi^{3+}$. C15 is cleaved to a moderate extent by racemic $Rh(TMP)_2phi^{3+}$, but not by the Δ enantiomer of this complex.

K-ras *AG oligonucleotide:* There are clear differences between the cleavage patterns on this oligonucleotide as compared with the K-*ras* CG oligomer. In the AG

Figure 3.3. Images of gels showing photocleavage by $Rh(X)_2phi^{3+}$ complexes on a5'-end-labelled oligonucleotide and mutants containing mismatches. **A.** K-*ras* CG. **B.** K-*ras* AG. **C.** K-*ras* TG. Lanes 1 and 18, and 2 and 17 correspond to photocleavage by Δ-$Rh(TMP)_2phi^{3+}$ and racemic $Rh(TMP)_2phi^{3+}$ respectively. Lanes 3 and 16, 4 and 15, and 5 and 14 correspond to photocleavage by racemic, Λ- and Δ-$Rh(phen)_2phi^{3+}$ respectively. Lanes 6 and 13 and 7 and 12 correspond to irradiation of DNA in the absence of metal complex and DNA in the absence of irradiation and metal complex, respectively. **D.** A histogram comparing photocleavage at each base by Δ- and Λ-$Rh(phen)_2phi^{3+}$, and Δ-$Rh(TMP)_2phi^{3+}$ and racemic $Rh(TMP)_2phi^{3+}$.

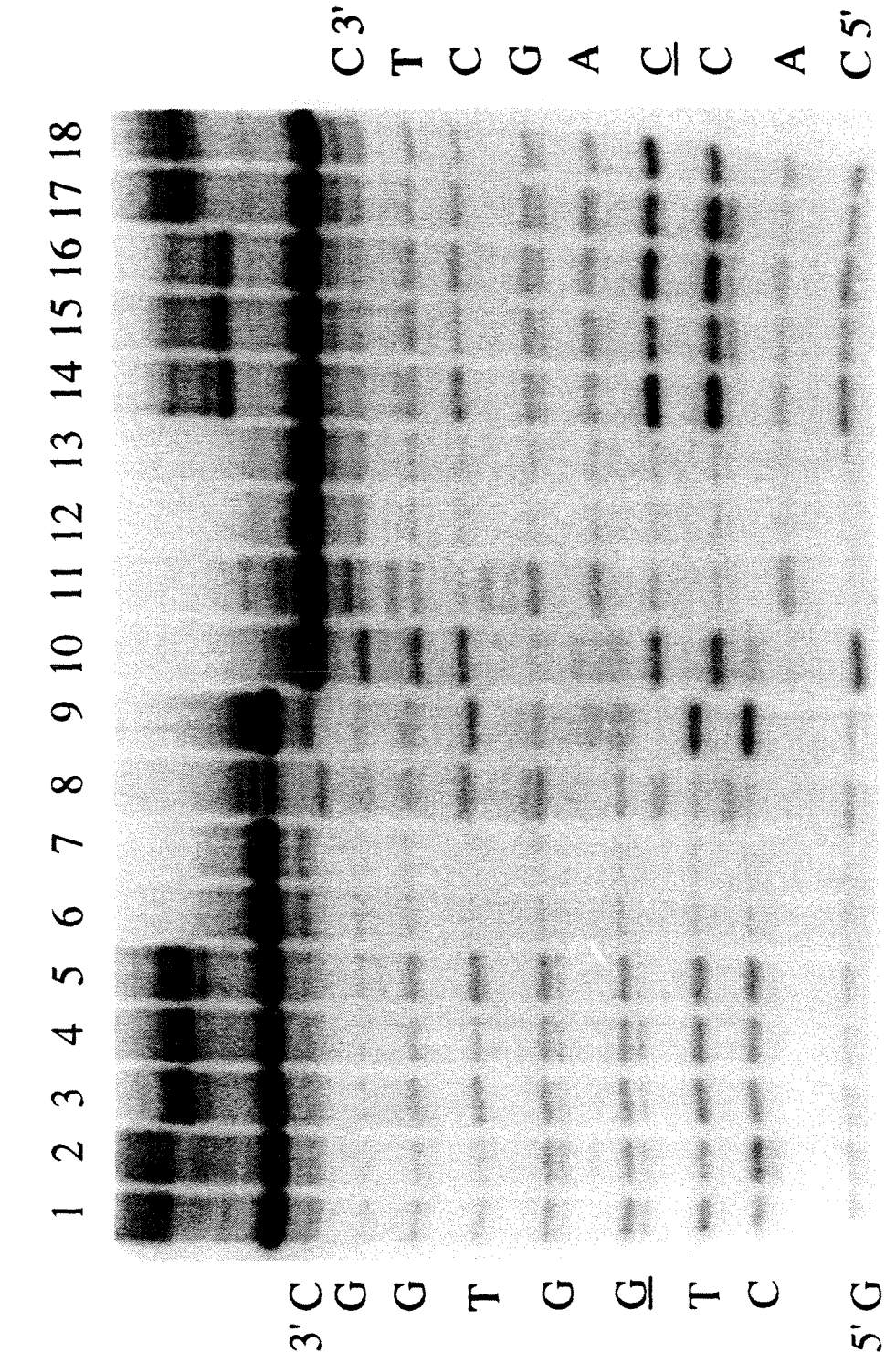
1 2 3 4 5 6 7 8 9 10 11 12 13 14 15 16 17 18
C 3'
T
C
G
A
C
C
A
C 5'
3'C
G
G
T
G
G
T
C
5'G

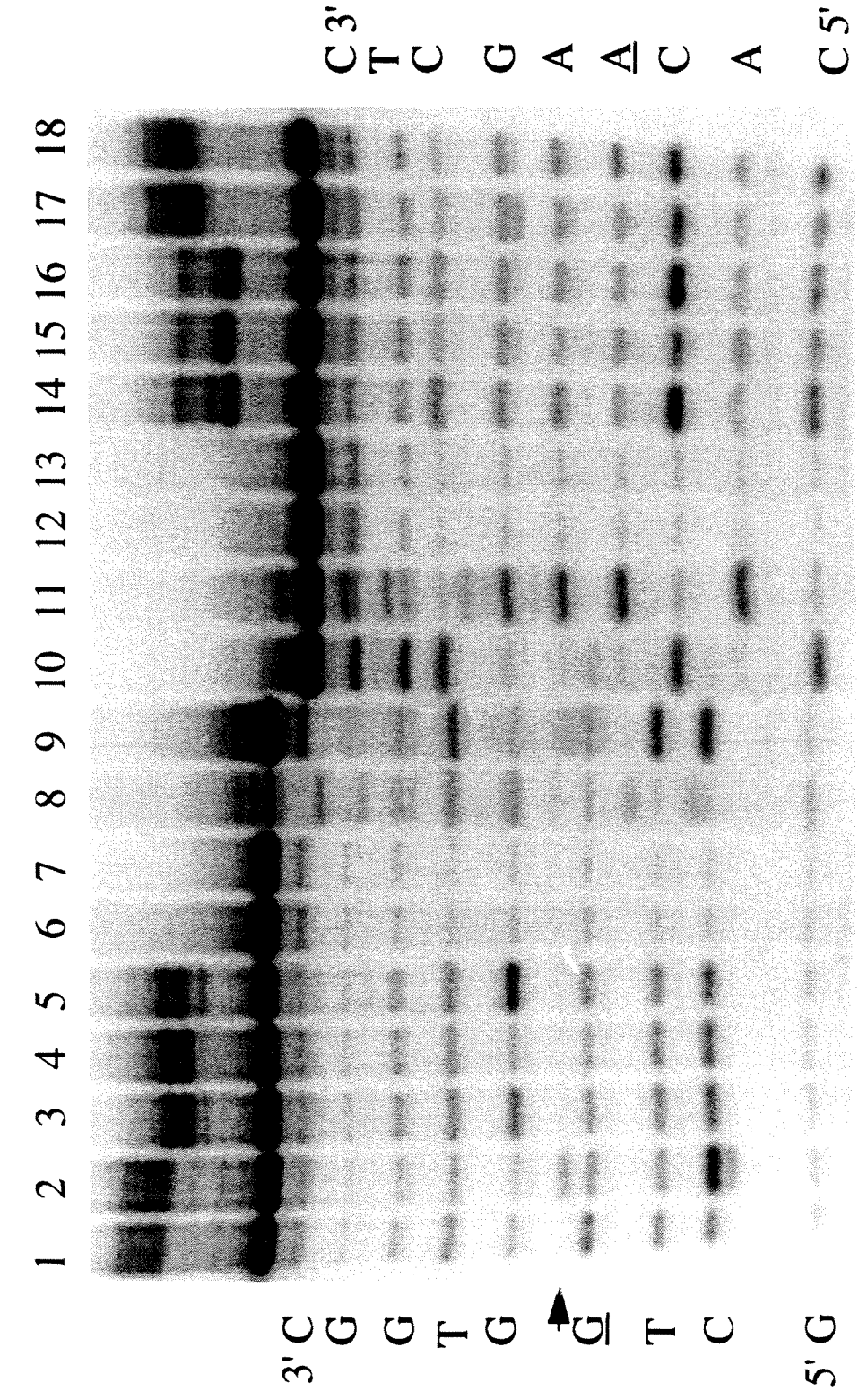
1 2 3 4 5 6 7 8 9 10 11 12 13 14 15 16 17 18
C 3'
T C G A A C A C 5'
3' C G G T G G T C 5' G

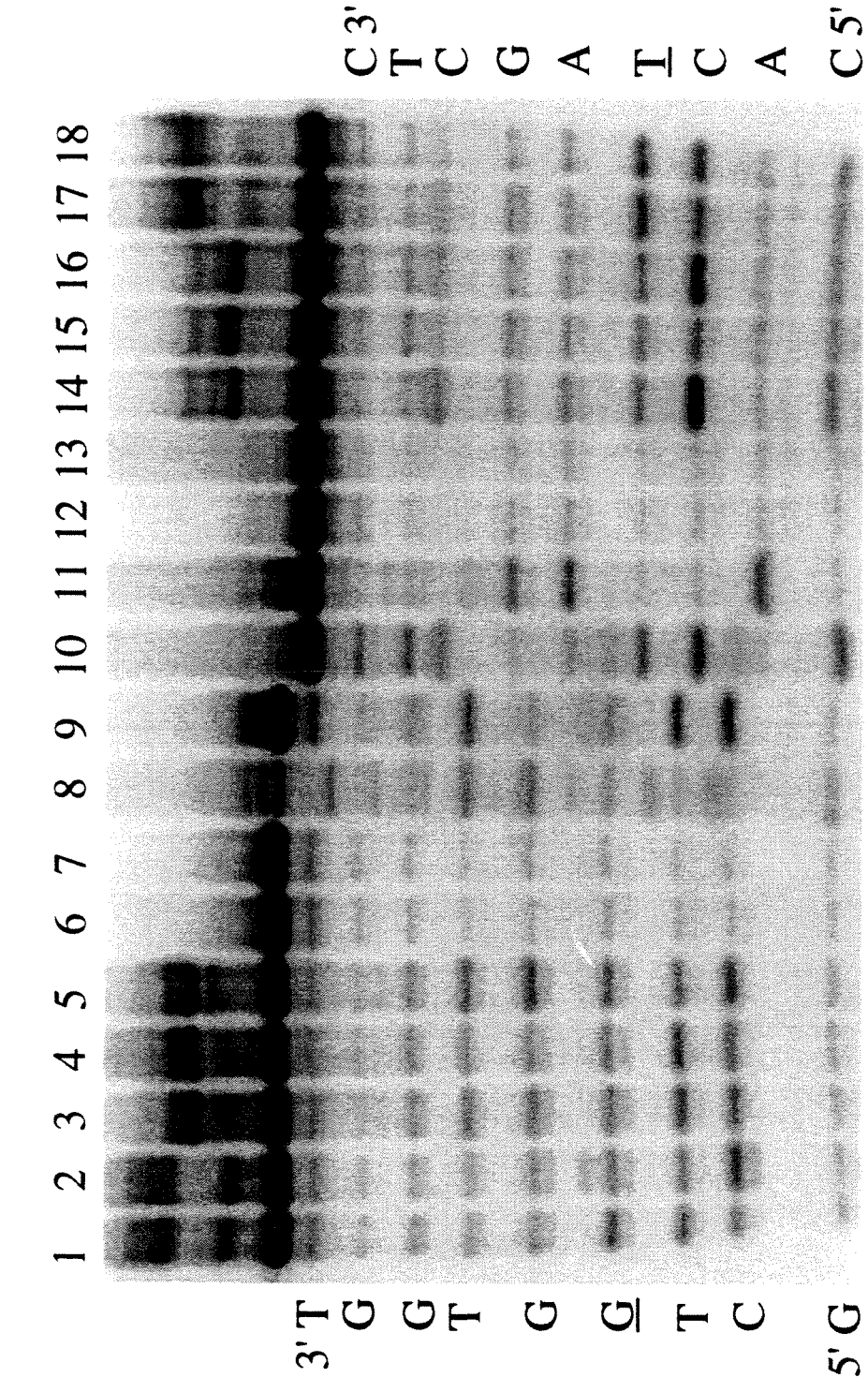
1 2 3 4 5 6 7 8 9 10 11 12 13 14 15 16 17 18
3'T G G T G G T C 5'G
C 3' T C G A T C A C 5'

$Rh(phen)_2phi^{3+}$

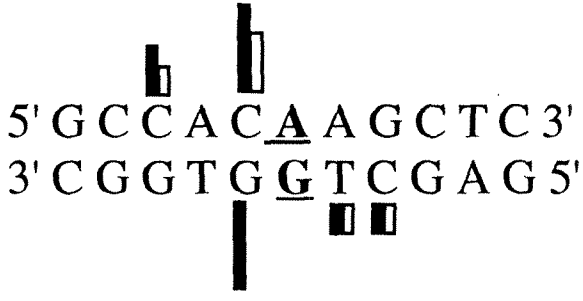

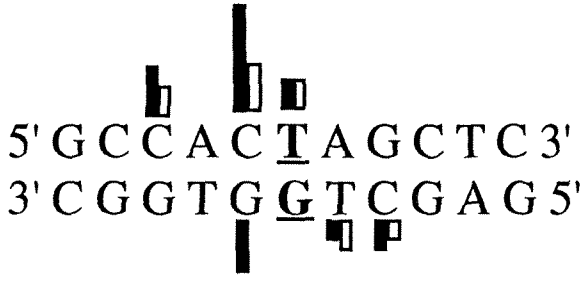

$Rh(TMP)_2phi^{3+}$

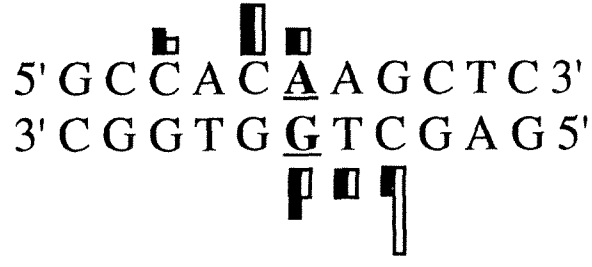

oligonucleotide, C6 is mutated to an A6. As may be observed in Figure 3.3B, the cleavage by each metal complex at this mutated base is weak. Cleavage at C5 has a slight enhancement of enantioselectivity. Cleavage on the other bases of this strand appears to remain the same as in K-*ras* CG. On the other strand of this oligonucleotide, G18, the guanine which is 3' to the mismatched guanine, is cleaved very strongly by Δ-$Rh(phen)_2phi^{3+}$. The cleavage also appears to be highly enantioselective. Interestingly, in the correctly paired oligonucleotide, G18 is cleaved only weakly by Δ-$Rh(phen)_2phi^{3+}$, or in fact, any of the other metal complexes. Therefore, Δ-$Rh(phen)_2phi^{3+}$ is discerning *a mismatch-induced structural change which specifically complements its right-handed chirality.*

For the correctly paired oligonucleotide, cleavage at G18 corresponds to intercalation between G18 and T19, as $Rh(phen)_2phi^{3+}$ has been shown to cleave with a 5' asymmetry[18]. 5'-G*G*TG-3' would be expected to be a particularly poor recognition site for Δ-$Rh(phen)_2phi^{3+}$, and may be understood in terms of a structure which is closed in the major groove. The low level of recognition in the correctly paired duplex is completely consistent with previously observations[19]. However, for the K-*ras* GA, it is not absolutely certain that cleavage at G18 corresponds to binding at the G18-G19 base step. Another possibility would be that the cleavage at G18 is a result of intercalation between the 5'-G17G18-3' base step, and that the A6G17 mismatch (and/or intercalation at the base step containing the mismatch) is disrupting the structure of DNA to such an extent that a hydrogen atom is abstracted from the sugar belonging to the 3' base instead of the 5' base. The hydrogen atom abstracted could be the C3'H, as the photoproduct runs with the same electrophoretic mobility as the Maxam-Gilbert band, which is representative of a 3'-phosphate end. However, this mechanism would have to be examined further before any definitive conclusions could be drawn.

$Rh(TMP)_2phi^{3+}$ also shows some interesting differences in cleavage on K-*ras* CG and K-*ras* AG. The moderate cleavage which is attributed to Λ-$Rh(TMP)_2phi^{3+}$ on

C15 in the correctly paired duplex, becomes a strong cleavage site in the oligonucleotide containing the AG mispair. Interestingly, C15 is *two* bases away from the mispair. Therefore, if $Rh(TMP)_2phi^{3+}$ is intercalating between C15 and T16, then Λ-$Rh(TMP)_2phi^{3+}$ is sensing the effect of having a mismatched base pair as a *flank*. This result, and the strong cleavage by Δ-$Rh(phen)_2phi^{3+}$ at G18, show that the structural change caused by the AG mismatch extends at least one base pair in each direction. This observation correlates well with what has been observed by NMR for this and other oligonucleotides containing mismatches[5a,20].

Another interesting observation is that both racemic and Δ-$Rh(TMP)_2phi^{3+}$ appear to cleave more strongly at G17 when it is part of a AG mismatch than when it is correctly paired. Although this effect is modest, the cleavage by $Rh(TMP)_2phi^{3+}$ at A6·*G17* is stronger than that by $Rh(phen)_2phi^{3+}$. Additionally, the enantiomers of this complex show differences in the photoproducts observed. Cleavage by the racemic complex appears to have a band running between G17 and G18 phosphates. This band is labelled with an arrow in Figure 3.3B. The Δ enantiomer of this complex shows no such band, but rather an enhanced cleavage band which migrates as a phosphate end. Therefore this photoproduct can be attributed to cleavage by the Λ-isomer. This band could likely correspond to the well-characterized 3'-phosphoglycaldehyde terminus[R]. It is not unexpected that there might be some differences in the photoproducts observed between the enantiomers of this complex. Differences in reactivity between enantiomers has been previously observed with $Rh(phen)_2phi^{3+}$ [8b].

*K-*ras *TG Oligonucleotide:* The photocleavage on this oligonucleotide possesses some characteristics in common with both K-*ras* AG and K-*ras* CG, and is shown in Figure 3.3C. Like the other oligonucleotides, cleavage by most of the complexes at C5 of K-*ras* TG appears to be strong; therefore the cleavage at this position 5' to the mismatch remains generally unaffected by either base substitution. However, it does appear that the *enantioselectivity* in cleavage by $Rh(phen)_2phi^{3+}$ is enhanced at this site. Additionally,

for racemic $Rh(TMP)_2phi^{3+}$ and Δ-$Rh(TMP)_2phi^{3+}$ the extent of cleavage appears to be almost as strong at T6 in the K-*ras* TG oligonucleotide as it is for the C6 in K-*ras* CG. In contrast, the cleavage by these complexes at A6 of the AG mismatch, was much diminished.

The increased cleavage at certain positions on the other strand that resulted from the AG mismatch was also observed for the TG mismatch-containing oligonucleotide, but to a lesser extent. Specifically, enantioselective cleavage by Δ-$Rh(phen)_2phi^{3+}$ was observed at G18, which is 3' to the mismatched base pair at a level which was intermediate to that observed for K-*ras* CG and K-*ras* AG. Additionally, the increase in cleavage at C15 by racemic (likely Λ-)$Rh(TMP)_2phi^{3+}$ is observed, but again to a lesser extent than when the AG mismatch is present. Finally, increased cleavage by Δ-$Rh(TMP)_2phi^{3+}$ was observed at T6·*G17*, the mismatched base. The effect here, although subtle, is about the same as that observed for the A6·*G17* mismatch.

3.4. Discussion

3.4.1. $Rh(X)_2phi^{3+}$ Complexes Recognize DNA Structural Mutations

The goal of these studies has been to examine the structure of DNA containing mismatched base pairs, rather than specifically targeting a particular mismatch. Clearly, the photocleavage by $Rh(phen)_2phi^{3+}$ and $Rh(TMP)_2phi^{3+}$ *is* sensitive to the alterations in local DNA structure which result from insertion of a mismatched base pair into a double helical duplex. In general, the oligonucleotide containing the AG mismatch shows greater differences in cleavage as compared with K-*ras* CG than does the TG mismatch mutant. The complexes showing the greatest enhancements in photocleavage at a particular base in comparison to the correctly paired 11mer were Δ-$Rh(phen)_2phi^{3+}$ and racemic $Rh(TMP)_2phi^{3+}$. Δ-$Rh(phen)_2phi^{3+}$ shows a strong and enantioselective cleavage at the base 3' to the AG mismatch of K-*ras* AG. Racemic (likely Λ-) shows an enhancement in cleavage at C15, which is two bases 5' to the AG mismatch. These same

enhancements were also observed with K-*ras* TG, but to a lesser degree. Conversely, the *loss* of cleavage by each metal complex studied at the mismatched base pair was also greater for A6 of the AG mismatch than it was for T6 of the TG mismatch. It may be qualitatively concluded, then, that the overall structure of K-*ras* AG is more perturbed than is the overall structure of K-*ras* TG, and that the structural perturbations occur in both the 5' and 3' directions.

How does $Rh(TMP)_2phi^{3+}$ recognize the presence of a mismatched base pair two bases away? It is entirely possible that the presence of the mismatches changes the positioning of T16, which is also to the 5' side of the mismatch. In this scenario, binding by $Rh(TMP)_2phi^{3+}$ would be facilitated by increased accessibility of the bases for stacking and/or increased interaction with the methyl group of T16.

$Rh(phen)_2phi^{3+}$ and $Rh(TMP)_2phi^{3+}$ exhibit patterns of cleavage similar to each other on the oligonucleotides examined, particularly K-*ras* CG, as illustrated in Figure 3.3D. However, one difference between these complexes is that the latter cleaves the bases comprising the mismatches to a greater extent. Interestingly, NMR studies of K-*ras* AG[5] demonstrate that both bases of the mismatch, A6 and G17, are displaced towards the *minor* groove. Perhaps, then, $Rh(TMP)_2phi^{3+}$ supplements a less than optimal stacking interaction with van der Waals interactions between its methyl groups and the DNA major groove. A similar explanation can be proffered in the case of the TG mismatch. Crystal structures[21] and molecular dynamics studies[22] show that the thymine of TG mismatches is displaced towards the *major* groove. This displacement should favor stacking by these complexes, and is also consistent with the greater intensity of cleavage on T6 of K-*ras* TG by both complexes as compared with A6 of K-*ras* AG.

It should be noted that a crystal structure of a closely related sequence with an AG mismatch is available[23]. The sequence of this structure is 5'-C*RCAAGCTG*GCG-3', with the section in italics indicating the region in common with K-*ras* AG, and with the mismatch in bold. R is a guanine in the crystal structure and an adenine in K-*ras*. The

AG mismatch in this structure exhibits an A(*syn*)- *G(anti)* conformation, which differs from the A(*anti*)-G(*anti*) conformation elucidated by NMR for K-*ras* AG[5]. The differences in mismatch conformation and flanking sequence make it difficult to make direct comparisons between photocleavage and crystallographic parameters, as was done in Chapter 2. However, some observations may be made. This crystal structure exhibits high propeller twisting in general. Interestingly, the guanine 3' to the mispaired guanine, which is equivalent to G18 in K-*ras*, shows quite different values for propeller twisting (0° and -20°) on the two sides of the asymmetrical crystal. Additionally, the roll angle of the 5'-GC-3' step is -3° on one side and -10° on the other side. Perhaps the strong cleavage by Δ-Rh(phen)$_2$phi^{3+} at this base can be explained by the flexibility of this structure. The helical twist values at this site (35° and 38°) are not, however, out of the ordinary, and do not suffice to explain the high enantioselectivity in cleavage at G18.

As observed with the enantiomers of Rh(phen)$_2$phi^{3+}, the enantiomers of Rh(TMP)$_2$phi^{3+} also show differences in the photoproducts which are observed. Large differences in photocleavage between racemic Rh(TMP)$_2$phi^{3+} and Δ-Rh(TMP)$_2$phi^{3+} may be attributed to the Λ-isomer. It is particularly noteworthy that the largest difference between the enantiomers of this complex in the observed photoproducts occurs at G17 of the AG mismatch. As observed with Rh(phen)$_2$phi^{3+}, the Δ-enantiomer produces relatively more of the 3'-phosphate end whereas the Λ enantiomer produces relatively less. Therefore, it may be inferred that the structure immediately surrounding the AG mismatch better complements the shape of the right-handed isomer of Rh(TMP)$_2$phi^{3+}. The enantioselective cleavage at neighboring G18 by Rh(phen)$_2$phi^{3+} also supports the right-handed helicity of the DNA structure in the vicinity of the mismatch.

Although similar in structure, Rh(phen)$_2$phi^{3+} and Rh(TMP)$_2$phi^{3+} do display differences in recognition of properly matched DNA in the context of long DNA strands. On the fragment studied, Rh(TMP)$_2$phi^{3+} shows a greater extent of cleavage than does Rh(phen)$_2$phi^{3+} at a number of sites, but a reduction at another site. These observations

indicate that having several methyl groups can increase affinity for sites not recognized by the parent complex; however, these same methyl groups also inhibit binding at other sites due to steric hindrance. A future avenue of investigation would involve examining photocleavage by $Rh(TMP)_2phi^{3+}$ on mismatches in the context of a long strand of DNA. Under conditions of lower concentration, it is possible that $Rh(TMP)_2phi^{3+}$ could preferentially recognize a mismatch in a particular sequence context.

3.4.2. Implications for DNA Repair

Little is understood about the structural and dynamic basis for DNA mismatch repair. One area which has been explored has involved examining the thermodynamic stability of oligonucleotide duplexes containing various mismatches, in an attempt to make correlations between stability of structure and repair efficiency. This type of study was performed[24] on oligonucleotides in a similar 5'-YXR-3' context as the K-*ras* oligonucleotides, where X is the mismatched base. It was demonstrated that, in broad terms, the higher the enthalpy of melting of a duplex containing a particular mismatch, the more efficiently the mismatch is repaired. Thus the overall trend for both stability and suitability as a repair substrate is Y·R > R·R > Y·Y. However, duplexes containing T·G and A·G mispairs have nearly identical melting temperatures, and additionally have nearly identical enthalpy and entropy of melting, as derived from base stack theory. The stability of single base mismatches has also been examined in the context of long DNA strands (>300bp) by temperature gradient gel electrophoresis[25]. For mismatches present in long DNA, it was discovered that, in all nearest neighbor sequence contexts, the TG and the AG mispairs were amongst the most stable. Therefore, the thermodynamic investigations of long DNA and oligonucleotides are completely consistent with one another. However, it is also known that TG mispairs are well repaired, whereas AG mispairs are poorly repaired[26]. Thus thermodynamic considerations in isolation can not

account for the differential repair of the TG and AG mismatches. There is likely to be an important structural aspect to mismatch repair as well.

GT mismatches and GA mismatches are not readily distinguished thermodynamically as both are structurally stable and can be incorporated within B form double helical DNA. It is interesting that the structural perturbations caused by mismatches in this context are often described as being slight. In the photocleavage studies described here, we see that seemingly small changes in structure can effect *consequential differences in recognition*. Metal complex probes of nucleic acid structure have elucidated differences in local DNA structure and have revealed that the GT mismatch has a much less destabilizing influence overall on DNA local structure than does the GA mismatch examined in the identical sequence context and under identical conditions. One explanation for the poor repair of AG mismatches invokes poor recognition by repair enzymes of the hydrogen bonding functionalities of this mispair. The studies described here show that metal complexes which do not rely upon hydrogen bonding for recognition are clearly able to recognize the altered structure in the vicinity of the mismatched bases via a shape selective mechanism. Therefore there remain two possible explanations for the poor repair of the AG mismatch. One possibility is that the AG mismatch lacks hydrogen bonding functionalities in the positions necessary for recognition by repair enzymes. Another possibility is that the type of mismatch-induced structural changes detected by metal complex intercalators serves to decrease the affinity of the repair enzyme for the sequence in the vicinity of the mismatch. The application of metal complex probes with and without hydrogen bonding functionalities to the study of DNA mismatches could help in differentiating the two possibilities.

References and Footnotes

1. Modrich, P. *Ann. Rev. Genet.* **1991**, *25*, 229-253.
2. Privé, G.G.; Heinemann, U.; Chandrasegaran, S.; Kan, L.-S.; Kopka, M.L.; Dickerson, R.E. *Science* **1987**, *238*, 498-238.
3. (a) de Vos, A.M.; Tong, L.; Milburn, M.V.; Matias, P.M.; Jancarik, J.; Noguchi, S.; Nishimura, S.; Miura, K.; Ohtsuka, E.; Kim, S.-H. *Science* **1988**, *239*, 888-893. (b) Tong, L.; de Vos, A.M.; Milburn, M.V.; Kim, S.-H. *J. Mol. Biol.* **217**, 503-516.
4. Nishimura, S.; Sekija, T. *Biochem. J.* **1987**, *243*, 313-327.
5. (a) Carbonnaux, C; van der Marel, G.A.; van Boom, J.H.; Guschlbauer, W.; Fazakerley, G.V. *Biochemistry* **1991**, *30*, 5549-5458. (b) Boulard, Y.; Cognet, J.A.H.; Gabarro-Arpa, J.; Le Bret, M.; Carbonnaux, C.; Fazakerley, G.V. *J. Mol. Biol.* **1995**, *246*, 194-208.
6. Cognet, J.A.H.; Boulard, Y.; Fazakerley, G.V. *J. Mol. Biol.* **1995**, *246*, 209-226.
7. (a) Chow, C.S.; Behlen, L.S.; Uhlenbeck, O.; Barton J.K. *Biochemistry* **1992**, *31*, 972-982. (b) Chow, C.S.; Hartmann, K.M.; Rawlings, S.L.; Huber, P.W.; Barton, J.K. *Biochemistry* **1992**, *31*, 3534-3542.
8. (a) Pyle, A.M.; Morii, T.; Barton, J.K. *J. Am. Chem Soc.* **1990**, *112*, 9432-9434. (b) Campisi, D.; Morii, T.; Barton, J.K. *Biochemistry* **1994**, *33*, 4130-4139.
9. (a) Sitlani, A.; Barton, J.K. *Biochemistry* **1994**, *33*, 12100-12108. (b) Sitlani, A.; Dupureur, C.M.; Barton, J.K. *J. Am. Chem. Soc.* **1993**, *115*, 12589-12590. (c) Pyle, A.M., Ph.D. Thesis, Columbia University, New York, 1989.
10. Krotz, A.H.; Kuo, L.Y.; Barton, J.K. *Inorg. Chem.* **1993**, *32*, 5963-5974.
11. Sitlani, A., Ph.D. thesis, California Institute of Technology, Pasadena, 1993.
12. David, S.D.; Barton, J.K. *J. Am. Chem Soc.* **1993**, *115*, 2984-2985.

13. Carruthers, M.H.; Barone, A.D.; Beaucage, S.L.; Dodds, D.R.; Fisher, E.F.; Mc Bride, L.J.; Matteucci, M.; Stabinsky, Z.; Tang, J.-Y. *Methods Enzymol.* **1987**, *154*, 287-313.

14. Pyle, A.M.; Chiang, M.; Barton, J.K. *Inorg. Chem.* **1990**, *29*, 4487-4495.

15. Enantiomers of $Rh(phen)_2phi^{3+}$ used in these experiments were provided by Drs. Cynthia Dupureur and Kevin Kingsbury. Racemic $Rh(dmbpy)_2phi^{3+}$ was donated by Ayesha Sitlani.

16. Maniatis, T.; Fritsch, E.F.; Sambrook, J. in *Molecular Cloning*; Cold Spring Harbor Laboratory Press: 1982 .

17. Krotz, A.H.; Hudson, B.P.; Barton, J.K. *J. Am. Chem. Soc.* **1993**, *115*, 12577-12578.

18. Sitlani, A.; Long, E.C.; Pyle, A.M.; Barton, J.K. *J. Am. Chem Soc.* **1992**, *114*, 2303-2312.

19. Chapter 2, this work.

20. (a) Gao, X.; Patel, D.J. *J. Am. Chem. Soc.* **1988**, *110*, 5178-5182. (b) Patel, D.J.; Kozolowski, S.A.; Ikura, S.; Itakura, K. *Biochemistry* **1984**, *23*, 3207-3217.

21. Brown, T.; Kennard, O.; Kneale, G.; Rabinovich, D. *Nature* **1985**, *315*, 604-606.

22. Mitra, R.; Pettitt, B.M.; Ramé, G.L.; Blake, R.D. *Nuc. Acids Res.* **1993**, *21*, 6028-6037.

23. Webster, G.; Sanderson, M.R.; Skelley, J.V.; Neidle, S.; Swann, P.F.; Li, B.F.; Tickle, I.J. *Proc. Natl. Acad. Sci., USA* **1990**, *87*, 6693-6697.

24. Werntges, H.; Steger, G.; Riesner, D.; Fritz, H.-J. *Nuc. Acids Res.* **1986**, *14*, 3773-3790.

25. Ke, S.H.; Wartell, R.M. *Nuc. Acids Res.* **1993**, *21*, 5137-5143.

26. (a) Dohet, C.; Wagner, R.; Radman, M. *Proc. Natl. Acad. Sci., USA* **1985**, *82*, 503-505. (b) Kramer, B.; Kramer, W.; Fritz, H.-J. *Cell* **1984**, *38*, 879-887. (c) Su, S.-S.; Lahue, R.S.; Au, K.G.; Modrich, P. *J. Biol. Chem.* **1988**, *263*, 6829-6835.

Chapter 4:

Shape-Selective Photocleavage of DNA Fragments by $Rh(phen)_2phi^{3+}$ and $Ru(TMP)_3^{2+}$

4.1. Introduction

An interesting problem in DNA structure, and how this structure may influence recognition, involves examining the conformational variations which occur along biologically relevant sequences. Additionally, some unique conformational features are only detectable in DNA above a certain length. However, the length of DNA sequences with biological relevance may be outside the range which can be handled by some biophysical techniques. Therefore, in order to examine the structure of DNA in the context of long DNA strands, enzymatic and chemical probes are required.

The Barton laboratory has developed transition metal complexes with useful properties as probes of nucleic acid solution structure. The two of the photoactive metal complexes which may be utilized in probing the structure of long DNA fragments are $Ru(TMP)_3^{2+}$ and enantiomerically resolved $Rh(phen)_2phi^{3+}$. The structures of these complexes are shown in Figure 4.1. Cleavage by $Ru(TMP)_3^{2+}$ is a reporter of minor groove width, and cleaves preferentially at regions with an A form structure. On the other hand, $Rh(phen)_2phi^{3+}$, unlike most other chemical and enzymatic structural probes, is a probe of major groove structure. Specifically, $Rh(phen)_2phi^{3+}$ cleaves at sites which are opened in the major groove. The enantiomers of this complex additionally have distinct recognition properties which provide information concerning distinct local structural parameters in the major groove. Therefore $Rh(phen)_2phi^{3+}$ and $Ru(TMP)_3^{2+}$ are complementary in the information they provide about DNA sequence-dependent structure. Thus these complexes have been exploited in mapping the structure of DNA sequences which contain protein binding sites, including the 5S RNA gene[1].

Two examples of DNA which may be biologically relevant are homopolymeric

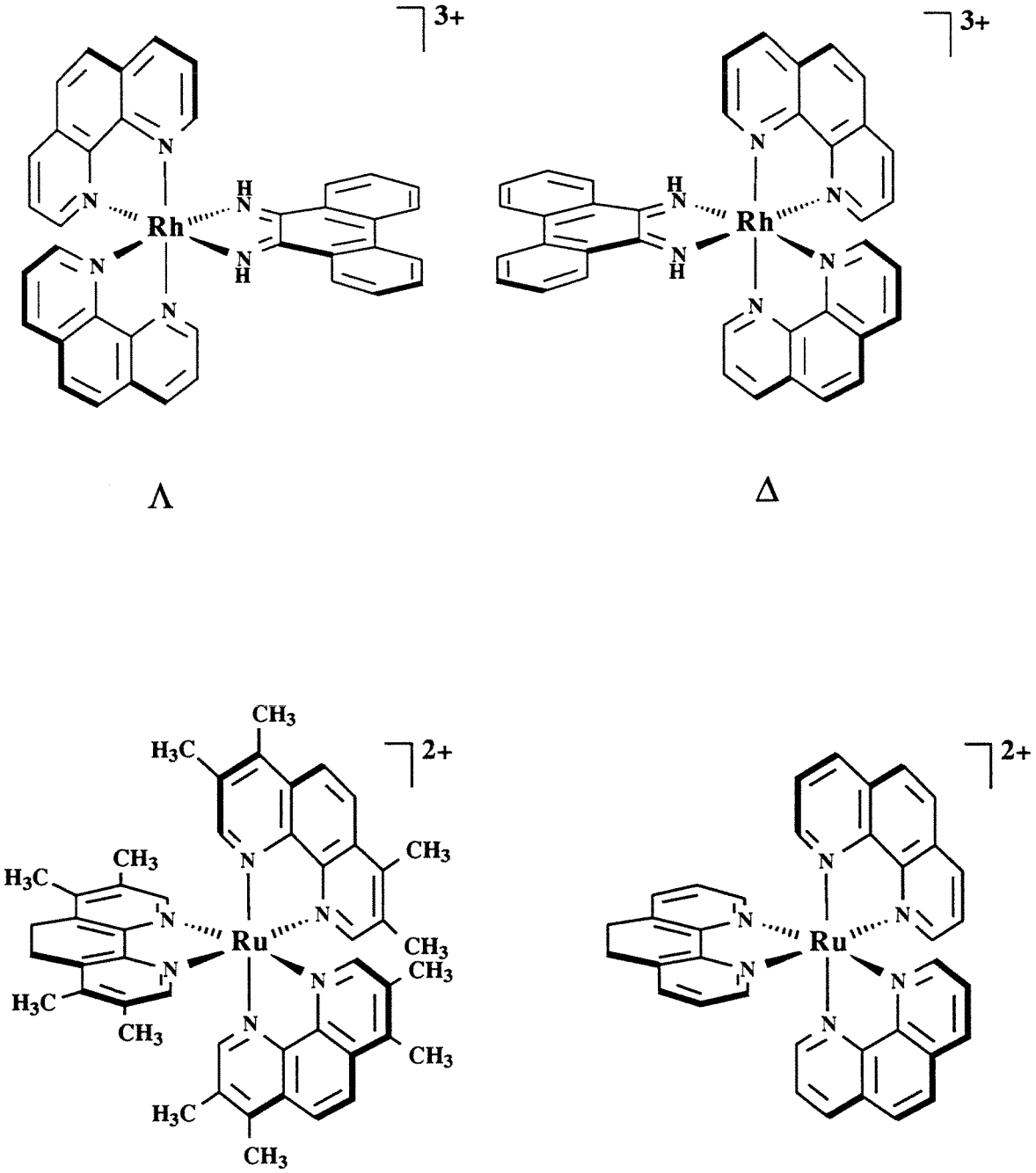

Figure 4.1. Structures of metal complexes used to examine DNA structure in the context of long fragments. (Top) The enantiomers of $Rh(phen)_2phi^{3+}$. (bottom) $Ru(TMP)_2phi^{3+}$ and $Ru(phen)_3^{2+}$.

stretches of guanines and adenines. Although long runs of guanines (>10) are not typical of naturally occurring DNA, they are found approximately 11 times more often than would be predicted statistically[2]. Additionally, many binding sites for zinc finger proteins are known to have one strand which is guanine-rich. The biological role for DNA containing A tracts is as yet uncertain, although it has been proposed to be important for the positioning of nucleosomes on DNA[3]. Sequences containing A_n tracts in phase with the helical repeat of DNA have been found to have reduced electrophoretic mobility. This anomaly is due to DNA bending. One model of bent DNA is shown in Figure 4.2. One remarkable property about sequences containing A tracts is that even seemingly closely related sequences can show different macroscopic bending properties. The most striking examples are the $(AAAATTTTCG)_n$ and $(TTTTAAAACG)_n$ multimers, which were shown by electrophoretic mobility methods to have bent and straight structures respectively[4]. Although A tracts have been studied by a wide variety of biophysical and biochemical methods, the exact nature of their structure, and how they contribute to DNA bending is still a matter of some controversy[5].

In this chapter, both G-rich stretches and A-rich stretches in the context of long DNA strands are examined by $Rh(phen)_2phi^{3+}$ enantiomers and $Ru(TMP)_3^{2+}$. Specifically, one fragment of interest contains the sequence 5'-TATA$(G)_7$TATA-3'. Photocleavage results by these complexes on this G stretch are consistent with a model for heteronomous DNA. Additionally, the $(A_4T_4CG)_n$ and $(T_4A_4\ CG)_n$ bent and nonbent multimers have been probed. Some structural features of these sequences will be discussed, and several models describing sequence-directed DNA bending will be considered.

4.2. Experimental

Materials. $Ru(TMP)_3^{2+}$ and Δ- and Λ-$Rh(phen)_2phi^{3+}$ were synthesized as described[6]. Restriction endonucleases *Hin*dIII and *Pvu*II, terminal deoxynucleotidyl

Figure 4.2. A model of a bent DNA structure. This model was derived from molecular mechanics. Figure from Reference 7.

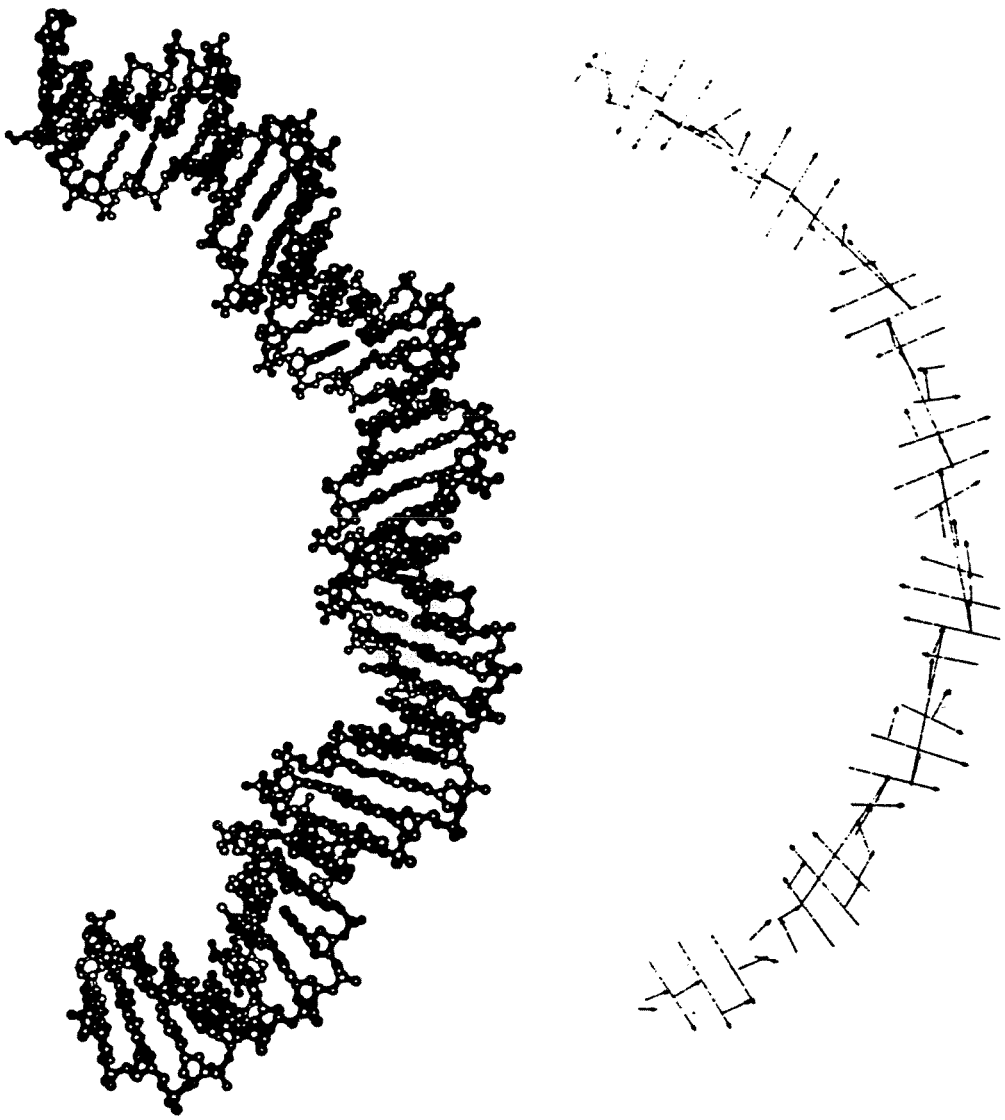

transferase, and T4 polynucleotide kinase were from Boehringer Mannheim; competent cell line DH5α was purchased from BRL. α-^{32}P-3'-dATP and γ-^{32}P-ATP were purchased from NEN. Oligonucleotides were synthesized on a Pharmacia-LKB Gene Assembler; cyanoethyl amidites were from Pharmacia. Plasmid pUC18 derivatives containing $(CGAAAATTTT)_5$ or $(CGTTTTAAAA)_5$ were kindly provided by Prof. T. D. Tullius.

Preparation of Labelled DNA fragments. A 18 base pair oligonucleotide insert, 5'-ATAT$(C)_7$ATAT-3' and its complementary strand, and 5'-TATA$(G)_7$TATA-3' were synthesized by standard automated methods, and purified by reverse phase C18 chromatography. To clone the insert, the 18 base pair duplex was ligated in the presence of Sma I-cleaved vector pUC18.[8] *E. coli* (DH5α) was transformed with the ligation mixture and plated on ampicillin plates. The resulting plasmids bearing a single copy of the insert were isolated by a modification of standard alkaline-lysis method. The nucleotides were numbered according to the parent plasmid pUC18, and the insert is positioned between the positions 436 and 437. Plasmid pJT18/C7 or /G7 DNA was digested with *Hind* III, then 3'-end-labelled with [α-^{32}P]-3'-dATP by using terminal deoxytransferase according to the company procedure. A second enzymatic digest, with *Pvu* II, yielded a 3'-end-labelled fragment 246 bp in length, containing the 18 base pair insert. This restriction fragment was isolated by nondenaturing polyacrylamide gel electrophoresis, followed by an electric elution. The isolated fragment was ethanol precipitated, with a 0.3M final concentration of sodium acetate. Digestion of pJT18/C7 with *Hind* III and subsequent treatment with calf intestine phosphatase, γ-^{32}P-dATP and T4 polynucleotide kinase, then *Pvu* II, yielded the 5'-end-labelled 245-bp fragment. 5'- and 3'-end-^{32}P-labelled fragments from the plasmid containing $(CGAAAATTTT)_5$ or $(CGTTTTAAAA)_5$ insert were obtained as described[9].

Photoreaction of 5'- and 3'-endlabelled DNA fragments with $Rh(phen)_2(phi)^{3+}$. Samples for irradiation contained ^{32}P-end-labelled fragment, 80 μM (nt) sonicated calf thymus DNA, and 25 mM sodium cacodylate buffer (pH 7.0). Samples prepared either

with or without 5 μM metal complex in final concentration. Irradiation was accomplished with 1000 W Xe/Hg lamp equipped with a monochrometer, at 313 nm for 40 seconds at ambient temperature. Subsequently, each reaction mixture was ethanol precipitated twice with 2.5 M ammonium acetate in final concentration, rinsed with 80% ethanol, and dried *in vacuo*. The resulting pellet was redissolved in 4 μL of 80% formamide/10 mM NaOH/1 mM EDTA dye, heat denatured, chilled on ice, then loaded onto 8% denaturing polyacrylamide sequencing gel containing 8.3 M urea. Chemical sequencing markers[10] were coelectrophoresed in adjacent lanes to determine the position of the nicks generated by the metal complexes. Autoradiography of the gels was carried out on Kodak, X-Omat AR film, and autoradiograms were then scanned with an LKB 2202 Ultrascan laser densitometer, equipped with a GelScan XL software.

Photoreaction of $Ru(TMP)_3^{2+}$ and $Ru(phen)_3^{2+}$ with 5'- and 3'- end labelled fragments. Fragments were endlabelled and isolated as described above. Samples contained final concentrations of 25mM sodium cacodylate buffer, 15 μM ruthenium complex and 100μM calf thymus DNA, for a nucleotide:metal ratio of 6:1 in a total reaction volume of 20μL. Reactions and controls also contained 1.2 mM histidine, which is usually added to the reactions using $Ru(TMP)_3^{2+}$. Histidine may serve as a solubilizing agent for this compound. Samples with and without ruthenium complex were irradiated by laser at 442nm, for 15 minutes. Ethanol precipitation was performed twice, as described above, and pellets rinsed with 80% ethanol, and dried. Subsequently the samples were treated with 100μL of 1M piperidine, and heated to 90°C for 30 minutes, and lyophilized. In order to remove the piperidine before loading to the gel, samples were resuspended in 50μL water and lyophilized twice more. Loading and autoradiography was the same as for the rhodium-reacted samples. Cleavage probabilities were determined from the results of the densitometric scan , corrected for the differential base reactivity of singlet oxygen by subtraction of $Ru(phen)_3^{2+}$ reactivity[11].

One experimental difficulty involved spurious cleavage of DNA in the controls of the C7 and G7 plasmid experiments which were not exposed to metal complex or light. Four very dark bands appeared in this control, in the region of the insert, making it difficult to analyze the cleavage patterns in the reaction lanes. This happened only on the 3' end labelled strand with both plasmids, and more strongly when the run of C's was on the 3' side. It was finally concluded that it was either some endonucleolytic activity of the terminal deoxytransferase or a contaminant in it which was responsible for the DNA cleavage[12].

4.3. Results and Discussion

4.3.1. Cleavage on Restriction Fragments with C7·G7 Inserts

The C7·G7 plasmid was probed with both $Rh(phen)_2phi^{3+}$ and $Ru(TMP)_3^{2+}$. An experiment utilizing racemic $Rh(phen)_2phi^{3+}$ at two different concentrations, and as a function of three different salt concentrations, is shown in Figure 4.3. For all lanes, it can be observed that $Rh(phen)_2phi^{3+}$ cleaves strongly on the C strand of the C7·G7insert, with the cleavage on the G7 strand very light by comparison. Additionally, at both metal complex concentrations (5μM and 20μM), it appears that salt lowers the overall intensity of the photocleavage. However, the relative intensities of cleavage at most sites stays the same. On the other hand, the site distribution of the C stretch does depend upon the concentration of $Rh(phen)_2phi^{3+}$ used. The cleavage in the C strand increases in intensity in the 5' to 3' direction for the lower concentration of metal complex, and in the 3' to 5' direction for the higher concentration of metal complex. This same concentration dependent cleavage pattern was also observed in the plasmid which had the insert oriented in the other direction. Perhaps the DNA conformation is somehow altered by the metal complex at high concentrations of $Rh(phen)_2phi^{3+}$. A plasmid with this insert was also examined by the enantiomers of $Rh(phen)_2phi^{3+}$ (data not shown). The C stretch is cleaved well by both enantiomers of this complex. This low level of enantiomeric

Figure 4.3. Autoradiogram showing cleavage by racemic $Rh(phen)_2phi^{3+}$ as a function of metal complex and salt concentrations, on 5'- and 3'-endlabelled fragments containing a C7·G7 insert. All samples were 25μM in sodium cacodylate buffer, pH=7.0. NaCl was added where noted. Lanes 1 and 20 and lanes 2 and 19 show DNA in the absence of metal and light and DNA irradiated in the absence of metal, respectively. Lanes 3 and 18 contain 5μM $Rh(phen)_2phi^{3+}$; lanes 4 and 17 contain 20μM metal complex; lanes 5 and 16 contain 5 μM metal complex and 1.25 mM NaCl; lanes 6 and 15 contain 20μM $Rh(phen)_2phi^{3+}$ and 1.25mM NaCl; lanes 7 and 14 contain 5 μM metal complex and 2.50mM NaCl; lanes 8 and 13 contain 20μM $Rh(phen)_2phi^{3+}$ and 2.5mM NaCl. Lanes 9 and 12 and lanes 10 and 11 are Maxam Gilbert G+A and C+T reactions, respectively.

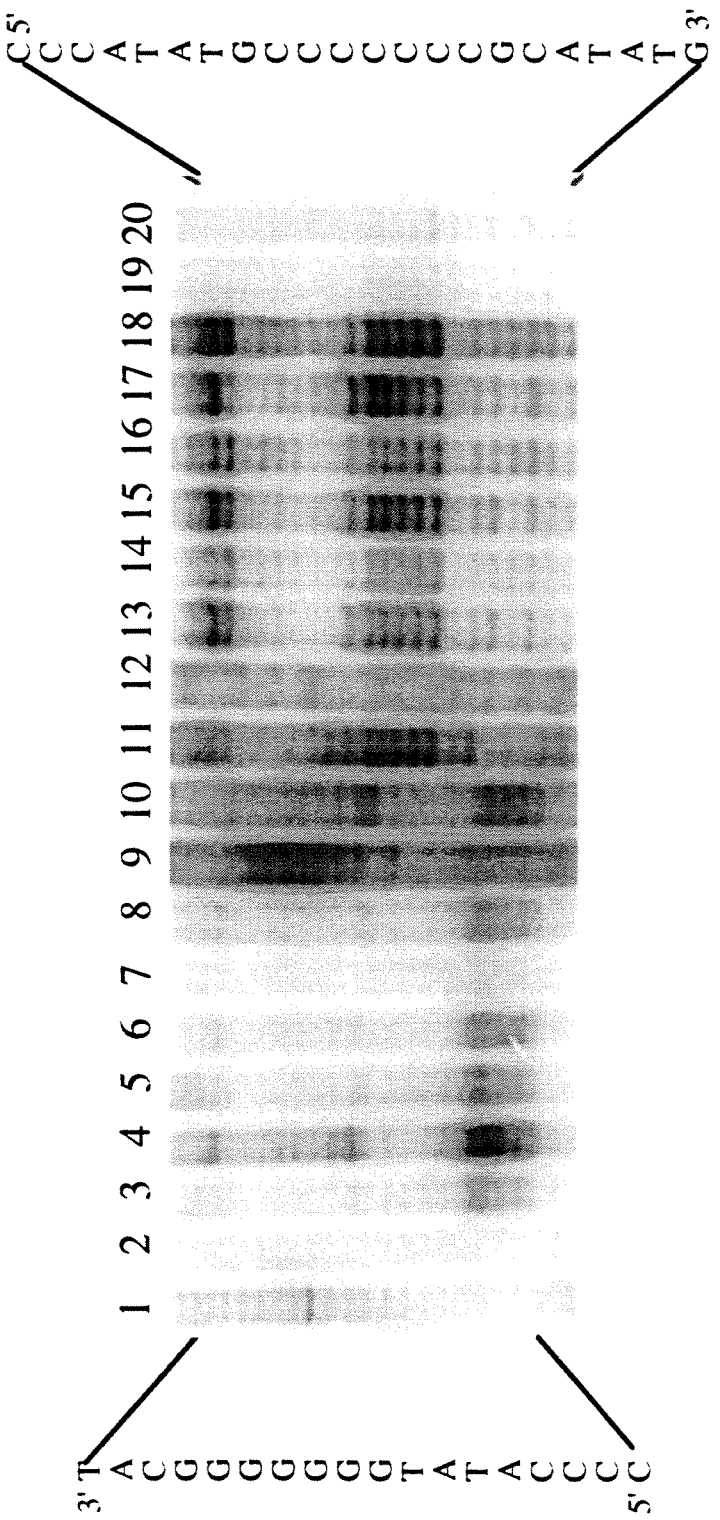
5' C C C A T A T G C C C C C C C C G C A T A T G 3'
1 2 3 4 5 6 7 8 9 10 11 12 13 14 15 16 17 18 19 20
3' T A C G G G G G G G T A T A C C C C 5'

discrimination is consistent with results which have been reported earlier[13], and is to be expected since these 5'-YY-3' steps do not have an axis of dyad symmetry.

The C7·G7 insert-containing fragment was also cleaved by $Ru(TMP)_3^{2+}$ and $Ru(phen)_3^{2+}$. Since the reaction mechanism of both these metal compounds involves a singlet oxygen mediated attack at guanines, $Ru(phen)_3^{2+}$ is used as a reaction control. As described in Chapter 1, sites at which there is relative more cleavage by $Ru(TMP)_3^{2+}$, as compared with $Ru(phen)_3^{2+}$, are likely to possess an A form structure. The differences between these complexes are shown in Figure 4.4. It can be seen that the cleavage for the C7 strand is higher for $Ru(TMP)_3^{2+}$ than for $Ru(phen)_3^{2+}$. However, in contrast to $Rh(phen)_2phi^{3+}$, $Ru(TMP)_3^{2+}$ cleaves the stretch relatively evenly. On the G-rich strand the $Ru(phen)_3^{2+}$ cut slightly more than the $Ru(TMP)_3^{2+}$.

4.3.2. Photocleavage On C7·G7 Stretches Is Consistent with a Heteronomous DNA Structure

It is interesting that for the homopolymeric stretch of the C7·G7 plasmid insert, the pyrimidine strand is strongly cleaved by $Rh(phen)_2(phi)^{3+}$, *and* preferentially by $Ru(TMP)_3^{2+}$ over $Ru(phen)_3^{2+}$. This combination of results is somewhat unexpected in that these metal complexes might appear to target different types of nucleic acid structures. $Rh(phen)_2phi^{3+}$, which binds by intercalation in an open major groove, does not recognize the narrow and deep major groove of A form double helices[14]. On the other hand, $Ru(TMP)_3^{2+}$ engages in a surface bound interaction in the minor groove, and as such can sense differences in groove width along the helix, favoring the wider A form. A structure that could be consistent with patterns of cleavage by both metal complexes is one in which the major groove is wide and the minor groove is also wide. One example of this type of DNA structure occurs when the two strands have different conformations. The term for this kind of structure is called heteronomous DNA, inferred from fiber diffraction studies of poly dA·poly dT [15], and other homopolymeric sequences. This structure is shown in

Figure 4.4. Autoradiogram showing cleavage by racemic $Ru(TMP)_3^{2+}$ and $Ru(phen)_3^{2+}$ on 5'- and 3'-endlabelled fragments containing a C7·G7 insert. Lanes 1 and 10 and lanes 2 and 9, are Maxam-Gilbert G and C+T reactions respectively. Lanes 3 and 8 are samples irradiated with no metal complex. Lanes 4 and 7 were irradiated in the presence of $Ru(TMP)_3^{2+}$. Lanes 5 and 6 were irradiated in the presence of $Ru(phen)_3^{2+}$. Conditions for the experiment are as described in the text.

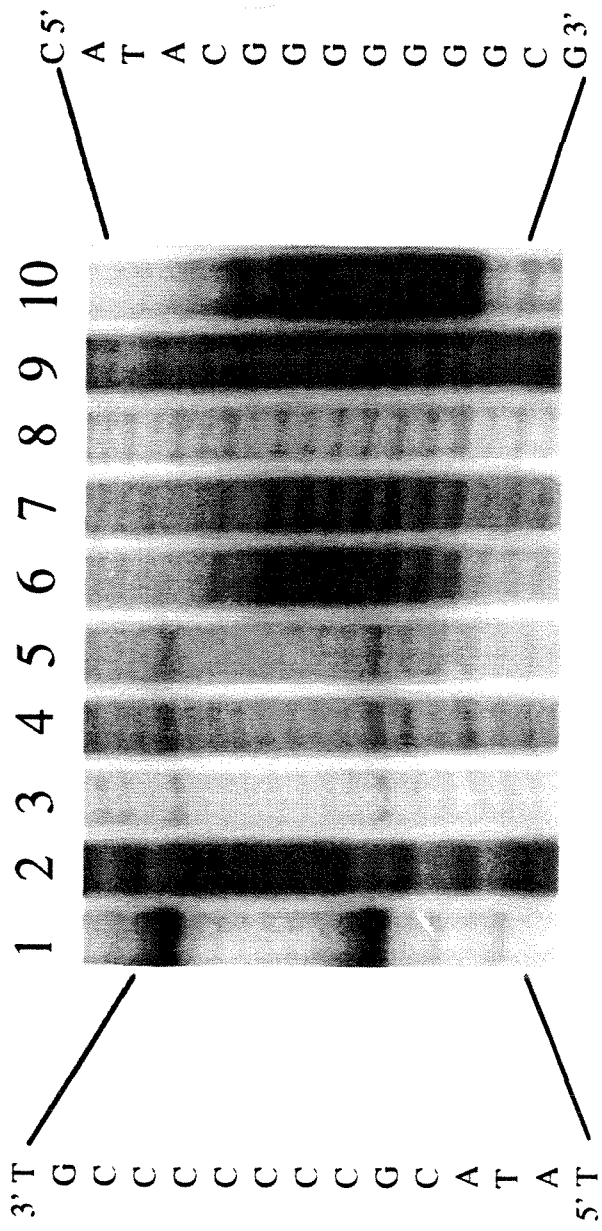
C 5'
A
T
A
C
G
G
G
G
G
G
G
C
G 3'
1 2 3 4 5 6 7 8 9 10
3' T
G
C
C
C
C
C
C
C
C
G
C
A
T
A
5' T

Figure 4.5. A model for heteronomous DNA, derived from fiber diffraction studies. It may be observed that in this model of DNA structure, contrary to the canonical A and B forms of DNA conformation, *both* the major groove and the minor groove are wide. Figure is from Reference 15.

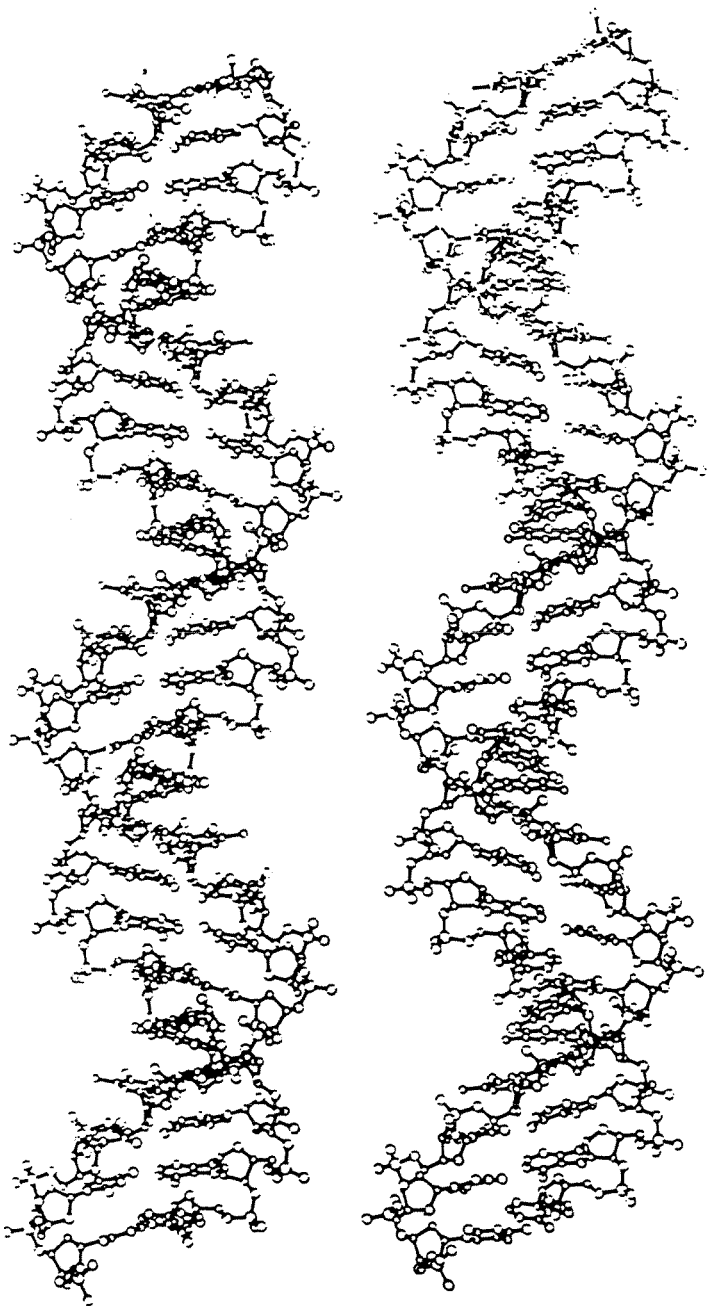

Figure 4.5.

In order for DNA base pairs to hydrogen bond correctly, the most strict constraint in double helical structure is that the phosphate-phosphate distances be within the range from 5.8-7.0 Å. This constraint still allows for variation in structure between the strands, since the phosphate torsional angles may change considerably without causing undue strain on the backbone. Differences in phosphate torsional angles may be compensated for by displacement of the bases on one strand away from the helical axis. These different phosphate angles correspond to different sugar puckering as well. A large angle is consistent with a $C_{2'}$-*endo* sugar conformation, whereas a smaller phosphate torsional angle is consistent with a $C_{3'}$- *endo* sugar conformation. The former is associated with B DNA and the latter is associated with A DNA. If these differing phosphate angles are consistently maintained for each strand, the result is that one strand appears to be structurally quite different from the other, without any disruption in the base pairing. In the model for heteronomous DNA, it is the pyrimidine strand which is being displaced from the helical axis, and has the B-like structure, whereas the purine strand has the A-like structure.

The photocleavage by both $Ru(TMP)_3^{2+}$ and $Rh(phen)_2phi^{3+}$ at the C_7 stretch in the context of long DNA argues for this type of model. The minor groove in this model is wide enough for the complex which cleaves at wide minor grooves. Additionally, if base stacking is present on the guanine-rich strand, then perhaps the stacking energy that would be gained by the intercalation of $Rh(phen)_2phi^{3+}$ would stabilize an interaction for $Rh(phen)_2phi^{3+}$ near the pyrimidines, allowing cleavage to preferentially occur on the pyrimidine strand. The abstraction of the C3' hydrogen atom has been shown to be the mechanism of cleavage by $Rh(phi)^{3+}$ complexes[16]. It might be therefore be argued that the $C_{3'}$-*endo* sugar puckering present on the purine strand in such a structure could favor the abstraction of the C3' hydrogen of the purines. However, it is not absolutely certain that it is the purine strand which adopts the A form, as fiber diffraction does not distinguish

between purine and pyrimidine bases. Additionally, sugar puckering is one of the DNA structural features which is likely to be changed upon intercalation. Therefore the photocleavage observed here is still consistent with this heteronomous model.

Cleavage by other probes of DNA structure has also been consistent with a heteronomous model for purine stretches. It is interesting that long G stretches, which do not alternate with Cs, have been shown to be resistant to cleavage by DNase I[17]. On the other hand, DNaseII, whose cleavage preferences are complementary to those of DNase I, cleaves very strongly on the G-rich strand of these stretches, and not at all on the C-rich strand. These preferences for DNaseII cleavage, although directly in opposition to those of the metal complexes examined here, may also be explained in terms of a heteronomous model of DNA structure[17]. In the heteronomous model, the phosphate-phosphate distances are at two extremes for the different strands; they are shorter for the purine strand than the pyrimidine strand. Therefore, if the structural feature that DNase II recognizes is the conformation of the DNA sugar-phosphate backbone, it would be expected that one strand would be cleaved preferentially to the other, and, indeed even to DNA composed of mixed sequences.

In summary, both $Rh(phen)_2phi^{3+}$ and $Ru(TMP)_3^{2+}$ have been shown to recognize the C-rich strand of a C7·G7 stretch. $Rh(phen)_2phi^{3+}$ shows concentration-dependent differences in site selection within the stretch, whereas $Ru(TMP)_3^{2+}$ appears to cleave the stretch fairly evenly. Both Δ- and Λ- $Rh(phen)_2phi^{3+}$ show the same preference for the C-rich stretch as compared with other sites, and the level of enantioselectivity is low. Finally, the results obtained here are consistent with a heteronomous model of DNA, in which the structures of the two strands are substantially different in regard to phosphate conformation and base displacement, resulting in wide major and wide minor grooves.

4.3.3. Photocleavage by Rh(phen)$_2$phi^{3+} on Fragments Containing A_4T_4 and T_4A_4-Tracts.

Fragments with $(A_4T_4CG)_n$ and $(T_4A_4CG)_n$ inserts were examined by the enantiomers of Rh(phen)$_2$phi^{3+}. As described above, the former correspond to DNA which is macroscopically bent, and the latter correspond to sequences which are nonbent. Gels showing the cleavage by these enantiomers on 3'-endlabelled fragments are shown in Figure 4.6 and Figure 4.7. In all cases, the same results were also obtained on 5'-endlabelled DNA (results not shown). Generally speaking, it is clearly observed that the cleavage pattern for Rh(phen)$_2$phi^{3+} is distinct for the two different types of DNA structures. For Δ-Rh(phen)$_2$phi^{3+}, on the 5'-A_4T_4CG-3' fragment, there is strong cleavage at the sequence 5'-TCGA-3'. There is considerable selectivity in cleavage over that of the Λ enantiomer at this site. The enantioselectivity in cleavage at this 5'-YYRR-3' step is completely consistent with cleavage by Δ-Rh(phen)$_2$phi^{3+} on other sequences of this type[18]. There is no strong cleavage within the A tract; however, not all positions of the A tract are cleaved to the same extent. These subtle differences in the cleavage of the A tract of this A_4T_4 sequence were also previously observed with racemic Rh(phen)$_2$phi^{3+}[19]. Here it is observed that there is not a high level of enantioselection in either position or intensity of cleavage within the A tracts which determine the structure of bent DNA. This low level of enantioselectivity in cleavage has also been previously observed for 5'-YY-3' steps, which have no C_2 dyad axis with which to discriminate the symmetry of the metal complex[13].

The cleavage distribution on the fragment containing the $(T_4A_4CG)_n$ insert differs significantly. A gel showing the cleavage on the 3'-endlabelled fragment is also shown in Figure 4.7. Again, the same results were obtained on the 5'-endlabelled fragment (data not shown). It may be seen for this sequence, which is not bent-inducible, there is strong cleavage by Δ-Rh(phen)$_2$phi^{3+} at the second and third T of the T_4 tract. Moderate cleavage by this enantiomer is observed at the fourth T of the T_4 tract and at 5'-ACGT-3'. For the

Figure 4.6. An autoradiogram showing cleavage by enantiomers of $Rh(phen)_2phi^{3+}$ on a 3'-endlabelled fragment containing $(A_4T_4CG)_n$ multimers. Lanes 1 and 2 show Maxam-Gilbert G+A and C+T reactions respectively. Lane 3 shows fragment in the absence of irradiation and metal. Lanes 4, 5, and 6 show photocleavage reactions by racemic, Λ- and Δ-$Rh(phen)_2phi^{3+}$, respectively. Lane 7 shows fragment irradiated in the absence of metal complex.

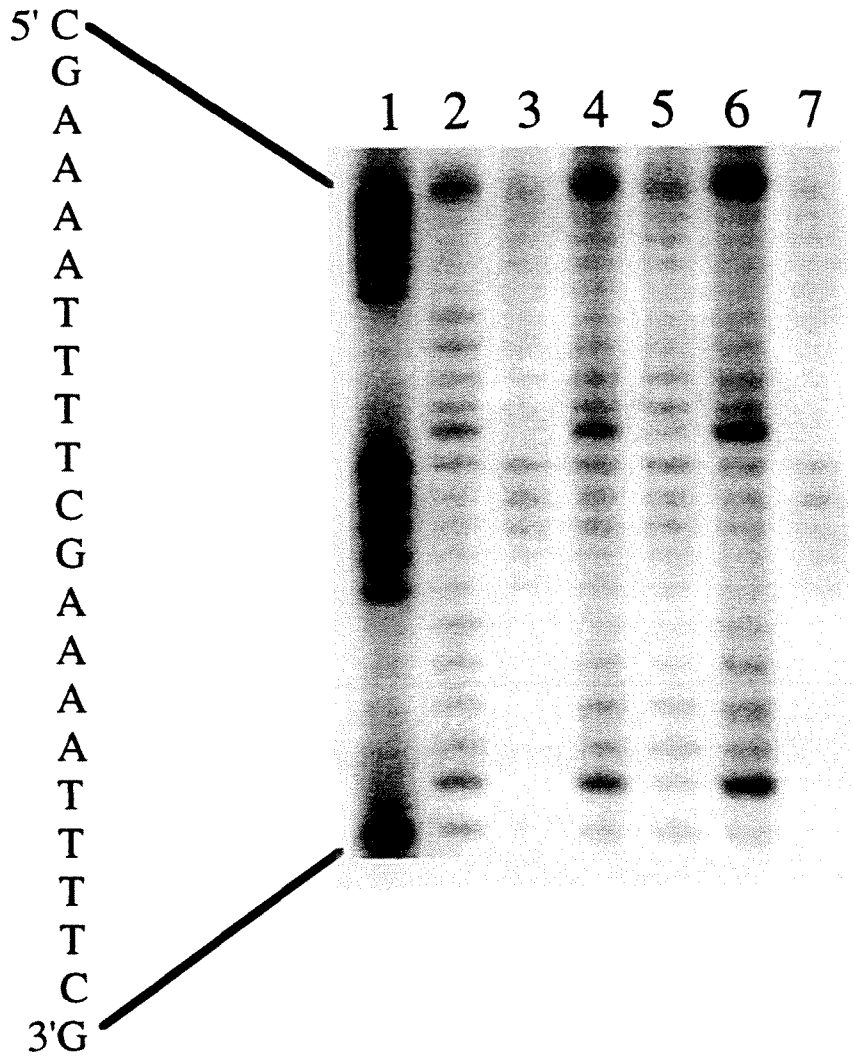
5' C
G
A
A
A
A
T
T
T
T
C
G
A
A
A
A
T
T
T
T
C
3'G
1 2 3 4 5 6 7

Figure 4.7. An autoradiogram showing cleavage by enantiomers of $Rh(phen)_2phi^{3+}$ on a 3'-endlabelled fragment containing $(T_4A_4CG)_n$ multimers. Lanes 1 and 2 show Maxam-Gilbert G+A and C+T reactions respectively. Lane 3 shows fragment in the absence of irradiation and metal. Lanes 4, 5, and 6 show photocleavage reactions by racemic, Λ- and Δ-$Rh(phen)_2phi^{3+}$, respectively. Lane 7 shows fragment irradiated in the absence of metal complex.

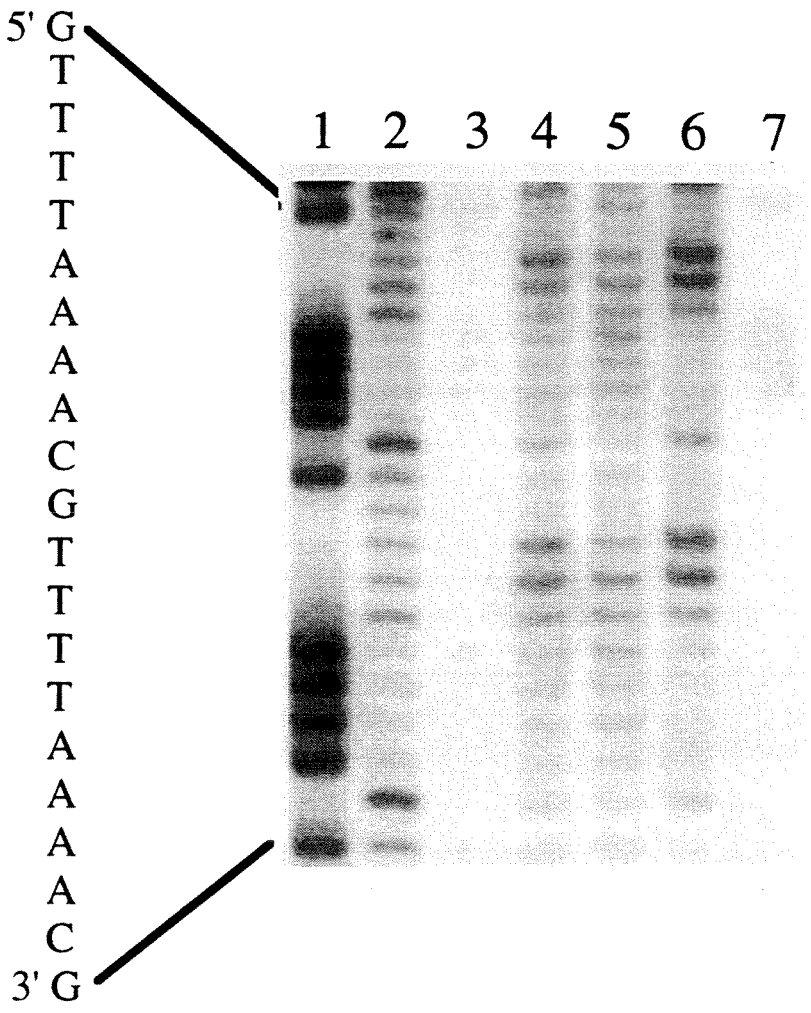
5' G
T
T
T
T
A
A
A
A
C
G
T
T
T
T
A
A
A
A
C
3' G
1 2 3 4 5 6 7

Λ-isomer of this complex, moderate cleavage is observed from the second T of the T_4 tract to the third A of the A_4 tract. Of these moderate sites, the cleavage is the strongest at the third T of the T tract. Therefore, the enantioselectivity in cleavage by Δ-Rh(phen)$_2$phi^{3+} over the Λ-isomer is strongest at T_2, and intermediate at T_3 and at 5'-ACGT-3'[20]. Interestingly, it appears that the first three A's of the A tract may be cleaved preferentially by the *Λ* -isomer. Therefore the photocleavage on the bent and nonbent sequences differs in cleavage position and in the observed enantioselectivity at sites within the AT-rich tract.

Interestingly, results obtained with Ru(TMP)$_3^{2+}$ on the A_4T_4CG sequence show a lower extent of cleavage than that of the parent compound Ru(phen)$_3^{2+}$. The difference in cleavage between the two complexes exhibits a repeated, periodically changing pattern, with cleavage by Ru(TMP)$_3^{2+}$ being relatively the highest at the third A, and lowest at the third T[21,22]. The pattern of exclusion of Ru(TMP)$_3^{2+}$ may be interpreted as a minor groove width which is compressed relative to that of B form DNA at this site. This photocleavage result corroborates studies performed with hydroxyl radical[21], and with NMR studies[23] which indicate a progressive narrowing of the minor groove of A tracts in the 5'-> 3' direction. However, this narrowing of the minor groove is also detected, to a smaller extent, by Ru(TMP)$_3^{2+}$ for the T_4A_4CG sequence. The positioning is different for this sequence, with the cleavage being the highest at the first A and lowest at the fourth A.

4.3.4. Models for Intrinsically Bent DNA Structure

The detailed structure of bent DNA is still a subject of some controversy. One problem in the study of bent DNA has been that, although the bent DNA is composed of relatively small sequence elements, a macroscopic bend is only realized after these elements have been repeated many times. Therefore, crystallographic studies which focus on a small sequence element may not be truly reflective of the solution structure of bent DNA. On the other hand, NMR has not been useful in determining a detailed three-

dimensional global view of bent DNA, although some local structural details have been elucidated.

Based upon evidence obtained by crystallographic, NMR, chemical probing, and gel electrophoresis methods, there have been a number of models which have been proposed for the structure of bent DNA. The first model is the junction model[24]. In this model, the A tracts of DNA are thought to be in the A form. Therefore, bends are created at the junctions between these A tract regions and adjoining regions which have a normal B form DNA conformation. In the junction model, the A tract is considered as a whole. In the wedge model of bent DNA structure[3,25], the bend is described in terms of a summation of the structures of dinucleotide steps of the A tract and adjoining regions of DNA. The structure of each step is described in terms of its roll or tilt wedge angles. In this model, bent DNA is described as having a smooth, curved structure, with the bend distributed over a number of base pairs. These models differ in that for the wedge model, each AA step is considered to be the same, whereas in the junction model, the structure of an AA step can vary depending on the surrounding sequence. It should be noted, however, that the wedge model and junction model are in fact similar[26], in that they both attribute bending of the helical axis to changes in base pair inclination.

Another model for bent DNA, derived from crystallographic studies of A tracts, is the non A tract bending model[27]. In this model, the A tracts are highly propeller twisted, and have inclination angles which closely resemble that of B form DNA. Accordingly, the structure of these A tracts is not dependent upon their sequence context. As implied by the name of this model, the source of the macroscopically measured bend of DNA results from sequences which are outside the A tract.

In yet another model, which may be termed the A tract bending model, the macroscopic bending of DNA is composed of A tracts which have a bent structure, and alternate with DNA which does not have a bent structure in phase with the helical repeat.

Therefore, the nonbent A tract bending model and the A tract bending model are at two logical extremes, and both differ from the junction/wedge model.

Our results are consistent with some of the observations made by crystallography, and with some aspects of the non A tract bending model. As defined by crystallography, all the bases in the A tracts are highly propeller twisted. This signifies that there is not a great degree of *differential* propeller twisting in the A tracts. This similarity in propeller twisting is consistent with 1) cleavage at sites in the A tract being distributed relatively evenly and 2) the small amount of enantiomeric discrimination observed in the A tract for the bent DNA sequence. Additionally, according to the non A tract bending model, the 5'-TA-3' step, and 5'-CG-3' step have a positive roll angle, which compresses the major groove, causing a local bend in the DNA. These bends are out of phase for the T_4A_4CG sequence but are in phase for the A_4T_4CG sequence. It is interesting that the cleavage that we see with Δ-Rh(phen)$_2$phi^{3+} is only moderate at these sequences in comparison with strong cleavage at the 5'-YY-3' steps for the T_4A_4 sequence. Specifically, the enantioselectivity is smaller at the 5'-T*T*AA-3' and 5'-A*C*GT-3' steps than at the second and third thymines in the T_4 tract. This behavior differs significantly from previously made observations about enantioselectivity. Perhaps the roll angle is closing down the major groove, inhibiting binding by the Δ enantiomer at this site. The Λ- enantiomer is not affected as much by this closing since it does not recognize preferentially the opening in the major groove defined by differential propeller twisting[28]. The aforementioned cleavage results are consistent with a non A tract model. However, the strong enantioselective cleavage at 5'-T*C*GA-3' indicates that the major groove is open by differential propeller twisting which, in this sequence context, overrides any compression of the major groove via the roll angle.

There is no evidence from these photocleavage experiments that the angle of base pair inclination is changing dramatically between the A tract and non A tract regions for bent DNA, as described by the junction model. Although Δ-Rh(phen)$_2$phi^{3+} does cleave

strongly at the 5'-TCGA-3' site of the bent DNA sequence, as mentioned above, this cleavage is strongly enantioselective. The strong enantioselectivity in cleavage is indicative of a site which has a large degree of differential propeller twisting. A large opening due to tilt would be expected to be recognized equally by both enantiomers, as tilt is not C2 symmetric about the dyad axis.

It should be mentioned that these metal complexes probes may perturb DNA structure after binding. In particular, intercalators have been shown to remove bends from DNA[29]. However, it has been determined for Δ-$Rh(phen)_2phi^{3+}$ that photocleavage correlates with structural features of DNA which have been determined by crystallography in the *absence* of metal complex[18]. This observation is corroborated by results summarized below, which indicate that these metal complex probes are able to detect structural features of bent DNA which are observable by use of other chemical probes and other techniques of examining DNA structure.

In summary, photocleavage by shape selective metal complexes on A_4T_4CG and T_4A_4CG sequences is consistent with some previously observed *local* structural characteristics of bent DNA. Photocleavage by $Ru(TMP)_3^{2+}$ and $Ru(phen)_3^{2+}$ indicates a narrowing of the minor groove in these AT rich regions, as deduced from NMR and $Fe(EDTA)^{2-}$ experiments. Additionally, photocleavage by the enantiomers of $Rh(phen)_2phi^{3+}$ is consistent with an A tract which has a highly propeller twisted structure throughout. However, these results do not completely correlate with any one of the several models which attempt to describe the origin of the *global* bend of DNA. The reason for this lack of agreement is likely due to the fact that under differing conditions, different conformations may be adapted by the DNA. Additionally, the models tend to rely on the assumption that a particular sequence will have a certain structure *regardless of the surrounding sequence*. Here it is observed, with both major and minor groove structural probes, that the structure of different sequence elements *does* differ based upon its

sequence context. Thus models which ignore contextual effects are likely to oversimplify the complexity of DNA solution structure.

References and Footnotes

1. Huber, P.W.; Morii, T.; Mei, H.-Y.; Barton, J.K. *Proc. Natl. Acad. Sci., USA* **1991**, *88*, 10801-10805.
2. McCall, M.; Brown, T.; Kennard, O. *J. Mol. Biol.* **1985**, *183*, 385-396.
3. Trivonov, E.N.; Sussman, J.L. *Proc. Natl. Acad. Sci. USA* **1980**, *77*, 3816-3820.
4. Hagerman, P.J. *Nature* **1986**, *321*, 449-450.
5. Goodsell, D.S.; Kaczor-Grzeskowiak, M.; Dickerson, R.E. *J. Mol. Biol.* **1994**, *239*, 79-96.
6. Pyle, A.M.; Chiang, M.; Barton, J.K. *Inorg. Chem.* **1990**, *29*, 4487-4495.
7. Diekmann, S. in *Nucleic Acids and Molecular Biology*, vol. 1 Springer-Verlag, Berlin: 1987.
8. Uchida, K.; Pyle, A.M.; Morii, T.; Barton, J.K. *Nuc. Acids Res.* **1989**, *17*, 10259-10279.
9. Burkhoff, A.M.; Tullius, T.D. *Nature* **1988**, *331*, 455-457.
10. Maxam, A.M.; Gilbert, W. *Methods Enzymol.* **1980**, *65*, 499-560.
11. Mei, H.-Y.; Barton, J.K. *Proc. Natl. Acad. Sci., USA* **1988**, *85*, 1339-1343.
12. This same type of endonucleolytic activity by terminal deoxytransferase was also observed with the *Nar*I dodecamer, which is also GC-rich. Reported results are from gels with clear controls.
13. Pyle, A.M.; Morii, T.; Barton, J.K. *J. Am. Chem Soc.* **1990**, *112*, 9432-9434.
14. Chow, C.S.; Barton, J.K. *J. Am. Chem. Soc.* **1990**, *112*, 2839-2841.
15. Arnott, S.; Chandrasekaran, R.; Hall, I.H.; Puigjaner, L.C. *Nuc. Acids Res.* **1983**, *11*, 4141-4155.

16. (a) Pyle, A.M.; Long, E.C.; Barton J.K. *J. Am. Chem. Soc.* **1989**, *111*, 4520-4522. (b) Sitlani, A.; Long, E.C.; Pyle, A.M.; Barton, J.K. *J. Am. Chem Soc.* **1992**, *114*, 2303-2312.

17. Drew, H.R.; Travers, A.A. *Cell* **1984**, *37*, 491-502.

18. Campisi, D.; Morii, T.; Barton *Biochemistry* **1994**, *33*, 4130-4139.

19. Morii, T.; Barton, J.K., unpublished results.

20. A large amount of enantioselective cleavage by Δ-Rh(phen)$_2$phi^{3+} is observed on the sequence 5'A*C*GT-3' in the context of an oligonucleotide. This is discussed in Chapter 3.

21. Tullius, T.D. *Methods Enzymol.* **1992**, *212*, 219-242.

22. This changing cleavage pattern by Ru(TMP)$_3^{2+}$ on AT-rich DNA is in contrast to the relatively even cleavage pattern by this complex observed for the C7 stretch.

23. (a) Lipanov, A.A.; Churprina, V.P. *Nuc. Acids Res.* **1987**, *15*, 5833-5844. (b) Behling, R.W.; Kearns, D.R. *Biochemistry* **1986**, *25*, 3335-3346.

24. (a) Wu, H,-M.; Crothers, D.M. *Nature* **1984**, *308*, 509-513. (b) Selsing, E.; Wells, R.D.; Alden, C.J.; Arnott, S. *J. Biol. Chem.* **1979**, *254*, 5417-5422. (c) Levene, S.D.; Crothers, D.M. *J. Biomol. Struct. Dynam.* **1983**, *1*, 429-435.

25. Ulanovsky, l. E.; Trivonov, E.N. *Nature* **1987**, *326*, 720-722.

26. Crothers, D.M. Haran, T.E., Nadeau, J.G. *J. Biol. Chem.* **1990**, *265*, 7093-7096.

27. (a) Calladine, C.R.; Drew, H.R.; McCall, M.J. *J. Mol. Biol.* **1988**, *201*, 127-137. (b) Nelson, H.C.M.; Finch, J.T.; Luisi, B.F.; Klug, A. *Nature* **1987**, *330*, 221-226. (c) Maroun, R.C.; Olson, W.K. *Biopolymers* **1988**, *27*, 585-603.

28. Differential propeller twisting is defined as the angle between purine planes as projected onto the plane defined by the helical and dyad axes. This parameter is quantitatively defined in Chapter 3.

29. Barcelo, F.; Muzard, G.; Mendoza, R.; Révet, B.; Roques, B.P.; Le Pecq, J.-B. *Biochemistry* **1991**, *30*, 4863-4873.

Chapter 5:
Effects of $M(L)_2X^{n+}$ Complexes on the Electrophoretic Mobility of DNA: Influence of Intercalating Ligand, Charge, and Chirality

5.1. Introduction

The study of DNA electrophoretic mobility provides much information regarding its conformation, both in isolation and in the presence of DNA-binding molecules. An important application of this technique has been to the study of DNA with a bent conformation. Bent DNA shows markedly reduced mobility compared with nonbent DNA with the identical base composition. As few other techniques provide evidence of DNA bending in solution, reduced electrophoretic mobility has become perhaps the primary criterion for establishing whether a particular DNA fragment has a bent conformation.

Gel retardation is also commonly used to examine protein-DNA interactions. As proteins are usually large in molecular weight compared with the DNA fragments to which they are binding, and bind in a specific fashion, DNA-protein complexes have a migration which is distinct from that of free DNA. This fact has allowed the routine application of gel retardation to the determination of protein- DNA binding constants[1]. Additionally, information concerning binding kinetics[2], stoichiometries, and protein-induced conformational changes of DNA[3] may be obtained from examination of the electrophoretic mobility of DNA-protein complexes. Although attempts are in progress to quantitate such parameters as protein-induced helical twist changes[4] from gel electrophoretic mobility, the technique is presently better applied towards an understanding of DNA bending and flexibility rather than the acquisition of detailed structural information.

In addition to its utility for measurements of protein-DNA interactions, the gel mobility shift assay has also found use in the study of small molecule-DNA interactions. Insight has been gained regarding DNA conformational changes produced by agents which bind covalently, e.g., cis-platin[5] and psoralen[6]. Gel retardation has also been useful in examining noncovalently bound ligands. It was unanticipated that small molecules would be able to comigrate with DNA in a gel matrix; since they are usually positively charged, the expectation is that they would migrate in the opposite direction of the DNA. Additionally, small molecule-DNA exchange rates tend to be fast, especially in comparison with the time required to perform an electrophoresis experiment (hours). However, a number of noncovalently interacting small molecules have been found to comigrate with DNA in a gel matrix, including surface binding molecules such as distamycin[7] and a number of intercalators[8].

In the Barton group, metallointercalators with many useful properties are used as probes of DNA structure. Their structures are shown in Figure 5.1. $Ru(L)_2dppz^{2+}$ complexes can serve as a molecular "light switch" for DNA, as they do not luminesce in aqueous solution but in the presence of DNA they glow brightly. $Ru(phen)_2dppz^{2+}$ has been shown to intercalate from the major groove by NMR spectroscopy[9]. $Rh(L)_2phi^{3+}$ complexes, as described in previous chapters, intercalate into the major groove of DNA and effect strand scission upon ultraviolet irradiation by a nondiffusable mechanism. Several lines of evidence point to the fact that $Ru(phen)_3^{2+}$ also intercalates into DNA, though with much lower affinity than the dppz and phi complexes. Its luminescence lifetime increases in the presence of DNA, and inhibition by anionic quenchers such as $Fe(CN)_6^{4-}$ is reduced[10].

This chapter concerns the application of gel retardation to the study of metal complex- DNA interactions. This technique has the advantage that it is not dependent upon photocleavage. Therefore complexes which cleave by different mechanisms, and even complexes which do not cleave DNA at all, may be directly compared. Here

Figure 5.1. Structures of the intercalators used in gel electrophoretic mobility shift assays. From top: $Ru(phen)_2dppz^{2+}$, $Rh(bpy)_2dppz^{3+}$, $Rh(phen)_2phi^{3+}$, ethidium bromide, and $Ru(phen)_3^{2+}$.

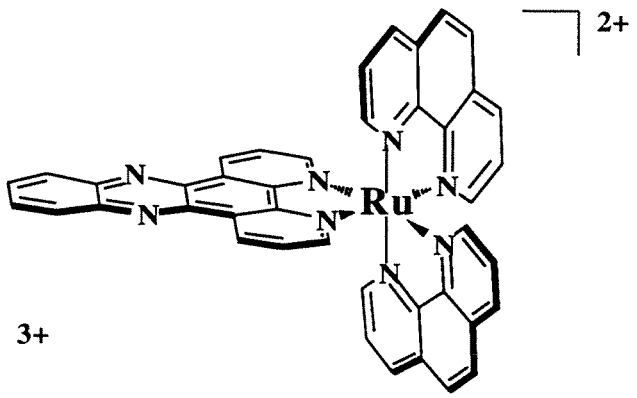
2+
N
Ru

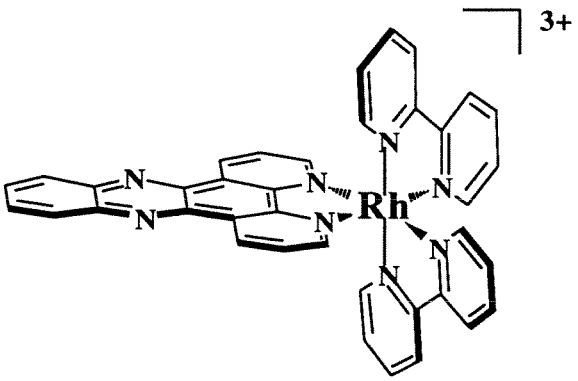
3+
N
Rh

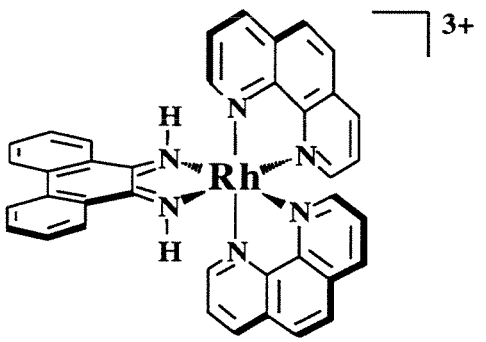
3+
H
N
Rh

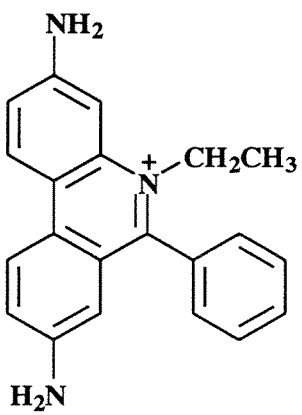
NH2
CH2CH3
N
H2N

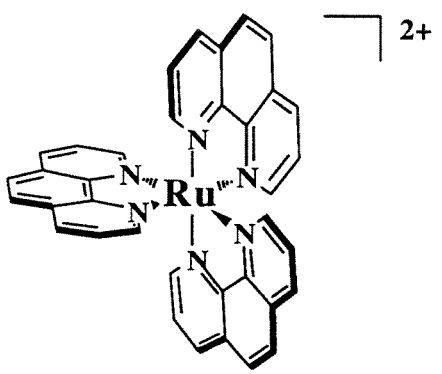
2+
N
Ru

following specific issues are addressed. The importance of the intercalating ligand in the retardation of DNA will be explored using three complexes which have identical ancillary ligands, but differing metal centers and intercalators: $Ru(phen)_2dppz^{2+}$, $Rh(phen)_2phi^{3+}$, and $Ru(phen)_3^{2+}$. The effect of metal complex chirality upon DNA conformational change will be assessed by use of the enantiomers of $Ru(phen)_2dppz^{2+}$ and $Rh(phen)_2phi^{3+}$. The Δ- and Λ- enantiomers of a given complex are identical in every respect except for the disposition of the ligands around the metal center. Additionally, the influence of the charge of these metal complexes upon DNA mobility will be examined using $Rh(bpy)_2dppz^{3+}$ and $Ru(bpy)_2dppz^{2+}$, which have identical ligands, but differing metal centers and charges. Finally, the effect of the absolute concentrations of DNA and metal upon DNA retardation will be discussed.

5.2. Experimental

Materials. pUC18 plasmid DNA was purchased from Boehringer Mannheim. All enzymes utilized were from commercial sources. [α- ^{32}P] dNTPs were purchased from NEN-Dupont. Ethidium bromide was purchased from Sigma. *rac*-$Rh(phen)_2phi^{3+}$ was synthesized as described previously[11]. Other racemic and enantiomerically resolved metal complexes were donated by members of the Barton group[12].

Instrumentation. Concentrations of metal complexes and DNA were based on absorption spectra in 50mM sodium cacodylate buffer, pH 7.0; these were recorded on a Cary 219 (Varian) spectrophotometer. A Gibco BRL double-sided vertical gel electrophoresis apparatus was used to elute the gels. Gels were dried using a Bio-Rad gel dryer, and exposed to a phosphorimaging plate for approximately 16 hours. Plates were scanned using a Molecular Dynamics phosphorimager. (Autoradiograms were analyzed by use of a LKB 2202 Ultrascan Laser Densitometer).

Gel Electrophoresis on DNA fragments. Approximately 60 μg of pUC18 plasmid DNA was linearized with the restriction enzyme *Hin*d III. A fraction of this linearized

DNA was subsequently used for labelling, the remainder was stored at -20°C. Labelling was accomplished by reaction with one or more α-^{32}P dNTPs and the Klenow fragment of DNA polymerase I. Labelled and unlabelled DNA in parallel were then digested with *Sca*I and *Eco*RI simultaneously, producing labelled fragments 90 bp and 908 bp in length, and an unlabelled fragment of 1727 bp.

Samples, unless otherwise indicated had final concentrations of 10mM Tris, 1mM EDTA pH 7.0, and 70μM bp DNA. Samples were typically incubated for approximately one hour at room temperature. Metal complex concentrations are as indicated; typical ranges are from 2μM to 58μM. Samples were suspended in 10X ficol dye and loaded at 4°C at 0V. Gels were run at 300V for 5 hours on a 5% polyacrylamide gel (29:1 mono:bis acrylamide ratio), in 0.25X TBE buffer (25mM Tris, 25mM borate, 0.5mM EDTA) unless otherwise indicated. Retardation data was quantified using ImageQuant software (phosphorimager), or Gel Scan XL (densitometer).

Experimental variables. Numerous sets of experimental conditions were used in order to obtain optimal data. Attempts at visualization by $Ru(phen)_2dppz^{2+}$ luminescence from the sample were unsuccessful, likely due to the relatively small amount present in a band. Attempts at visualizing DNA in 5% polyacrylamide by ethidium bromide also proved difficult. The percentage of crosslinker in the polyacrylamide did not have much of an effect on the retardation observed. However, the 29:1 mono:bis acrylamide ratio appeared to give sharper bands than 5% acrylamide with a 80:1 ratio, which is sometimes used for gel retardation of DNA by proteins. The ionic strength of the running buffer appeared to be important, as gels run in the low ionic strength buffer (0.25X TBE) produced better quality data than those run in a high ionic strength buffer (1X TBE). This low ionic strength condition is commonly used for binding constant determinations with proteins. Excessive diffusion of bands occurred when a low voltage over a long time period, e.g. 70V for 18 hours, was used. The length of DNA fragment used affected the extent of retardation, as observed elsewhere[8c, 13]. For

example, at DNA: bp ratios which produced a great extent of retardation for the 908mer, there was a smaller amount of retardation for a 406mer, and a trace of retardation for a120mer. It is not known with certainty what the origin of this effect is; it is perhaps the result of longer DNA fragments having a higher local concentration in bp in a band for the same number of DNA strands.

5.3. Results

5.3.1. Gel Mobility Shifts by Racemic $Ru(phen)_2dppz^{2+}$, $Rh(phen)_2phi^{3+}$, and $Ru(phen)_3^{2+}$: Effect of Intercalating Ligand

In order to examine the effect of intercalating ligand upon DNA electrophoretic mobility, the following series of racemic complexes was utilized: $Ru(phen)_2dppz^{2+}$, $Rh(phen)_2phi^{3+}$, and $Ru(phen)_3^{2+}$. Ethidium bromide was also examined for comparison. It has been previously observed that ethidium bromide can alter DNA electrophoretic mobility[8a,8c]. Under the standard conditions described above, $Ru(phen)_2dppz^{2+}$, $Rh(phen)_2phi^{3+}$, and ethidium bromide are able to retard DNA mobility whereas $Ru(phen)_3^{2+}$ does not. Figure 5.2 shows a plot of gel mobility shifts by the three racemic complexes and ethidium bromide vs the log of the concentration of DNA binding ligand. As may be seen from this plot, the extent of retardation (R_L= [mobility of unbound DNA fragment/mobility of DNA fragment in the presence of ligand]) increases with increasing metal complex concentration. Some of the mobility change is likely due to an effective lengthening of the DNA fragment by insertion of the intercalating ligand into the helix stack. At all concentrations, the trend of effect on DNA migration by the racemic complexes is as follows: $Ru(phen)_2dppz^{2+}$ > $Rh(phen)_2phi^{3+}$ > Et Br > $Ru(phen)_3^{2+}$. This trend correlates with the surface area of the intercalating ligand, i.e., the larger the area of the ligand which is accessible for stacking, the more efficiently the complex can stack. However, other factors such as charge and ancillary ligands are also involved, as described below.

Figure 5.2. Plot showing comparison of the effect of different intercalators upon DNA electrophoretic mobility. R_L is determined as described in the text. There is a direct correlation between the accessibility of the intercalating ligand and the observed extent of DNA retardation.

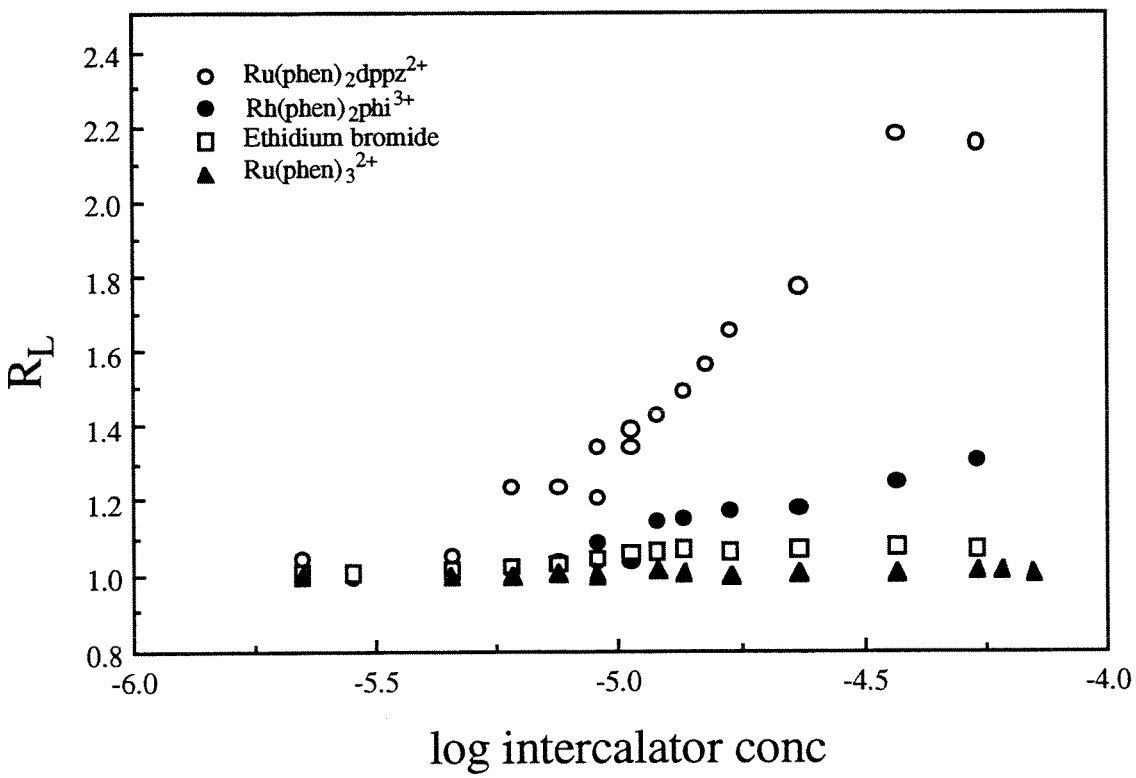
Ru(phen)2dppz2+
Rh(phen)2phi3+
Ethidium bromide
Ru(phen)32+
RL
2.4
2.2
2.0
1.8
1.6
1.4
1.2
1.0
0.8
-6.0
-5.5
-5.0
-4.5
-4.0
log intercalator conc

Although no detectable retardation of DNA by $Ru(phen)_3^{2+}$ occurs under the standard conditions of this experiment, conditions which are more favorable for binding by this complex do decrease DNA mobility, which is shown in Figure 5.3. However, these conditions involve significantly higher concentrations of metal complex, and the observed effect is small. The small effect in DNA mobility by $Ru(phen)_3^{2+}$ may be explained by its low affinity for DNA.

5.3.2. Enantioselectivity in Metal Complex-Induced Electrophoretic Mobility Change

In order to address the effect of metal complex chirality upon DNA retardation, the Δ and Λ enantiomers of $Ru(phen)_2dppz^{2+}$ and $Rh(phen)_2phi^{3+}$ were used to effect retardation on the 908mer DNA fragment. As mentioned in the previous section, the racemates of both complexes retard DNA mobility. A typical retardation gel is shown in Figure 5.4. This gel shows the effect of increasing concentrations of Δ-$Ru(phen)_2dppz^{2+}$ on the mobility of this DNA fragment. It may be seen that the addition of this complex has a dramatic effect on the mobility of the DNA. A quantitative comparison between Δ-$Ru(phen)_2dppz^{2+}$ and Λ-$Ru(phen)_2dppz^{2+}$ is shown in Figure 5.5(top). The plot in Figure 5.5(top) shows that for both these enantiomers there is a decrease in DNA mobility with increase in $Ru(phen)_2dppz^{2+}$ concentration. However, at all concentrations there is a greater effect for the Δ enantiomer than the Λ enantiomer, which is especially noticeable at higher Ru:DNA ratios. Thus two complexes which are identical except for their chirality show differences in their effect on DNA retardation. Enantioselectivity in retardation of DNA is also observed for $Rh(phen)_2phi^{3+}$, as shown in Figure 5.5(bottom). Once again, there is an increase in the extent of retardation observed with an increase in metal complex concentration for both isomers. It should be noted, however, that the mobility of the DNA in the presence of Λ-$Rh(phen)_2phi^{3+}$ appears to be biphasic in nature. This characteristic is not shared by any of the other intercalators examined.

Figure 5.3. An image of a gel showing the effect of $Ru(phen)_3^{2+}$ on the mobility of a 908mer fragment. Samples were incubated at room temperature for 2 hours. This gel was run at 150V for 5 hours at 4°C. Lanes 1 and 7, DNA control at 70μM bp; lane 2, 2mM DNA bp and 2mM $Ru(phen)_3^{2+}$; lane 3, DNA control at 1mM bp; lane 4, 1mM DNA bp and 1mM $Ru(phen)_3^{2+}$; lane 5, 1mM DNA bp and 2mM $Ru(phen)_3^{2+}$; lane 5, 1mM DNA bp and 2mM $Ru(phen)_3^{2+}$; lane 6, 70μM DNA bp and 2mM $Ru(phen)_3^{2+}$. Lanes 2, 4, and 5 show a small extent of retardation. The reduced mobility of this DNA fragment is clear in lane 6.

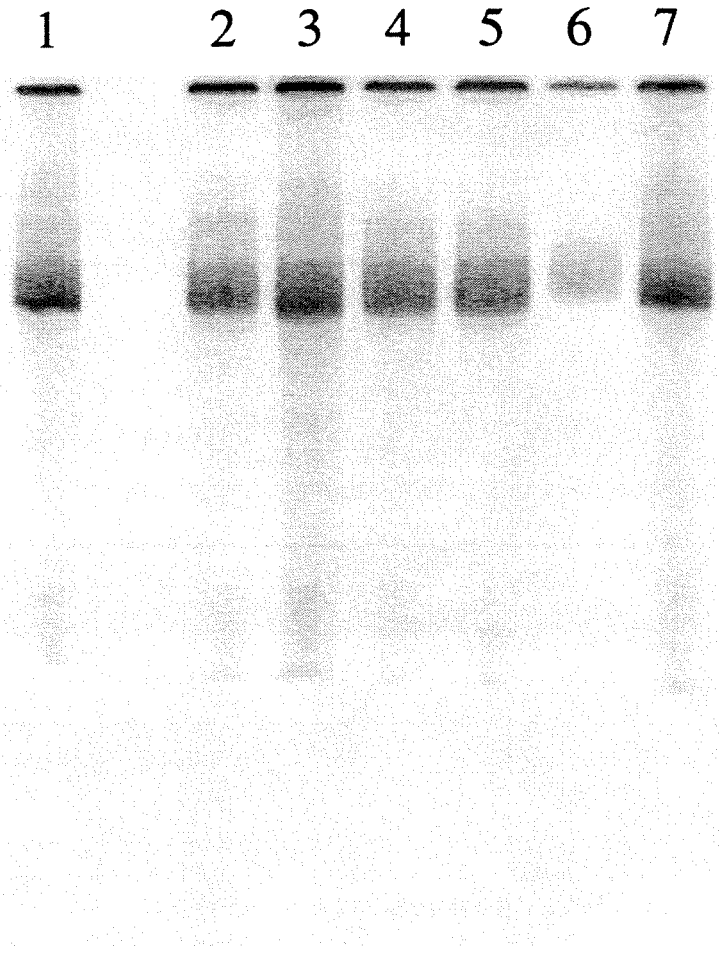
1
2
3
4
5
6
7

Figure 5.4. An image of a representative gel showing reduction in the mobility of a 908mer DNA fragment by Δ-Ru(phen)$_2$dppz^{2+}. Lanes 1, 9, 10, and 18 , DNA control; lanes 2-8 have Δ-Ru(phen)$_2$dppz^{2+} concentrations (μM) of 2.2, 2.8, 4.5, 6, 7.5, 9, and 10.5 respectively; lanes 11-17 have Δ-Ru(phen)$_2$dppz^{2+} concentrations of 10.5 (repetition), 12, 13.5, 15, 16.8, 23.3, 36, and 53.8 respectively.

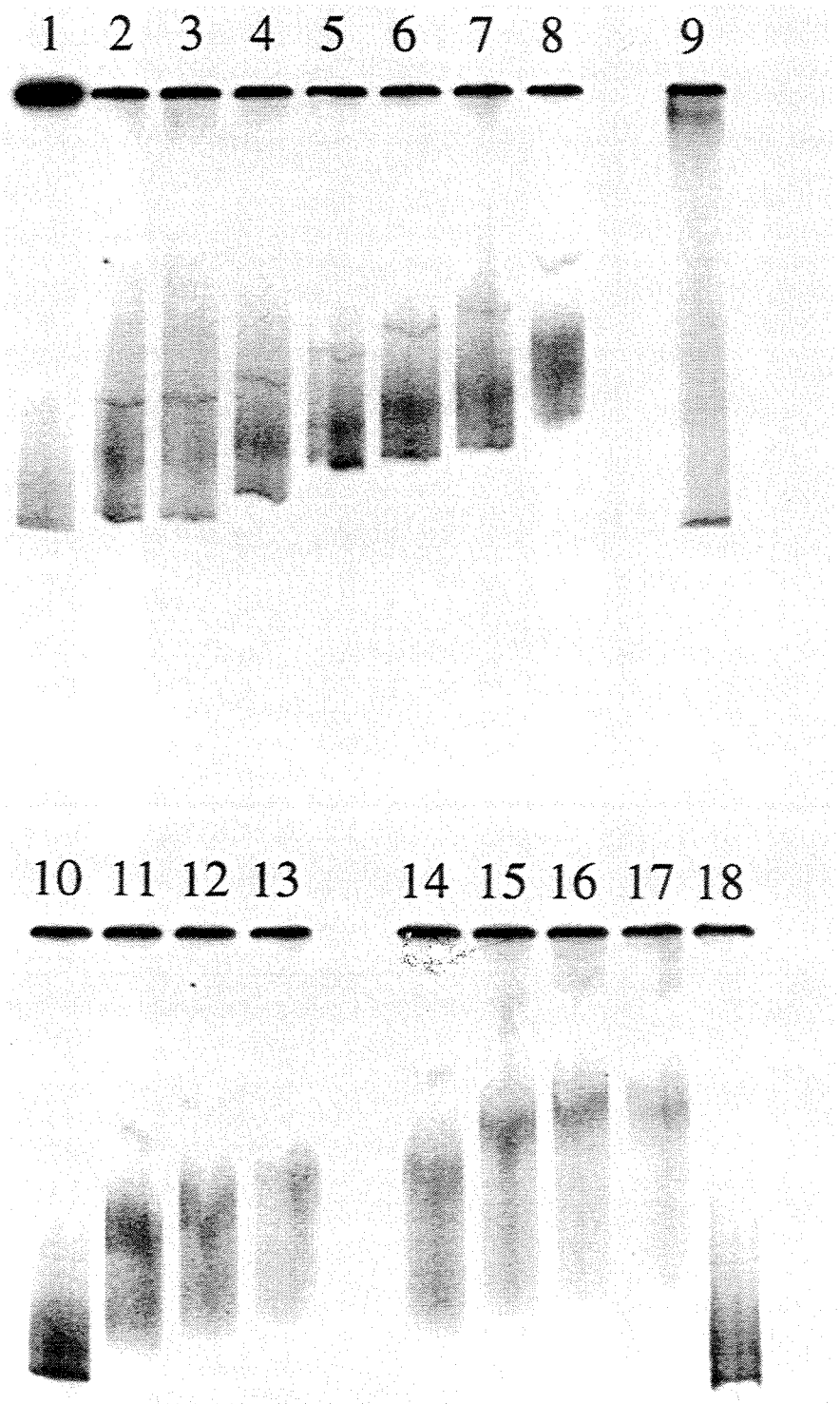
1 2 3 4 5 6 7 8 9
10 11 12 13 14 15 16 17 18

Figure 5.5. Plots showing a comparison of the effect of enantioselectivity upon DNA retardation for $Ru(phen)_2dppz^{2+}$ and $Rh(phen)_2phi^{3+}$. R_L is determined as described in the text. (top panel) A plot showing the change in DNA mobility vs the log of the metal complex concentration for Δ- and Λ-$Ru(phen)_2dppz^{2+}$. (bottom panel) A plot showing DNA retardation as a function of the log of $Rh(phen)_2phi^{3+}$ concentrations for both enantiomers. Note the smaller scale of this plot.

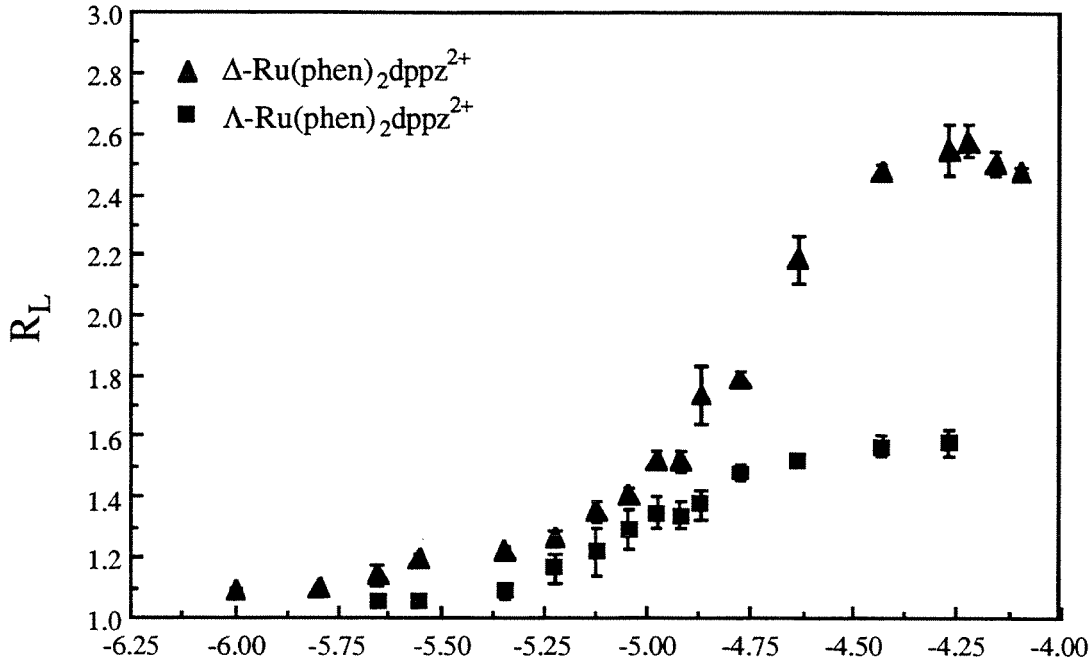
Δ-Ru(phen)2dppz2+
Λ-Ru(phen)2dppz2+
RL
3.0
2.8
2.6
2.4
2.2
2.0
1.8
1.6
1.4
1.2
1.0
-6.25
-6.00
-5.75
-5.50
-5.25
-5.00
-4.75
-4.50
-4.25
-4.00
log metal complex conc

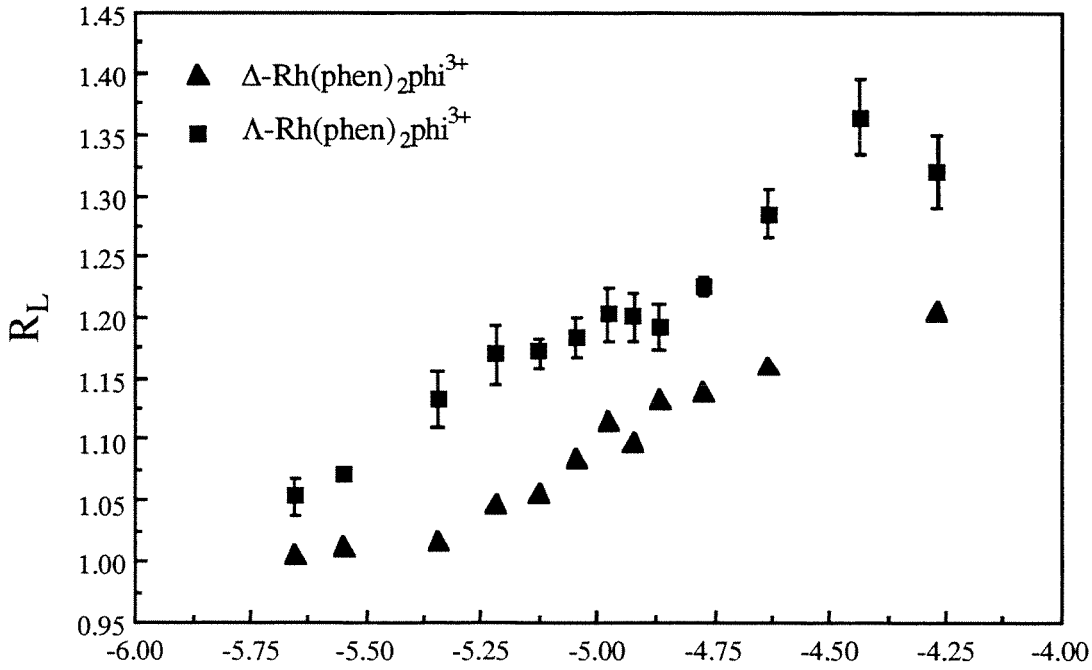
Δ-Rh(phen)2phi3+
Λ-Rh(phen)2phi3+
RL
1.45
1.40
1.35
1.30
1.25
1.20
1.15
1.10
1.05
1.00
0.95
-6.00
-5.75
-5.50
-5.25
-5.00
-4.75
-4.50
-4.25
-4.00
log metal complex conc

Additionally, the enantioselectivity of retardation is opposite to that observed with $Ru(phen)_2dppz^{2+}$; for $Rh(phen)_2phi^{3+}$, it is the *Λ -isomer* which has the greater effect upon DNA mobility than the Δ isomer. It is unlikely that the origin of this difference results from differential intercalation by Λ-$Rh(phen)_2phi^{3+}$ and Δ-$Rh(phen)_2phi^{3+}$, since photocleavage data are consistent with the Δ enantiomer showing preferential cleavage of DNA and photocleavage requires intercalation. As mentioned in Chapter 2, there are some sites which Δ-$Rh(phen)_2phi^{3+}$ cleaves to an equal or greater extent than Λ-$Rh(phen)_2phi^{3+}$, but there are no sites at which Λ-$Rh(phen)_2phi^{3+}$ cleaves to an appreciably greater extent than Δ-$Rh(phen)_2phi^{3+}$. NMR results also show preferential binding by the Δ isomer; the spectrum of Λ-$Rh(phen)_2phi^{3+}$ exhibits broader linewidths indicative of faster exchange and lessened specificity. Therefore this differential mobility may be explained by a) different conformational changes induced by intercalation by Δ-$Rh(phen)_2phi^{3+}$ versus Λ-$Rh(phen)_2phi^{3+}$, or b) a binding mode other than intercalation. The fact that the Λ > Δ trend is observed at all concentrations of $Rh(phen)_2phi^{3+}$ and not just the higher concentrations points to the former explanation.

Therefore, it may be observed that although the primary effect on DNA mobility is due to the nature of the intercalator, the chirality of the metal complexes produces differential mobilities as well.

5.3.3. The Effect of Metal Complex Charge upon DNA Retardation

$Ru(phen)_2dppz^{2+}$ and $Rh(phen)_2phi^{3+}$ have different intercalating ligands, which lead to their differential effects upon DNA retardation as described above. However, they also differ in their metal center, and therefore their overall charge. It was not clear whether a more positively charged complex would retard the DNA to a greater extent due to charge neutralization; another possibility would be that the application of a voltage would more effectively separate the metal complex and DNA. In order to examine specifically the effects of charge on DNA mobility the racemic complexes

$Rh(bpy)_2dppz^{3+}$ and $Ru(bpy)_2dppz^{2+}$ were compared. These complexes are identical except for their metal centers and their charges. Figure 5.6 shows differences in the retardation induced by $Rh(bpy)_2dppz^{3+}$ and $Ru(bpy)_2dppz^{2+}$. There is not much difference in the extent of retardation of the 908mer fragment at low concentrations of metal complex (2 μM). However, at the middle concentration range (6-17 μM), $Rh(bpy)_2dppz^{3+}$ reproducibly retards DNA to a greater extent than $Ru(bpy)_2dppz^{2+}$. At the highest concentrations of metal complex examined (50-70 μM) strong, reproducible retardation by $Rh(bpy)_2dppz^{3+}$ is observed, whereas the retardation by $Ru(bpy)_2dppz^{2+}$ is weaker and not as reproducible. These results are consistent with a contribution of charge neutralization by the metal complexes to the extent of retardation observed, i.e., with all else being equal, a greater extent of retardation is observed with the more positively charged metal complex.

Another interesting observation from these results is that the ancillary ligands of these complexes also influences DNA mobility. As may be observed in Figures 5.2 and 5.6, racemic $Ru(phen)_2dppz^{2+}$ retards DNA mobility to a greater extent than racemic $Rh(bpy)_2dppz^{3+}$. The maximal R_L for $Ru(phen)_2dppz^{2+}$ is 2.2 whereas the maximal R_L for $Rh(bpy)_2dppz^{3+}$ is less than 1.4. If the extent of retardation were dominated by a charge effect, it might be expected that $Rh(bpy)_2dppz^{3+}$ would have a greater effect on DNA mobility than $Ru(phen)_2dppz^{2+}$. Thus we see that the hydrophobicity of the ancillary ligands has a considerable influence upon the DNA retardation by these metal complexes, and not just the size of the intercalating ligand. Additionally, the hydrophobicity of the ancillary ligands appears to outweigh the effects of the charge of the metal complex.

Figure 5.6. Plots depicting an examination of the effect of metal complex charge upon DNA retardation. Shown is a plot of the apparent length of DNA vs the metal complex concentration for $Rh(bpy)_2dppz^{3+}$ and $Ru(bpy)_2dppz^{2+}$. R_L is determined as described in the text. Note the smaller scale for this plot as compared with that of Figure 5.4(top).

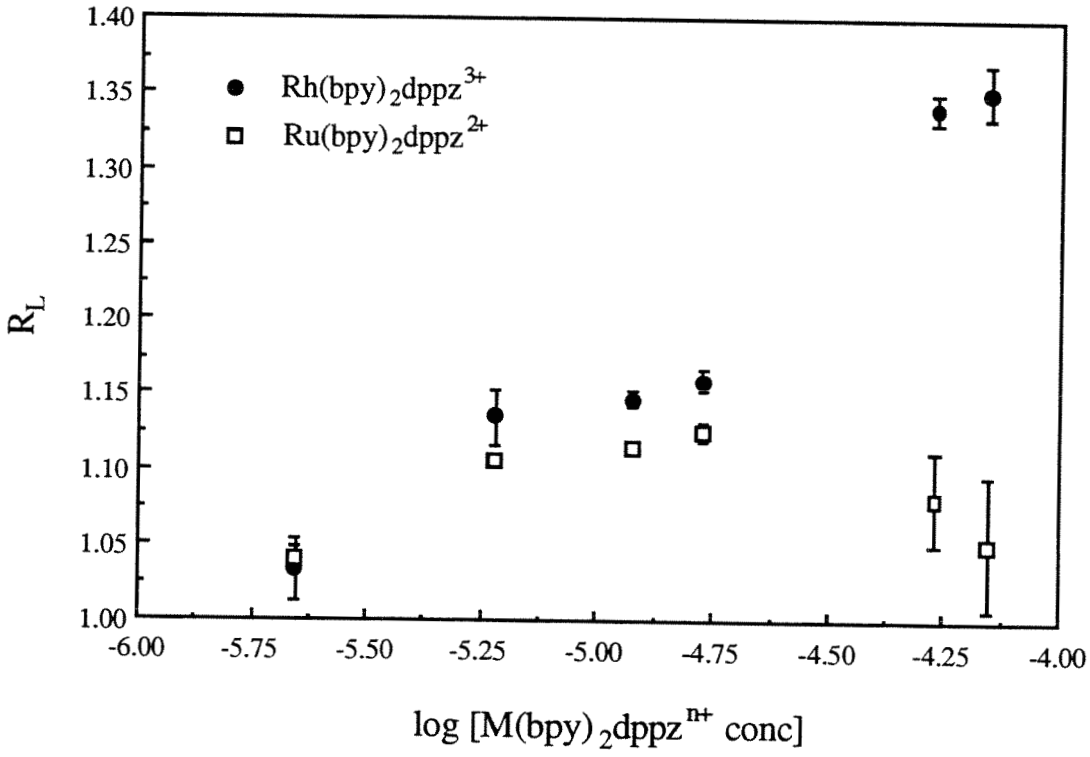
1.40
1.35
1.30
1.25
1.20
1.15
1.10
1.05
1.00
R_L
Rh(bpy)$_2$dppz^{3+}
Ru(bpy)$_2$dppz^{2+}
-6.00
-5.75
-5.50
-5.25
-5.00
-4.75
-4.50
-4.25
-4.00
log [M(bpy)$_2$dppz^{n+} conc]

5.3.4. The Effect of Absolute Concentrations of DNA and Metal Complex upon DNA Mobility

The importance of the absolute concentrations of DNA fragment and metal complexes on DNA retardation was also examined (data not shown). An experiment utilizing racemic $Ru(phen)_2dppz^{2+}$ at the same DNA:metal complex ratios as the experiment in Figure 5.2, but lowering the absolute concentrations by a factor of 200 eliminated retardation of the 908mer. When ratios of DNA bp: *rac*-$Ru(phen)_2dppz^{2+}$ are held constant in the range from 1.3 to 3.0, a great extent of retardation occurs at 70μM bp, as described above. However, a reduction of DNA concentration by about a factor of 6 severely hampers the retardation by this complex. At 2μM bp, only a trace of retardation is observed. Even a change by a factor of 2 in the absolute concentrations of Δ–$Ru(phen)_2dppz^{2+}$ significantly reduced the extent of retardation observed, particularly at low DNA bp: metal complex ratios. Another illustration of the importance of the absolute concentration of DNA is that at a constant *rac*-$Ru(phen)_2dppz^{2+}$ concentration of 37μM, the extent of retardation increases with increasing DNA concentration. Thus it has been demonstrated that the absolute concentrations of *both* DNA and metal complex in the gel matrix have a great influence upon the retardation of DNA.

5.4. Discussion

5.4.1. Comparison of Retardation by DNA-Binding Molecules

All the metal complexes studied have been shown to have an effect on DNA mobility in some concentration range. However, the extent to which these metal complexes retard DNA mobility varies widely. The overall trend of the magnitude of the retardation is as follows: Δ-$Ru(phen)_2dppz^{2+}$ > Λ-$Ru(phen)_2dppz^{2+}$ > Λ-$Rh(phen)_2phi^{3+}$ ≥ *rac*-$Rh(bpy)_2dppz^{3+}$ ≥ Δ-$Rh(phen)_2phi^{3+}$ > ethidium bromide >> $Ru(phen)_3^{2+}$. As can be seen from this trend, when the ancillary ligands are phenanthrolines, it is the nature of the intercalator which has the greatest effect upon DNA mobility. $Ru(phen)_2dppz^{2+}$,

which has the greatest propensity for base pair overlap, shows the largest effect. The phi ligand is also shown here to be an effective intercalator, as differences in DNA mobility are observed at the same concentrations used for $Ru(phen)_2dppz^{2+}$. $Ru(phen)_3^{2+}$, which is an intercalating and groove binding molecule, shows a much diminished effect, and only at significantly higher concentrations. Although the phi and phenanthroline ligands are comparable in area, in the context of the octahedral geometry of the complexes, the phenanthroline ligand is *less accessible* to stacking between the base pairs than the phi ligand. This shape also contributes to the low binding affinity of $Ru(phen)_3^{2+}$ for DNA, which is about 10^3 lower than that of $Rh(phen)_2phi^{3+}$. It is this low binding affinity, and not the surface binding mode of $Ru(phen)_3^{2+}$ which results in the small amount of retardation observed, since other groove binders with higher affinity for DNA, such as distamycin[8c], show a significant effect upon DNA mobility.

How does DNA retardation by these metal complexes compare to that observed for other DNA-binding small molecules under similar conditions? For the 908mer examined here the maximal amount of retardation (R_L) by Δ-$Ru(phen)_2dppz^{2+}$ (2.6) is significantly greater than that by ethidium bromide (1.1). The maximum R_L is also slightly greater than that measured on mixed sequence DNA for ditercalinium (2.4)[8c], a bisintercalator with a +2 charge. Ethidium dimer, on the other hand, is capable of retarding mixed sequence DNA to a greater extent (R_L=3.8)[8c] than Δ-$Ru(phen)_2dppz^{2+}$ and all the previously mentioned compounds under similar conditions to those used in this work. The high charge of ethidium dimer (+4) would be expected to contribute to its efficacy in retarding DNA as compared with that of $Ru(phen)_2dppz^{2+}$ and the other compounds. Additionally, although ethidium dimer was once thought to be a monointercalator[14], it has been demonstrated by NMR that this DNA binding molecule is in exchange between monointercalating and bisintercalating modes[15]. Therefore, the large extent of retardation by ethidium dimer in comparison to other compounds may be explained by its charge and/or the differing binding modes of these molecules.

Although charge appears to be important for retardation by other intercalators, $Ru(phen)_2dppz^{2+}$ retards DNA to a much greater extent than does $Rh(phen)_2phi^{3+}$, even though formally it is not as positively charged. There are two possible explanations for this effect. First, since the pK_a of $Rh(phen)_2phi^{3+}$ is approximately 6.2[16], the phi ligand is likely to be mostly deprotonated at pH 7.0, which leads to an overall net charge of +2 for this complex at this pH, assuming the interaction with DNA does not change the pK_a significantly. Secondly, it might be reasoned that since $Ru(phen)_2dppz^{2+}$ has a greater overall binding constant to DNA, it is remaining associated with the DNA to a greater extent than is $Rh(phen)_2phi^{3+}$ in the gel matrix. This explanation, however, is questionable, as the K_a of $Rh(phen)_2phi^{3+}$ is high enough that it should be almost completely bound *in solution* throughout the concentration range studied here. Additionally, greater differences are observed in extent of DNA retardation by $Rh(phen)_2phi^{3+}$ and $Ru(phen)_2dppz^{2+}$ in the higher concentration range than in the lower concentration range. This observation would also be consistent with $Rh(phen)_2phi^{3+}$ being completely bound in the lower concentration range.

5.4.2. Factors Influencing Retardation by $M(L)_2X^{n+}$ Complexes

Sequence selectivity of these metallointercalators is one factor which could have an influence on their effect upon DNA mobility. The site selection of $Rh(phen)_2phi^{3+}$ has been well characterized[17], as it photocleaves DNA. Δ-$Rh(phen)_2phi^{3+}$ shows a strong preference for 5'-*YY*R-3' and an intermediate extent of cleavage at pyrimidine stretches. Λ-$Rh(phen)_2phi^{3+}$ shows an equal extent of cleavage for the pyrimidine stretches, and no preference for the 5'-YR-3' steps. NMR also shows greater site specificity by Δ-$Rh(phen)_2phi^{3+}$ than by the Λ enantiomer[18]. The sequence selectivity of $Ru(phen)_2dppz^{2+}$ has not been as well characterized. However, different types of experiments, including NMR[19], binding stoichiometries to DNA as measured by fluorescence[20], and singlet oxygen cleavage experiments on correctly paired DNA[21] all

suggest that both enantiomers of $Ru(phen)_2dppz^{2+}$ have a limited sequence selectivity. Binding by the dppz complexes in a more or less random manner may more effectively retard DNA mobility than binding by phi at specific sites. However, differences in sequence selectivity do not fully explain the observed difference in enantioselectivity of retardation by $Ru(phen)_2dppz^{2+}$.

What, then, are the factors leading to the reduced mobility of DNA by these metal complexes? The hydrophobicity of these metal complexes appears to be an important factor in this regard. As mentioned above, the accessible hydrophobic area of the intercalating ligand available for π stacking with the DNA bases correlates with the observed trend of retardation by the complexes. Additionally, the hydrophobicity of the ancillary ligands also appears to have an effect upon retardation, since $Ru(phen)_2dppz^{2+}$ has a much greater effect upon DNA mobility than does either $Rh(bpy)_2dppz^{3+}$ or $Ru(bpy)_2dppz^{2+}$. Another parameter which shows a dependence upon metal complex hydrophobicity is exchange rate, as measured by NMR spectroscopy, that is, the more hydrophobic the complex, the slower the exchange rate. Therefore, the above-mentioned trends in DNA retardation by the metal complexes correlate with observed trends in their exchange rates. The enantioselectivity by $Ru(phen)_2dppz^{2+}$ also correlates with that of exchange. However although $Rh(phen)_2phi^{3+}$ shows a $\Lambda > \Delta$ trend for DNA retardation, NMR shows it to be in faster exchange than the Δ-isomer. Some possible reasons for the observed enantioselectivity in DNA retardation by these complexes will be discussed below.

Additionally, it is likely the retardation of DNA observed here is due *in part* to a reduction in charge density, resulting from the lengthening of the DNA molecule by insertion of the intercalating ligand accompanied by charge neutralization of the phosphate backbone. Indeed, these results show that the more positively charged $Rh(bpy)_2dppz^{3+}$ retards DNA mobility more reproducibly and to a greater extent in the 6μM- 70μM concentration range than does $Ru(bpy)_2dppz^{2+}$. However, there are a

number of findings which contradict charge as being the overriding contribution to the alteration in DNA mobility by these metal complexes. First, *rac*-$Ru(phen)_2dppz^{2+}$ reduces DNA mobility to a significantly greater extent than does *rac*-$Rh(bpy)_2dppz^{3+}$, which is in opposition to expectations based upon metal complex charge being the predominant component to the retardation. Secondly, there are notable differences between retardation by two enantiomers of the same complex, which would also not be predicted if the retardation is occurring mainly by way of charge neutralization. It has been noted from comparisons of DNA mobility in the presence of ethidium bromide(+1) and propidium iodide(+2) that charge neutralization plays a more significant role in the retardation of gel mobility than does the increased contour length of the DNA[22]. However, the conclusion that the lowering of charge density is the major contribution to DNA retardation was based on data from a different gel matrix than utilized here. 1% agarose possesses a pore size of 1000-3000 Å, considerably larger than the persistence length of DNA (500 Å). In contrast the pore size of the 5% polyacrylamide used here is 20-35 Å. Therefore it is likely that the polyacrylamide matrix would be sensitive to another potential contribution to the observed retardation by these metal complexes, i.e., their deformation of DNA structure.

Some types of DNA conformational change that might be expected to influence DNA electrophoretic mobility are considerations such as stiffening or kinking. The stiffening of the DNA helix caused by intercalation may be quantified using such techniques as linear dichroism and viscometry. The orientation factor, S, which is derived from linear dichroism, shows a greater stiffening of DNA by Λ-$Ru(phen)_2dppz^{2+}$ than the Δ-isomer[23]. However, it has recently been found that Δ- and Λ-$Ru(phen)_2dppz^{2+}$ show essentially identical viscometric behavior[20], which indicates an equal extent of stiffening of DNA by both enantiomers of $Ru(phen)_2dppz^{2+}$. Therefore, stiffening in isolation is not likely to be the cause of the enantioselectivity in retardation ($\Delta > \Lambda$) by $Ru(phen)_2dppz^{2+}$. However, stiffening, in combination with other structural

deformations such as kinking might explain differences in retardation by phi and dppz intercalators, and could possibly explain the trend of $\Lambda > \Delta$ for $Rh(phen)_2phi^{3+}$. Additionally, other conformational changes besides stiffening could explain the enantioselectivity for $Ru(phen)_2dppz^{2+}$.

Another conformational change that contributes to differences between the complexes in effecting DNA retardation is helical unwinding. Intercalation involves a separation of DNA base pairs by the insertion of the ligand with a concomitant unwinding of the DNA base step. Such changes in the DNA phosphate backbone geometry have also been observed by ^{31}P NMR spectroscopy for these complexes[19,24]. The extent of unwinding of DNA can be measured using a topoisomerase assay. Some preliminary experiments with topoisomerase[21] have shown that Δ-$Ru(phen)_2dppz^{2+}$ unwinds DNA to a greater extent than does Λ-$Ru(phen)_2dppz^{2+}$ (25° vs 18°). Such differences in the average extent of unwinding by the metal complexes could effect differences in the apparent length of DNA.

It was unexpected that Λ-$Rh(phen)_2phi^{3+}$ would have a greater effect upon DNA mobility than Δ-$Rh(phen)_2phi^{3+}$. Although not easy to explain, there have been some observations using other techniques which would be consistent with a $\Lambda > \Delta$ trend. A low affinity binding mode observed by equilibrium dialysis[16] on $Rh(phen)_2phi^{3+}$, shows enantiomeric preference for the Λ-isomer. However, this low affinity binding mode is only observed at high concentrations of $Rh(phen)_2phi^{3+}$, and where [M] bound stops increasing sharply. This binding preference by Λ-$Rh(phen)_2phi^{3+}$ is likely to correspond to a surface binding interaction. By analogy to $Ru(phen)_3^{2+}$, a surface binding mode of Λ-$Rh(phen)_2phi^{3+}$ would involve van der Waals interactions between two phenanthroline ligands and the minor groove of DNA. Therefore, the affinity of Λ-$Rh(phen)_2phi^{3+}$ for DNA through a surface bound interaction would be expected to be very *weak* (10^3). The lack of retardation by $Ru(phen)_3^{2+}$ under the standard concentrations utilized here demonstrates that weak binding modes are incapable of producing a large effect upon

DNA mobility. Therefore, a surface bound mode for Λ-Rh(phen)$_2$phi^{3+} cannot explain the enantiomeric preference (Λ > Δ) observed in the standard concentration range utilized here (10^{-6}-10^{-4}M). Additionally, it is not obvious that Λ-Rh(phen)$_2$phi^{3+} would even have a greater effect upon DNA mobility in a surface bound mode than either enantiomer would in an intercalative mode.

Therefore, the large effects upon DNA mobility are likely to be due to a higher affinity binding mode for Λ-Rh(phen)$_2$phi^{3+}. There are a number of lines of evidence that are consistent with an intercalative binding mode for Λ-Rh(phen)$_2$phi^{3+}. First, *both* enantiomers of Rh(phen)$_2$phi^{3+} show an equivalent amount of photocleavage at sequences such as 5'-*YY*-3' in the 10^{-6}-10^{-5}M concentration range; since photocleavage requires intercalation, Λ-Rh(phen)$_2$phi^{3+} is certain to be binding by intercalation at these sites. A second line of evidence involves the upfield chemical shift changes observed for the protons situated on intercalators upon binding to DNA[25]. Similar upfield chemical shift changes of phi ligand protons are measured for both enantiomers of this complex[24], and there is direct NMR evidence of an intercalative binding mode for Δ-Rh(phen)$_2$phi^{3+}. Additionally, both enantiomers induce characteristic downfield chemical shift changes in DNA phosphorus resonances, as detected by ^{31}P NMR[24]. This observation is also consistent with intercalation by Λ-Rh(phen)$_2$phi^{3+}.

How may the Λ > Δ trend in DNA retardation be explained for Rh(phen)$_2$phi^{3+}? A number of experimental observations are consistent with DNA conformational destabilization by Λ-Rh(phen)$_2$phi^{3+}. For example, this metal complex shows some interesting thermodynamic behavior with DNA. Intercalation by these metal complexes generally results in an increase of duplex melting temperature, as observed by NMR and UV absorption spectroscopy. This increase in T_m indicates the thermodynamic stabilization of the duplex. Λ-Rh(phen)$_2$phi^{3+} shows significantly less stabilization of the duplex as detected by NMR and absorption spectroscopy[21,24] than does the Δ-isomer. Additionally, a Λ-isomer of a Rh(phen)$_2$phi^{3+} analog, Λ-1-Rh(MGP)$_2$phi^{5+} (MGP=4-

guanidylmethyl), induces a severe conformational change at a specific site of binding, which involves an unwinding of the DNA helix by approximately 70°[26]. These results, taken together, suggest some type of conformational destabilization of the DNA upon intercalative binding by Λ-$Rh(phen)_2phi^{3+}$. It is interesting that viscometry experiments show that with increasing Δ-$Ru(phen)_3^{2+}$ concentration, an initial decrease in DNA length is followed by a subsequent increase in DNA length[27]. These results, have also been interpreted in terms of a metal complex-induced kink in the DNA structure, and have some similarity to the biphasic nature of retardation by Λ-$Rh(phen)_2phi^{3+}$ observed here[28].

In conclusion, all the octahedral metal complexes studied here yield an effect on DNA electrophoretic mobility. The differing extents of retardation by these complexes may be explained by a combination of factors. The most important contribution appears to be the hydrophobicity of both intercalating and ancillary ligands, which also has an effect on the exchange rates of these complexes with DNA. With all other factors being equal, metal complex charge also has an influence upon the observed retardation of DNA mobility. Finally, differences between the enantiomers of a given complex are attributed to their differing effects upon DNA unwinding and other aspects of DNA conformation.

References and Footnotes

1. Carey, J. *Methods Enzymol.* **1991**, *208*, 103-117
2. Gerstle, J.T.; Fried, M.G. *Electrophoresis* **1993**, *14*, 725-731.
3. (a) Crothers, D.M.; Gartenberg, M.R.; Shrader, T.E. *Methods Enzymol.* **1991**, *208*, 118-146. (b) Harrington, R.E. *Electrophoresis* **1993**, *14*, 732-746.
4. Niederweis, M.; Hillen, W. *Electrophoresis* **1993**, *14*, 693-698.
5. Rice, J.A.; Crothers, D.M.; Pinto, A.L.; Lippard, S.J. *Proc. Natl. Acad. USA* **1988**, *85*, 4158-4161.
6. (a) Sinden, R.R.; Hagerman, P.J. *Biochemistry* **1984**, *23*, 6299-6303. (b) Haran, T.E.; Crothers, D.M. *Biochemistry* **1988**, *27*, 6967-6971.
7. Wu, H.-M; Crothers, D.M. *Nature* **1981**, *308*, 509-513.
8. (a) Nielsen, P.E.; Zhen, W.; Henriksen, U.; Buchardt *Biochemistry* **1988**, *27*, 67-73. (b) Glazer, A.N.; Peck, K.; Mathies, R.A. *Proc. Natl. Acad. USA* **1990**, *87*, 3851-3855. (c) Barcelo, F.; Muzard, G.; Mendoza, R.; Révet, B.; Roques, B.P.; Le Pecq, J.-B. *Biochemistry* **1991**, *30*, 4863-4873.
9. (a) Dupureur, C.M.; Barton, J.K. *J. Am. Chem. Soc.* **1994**, *116*, 10286-10287. (b) Dupureur, C.M.; Barton, J.K., manuscript submitted.
10. (a) Barton, J.K.; Goldberg, J.M.; Kumar, C.V.; Turro, N.J. *J. Am. Chem. Soc.* **1986**, *108*, 2081-2088. (b) Kumar, C.V.; Barton, J.K.; Turro, N.J. *J. Am. Chem. Soc.* **1985**, *107*, 5518-5523.
11. Pyle, A.M.; Chiang, M.; Barton, J.K. *Inorg. Chem* **1990**, *29*, 4487-4495.
12. Δ-, Λ-, *rac*-$Ru(phen)_2dppz^{2+}$, and $Ru(bpy)_2dppz^{2+}$ were provided by Yonchu Jenkins. Drs. Cindy Dupureur and Kevin Kingsbury provided Δ- and Λ-$Rh(phen)_2phi^{3+}$. $Rh(bpy)_2dppz^{3+}$ was synthesized by Alan Friedman.

13. He, G.-X.; Browne, K.A.; Groppe, J.C.; Blaskó, A., Mei, H.-Y.; Bruice, T.C. *J. Amer. Chem. Soc.* **1993**, *115*, 7061-7071.

14. Gaugain, B.; Barbet, J.; Oberlin, R.; Roques, B.P.; Le Pecq, J.-B. *Biochemistry* **1978**, 5078-5088.

15. Delbarre, A.; Gourevitch, M.I.; Gaugain, B.; Le Pecq, J.-B.; Roques, B.P. *Nuc. Acids Res.* **1983**, *11*, 4467-4482.

16. Pyle, A.M. Ph.D. dissertation, Columbia University, 1989.

17. (a) Pyle, A.M.; Morii, T.; Barton, J.K. *J. Am. Chem. Soc.* **1990**, *112*, 9432-9434. (b) Campisi, D.; Morii, T.; Barton *Biochemistry* **1994**, *33*, 4130-4139.

18. David, S.S.; Barton, J.K. *J. Am. Chem Soc.* **1993** *115,* 2984-2985.

19. Dupureur, C.M.; Barton, J.K., manuscript submitted, 1995.

20. Haq, I.; Lincoln, P.; Suh, D.; Nordén, B.; Chowdhry, B.Z.; Chaires, J.B *J. Am. Chem. Soc.* **1995**, *117*, 4788-4796.

21. Jenkins, Y.C.; Barton, J.K., unpublished results.

22. Reese, H.R. *Biopolymers* **1994**, *34*, 1349-1358.

23. Hiort, C.; Lincoln, P.; Nordén, B.; *J. Am. Chem. Soc.* **1993**, *115*, 3448-3454.

24. Dupureur, C.M.; Barton, J.K., unpublished results.

25. Feigon, J.; Denny, W.A.; Leupin, W.; Keans, D.R. *J. Med. Chem.* **1984**, *27*, 450-465.

26. Terbrueggen, R.H.; Barton, J.K. *Biochemistry* **1995**, in press.

27. Satyanarayana, S.; Dabrowiak, J.C.; Chaires, J.B. *Biochemistry* **1993**, *32*, 2573-2584.

28. The observed DNA length as a function of metal complex shows a more complex trend with the gel retardation than with the viscometry. This discrepancy may be due to the longer length DNA used in these retardation assays (908bp) as compared with the viscometric experiments (~200bp).

Chapter 6:

Conclusions and Perspectives

It has been more than a decade since the first high-resolution crystal structure of DNA in the B form has been solved. Previously, DNA had been considered to possess a regular polymeric structure. The range of local conformational heterogeneity observed within B DNA form was unanticipated, and attempts were made to define precisely how DNA sequence dictates its three-dimensional structure. However, as more structures were solved, early sets of proposed rules for DNA structure were not always found to be heeded.

The work described herein has involved the application of transition metal complexes to the study of DNA conformational variation in solution. The group of complexes utilized here bind noncovalently to DNA by means of a shape-selective mechanism. These complexes also possess useful photochemical properties which instruct us about DNA conformation on many levels. For example, $Ru(TMP)_3^{2+}$ detects variations in minor groove width, and is a probe for the A conformation. In a complementary fashion, $Rh(phi)^{3+}$ complexes bind in the major groove of DNA and therefore provide information about local major groove structure. The location of binding of $Rh(phi)^{3+}$ complexes is in contradistinction to that of most other chemical and enzymatic DNA probes. Whereas most other probes tend to recognize structural features of the DNA backbone and minor groove, $Rh(phi)^{3+}$ complexes are uniquely suited for examining the structure of the DNA *major* groove. Together with $Ru(TMP)_3^{2+}$, $Rh(phen)_2phi^{3+}$ can provide information about DNA groove width.

Another distinguishing feature of complexes such as $Rh(phen)_2phi^{3+}$ is their intercalation into DNA. This mode of association between the intercalating ligand and the DNA base pairs is necessarily sensitive to considerations of DNA stacking and disposition of the DNA bases. These important components of DNA structure are not easily determined by other techniques such as NMR spectroscopy. Therefore, again, use of these

transition metal probes serves to complement the use of other methods in studying DNA solution structure.

The intercalation of these metal complexes is modulated by their nonintercalating, or ancillary ligands. These ancillary ligands provide steric bulk which is an important means by which to discriminate among DNA sites. In this regard, Δ-$Rh(phen)_2phi^{3+}$ has been developed here into a probe of DNA sites which are opened in the major groove, in particular by the propeller twisting of successive DNA base pairs.

Aside from being useful as probes of DNA structure, this class of transition metal complexes are also interesting as rudimentary models of DNA recognition by proteins. Like proteins, $Rh(phen)_2phi^{3+}$, for example, recognizes DNA major groove shape. However, unlike proteins, $Rh(phen)_2phi^{3+}$ lacks hydrogen bonding functionalities, and therefore is not sensitive to the precise positioning of the functionalities in the major groove of DNA. This metal complex shares binding sites in common with proteins and has also been used as a probe of protein binding regions of DNA. Interestingly, however, Δ-$Rh(phen)_2phi^{3+}$ recognizes a mismatch-induced structural perturbation which is apparently not well detected by repair enzymes. It will be interesting to learn whether binding by these metal complexes to other DNA sequences and other mismatches can provide insights into such issues as indirect readout and DNA repair.